Alma Mater Studiorum · Università di Bologna

Scuola di Scienze
Dipartimento di Fisica e Astronomia
Corso di Laurea Magistrale in Fisica

Validation of a test for the physical performance evaluation of elderly and diseased subjects

Relatore:
Prof. Romano Zannoli

Presentata da:
Maria Francesca Morrone

Correlatore:
Dott. Ivan Corazza

Anno Accademico 2017/2018

“ Sembra così saggio, il corpo,
che mai potrò abituarmi ad abitare
dentro uno scheletro così sapiente di fatica.
Non è nostro il corpo,
appartiene invece ad un’antichità
che ce lo ha prestato dopo averlo perfezionato
in millenni di usura, sforzo, resistenza.
Una catena innumerevoli di antenati
ci consegna una macchina rifinita da abitare,
metà casa metà officina.
E riusciamo a conoscerla solo quando
la sottoponiamo al carico di lavoro. ”

Sulla traccia di Nives
Erri De Luca

Sommario

In questo lavoro di tesi è stato validato un test sottomassimale per la valutazione funzionale di soggetti con prestazioni fisiche limitate (anziani e pazienti con malattie cardiovascolari), anche inseriti in programmi riabilitativi.

Il "test of performance" (TOP) è di facile esecuzione, rappresenta un'alternativa al "test cardiopolmonare", molto più complesso, e prevede lo sviluppo di strumentazione e algoritmi di valutazione specifici. Nella modalità più semplice viene registrato il solo segnale elettrocardiografico (ECG) durante una prova da sforzo a basso carico, eseguita secondo un protocollo che prevede la suddivisione del test in due fasi. Nella prima fase si svolge il "tilt test" in cui il paziente passa dal clinostatismo all'ortostatismo, per valutare la funzionalità del sistema nervoso autonomo. Nella seconda fase il paziente esegue il test da sforzo sul cicloergometro a due carichi di lavoro diversi, inizialmente un carico lieve e poi uno moderato. Il test è basato sulla analisi delle modalità di adeguamento elettrocardiografico ai diversi livelli di sforzo e nella fase di recupero.

Il segnale acquisito durante il tilt test è analizzato utilizzando metodi che quantificano la variabilità della frequenza cardiaca (HRV), che permette di valutare il bilanciamento tra l'attività del sistema vagale e del sistema simpatico. L'analisi HRV viene eseguita nel dominio del tempo, e nel dominio della frequenza.

Il segnale elettrocardiografico rilevato durante la successiva fase a carico crescente, viene analizzato valutando le modalità di adeguamento della frequenza cardiaca sia per i cambiamenti sia per le stabilizzazioni. Particolare attenzione viene data all'analisi della fase adattativa al diverso carico e alla fase di recupero dopo lo sforzo. Da queste analisi, mediate confronto tra diverse classi di pazienti, si ritiene di potere ottenere parametri quantitativi di efficienza funzionale.

Abstract

This thesis is focused on the validation of a sub-maximal test for the evaluation of subjects with limited physical performance, such as elderly subjects or patients with cardiovascular diseases.

The "Test of Performance" is an alternative to the complex standard procedure, suitable for subjects with normal or enhanced performance. In the simplest protocol we applied , only the electrocardiographic signal is recorded in basal condition and during a low load exercise test, with two subsequent phases. In the first phase a "tilt test" is executed to evaluate the autonomic nervous system intervention. In the second phase the patient performs a stress test on the ergometer with a light load and then a moderate one.

The ECG signal sampled during the tilt test is used to quantify the Heart Rate Variability (HRV), in time domain and frequency domain. The signal taken during the phase of stress is analyzed to evaluate the heart rate trend during TOP test execution, especially in moments of light to moderate workload changes, and recovery. From the analysis of the response adaptive phase of ECG to the load and of the recovery phase it is possible to quantify the individual physical performance.

This test can also be used in rehabilitation programs, where the subjects are involved in periodic workload changes, to monitor the results and to adapt the protocols.

Contents

Introduction

Physical efficiency corresponds to the individual ability to perform, in an effective and satisfactory way, certain motor tasks in the normal activities of daily life with a functional reserve that enables him to cope with emergency needs without undue labor and with the ability to recover and complete restoration. The use of the tests aims to investigate individual skills and then propose targeted interventions. It offers the possibility of evaluating the existing situation and then planning the training processes in the short, medium and long term.

The first chapter describes the anatomy and physiology of the main systems involved in the evaluation of physical performance in order to identify the quantative parameters that determine the correct functioning during the activity.

The second chapter describes Cardiopulmonary exercise testing (CPX) that is a form of exercise testing that measures ventilatory and gas exchange, heart rate, electrocardiogram, and blood pressure to provide detailed information on the cardiovascular, pulmonary, and muscular systems. This testing allows an accurate quantification of functional capacity/measure of exercise tolerance, diagnosis of cardiopulmonary disease, disease-progression monitoring or response to intervention, and the prescription of exercise and training. CPX directly measures inhaled and exhaled ventilator gases to determine the maximal oxygen uptake, which reflects the body's maximal use of oxygen and defines the limits of the cardiopulmonary system.

The third chapter describes the test of performance which is a sub-maximal test aimed at evaluating the physical performance of elderly, sick and with cardiovascular, respiratory and musculoskeletal limitations. The test of performance is based on the taking of an electrocardiographic (ECG) signal during the performance of an exercise test established by an experimental protocol. From the ECG signal it is possible to obtain the patient's heart rate as a quantitative parameter to be monitored to evaluate the

physical adaptation in the different working conditions prescribed by the experimental protocol.

The fourth chapter describes the instrumentation used, the experimental protocol, the subjects chosen for the execution of the test and the methods used for signal analysis. The experimental protocol is designed for subjects with limited performance, so the test to which the patient is subjected is sub-maximal, or the workloads are mild or moderate so as not to bring the subject to exhaustion. Signal analysis was performed by dividing the signal into two parts related to the tilt test and top test phases. Once the RR intervals have been detected in the ECG signal for the tilt test phase an analysis of the time and frequency domain is carried out.

In the fifth chapter, the results of the analysis were shown for each subject using figures and tables

In the sixth chapter the results obtained were discussed with appropriate comparisons between the cases.

Chapter 1

The main systems involved for the physical performance evaluation

During physical activity the body tends to regulate its physiological processes to maintain homeostasis, a necessary internal steady condition. The dynamic state of equilibrium foresees a controlled variability of the functions performed mainly by the cardiovascular, respiratory, musculoskeletal and autonomic nervous systems. Depending on the intensity of physical activity, biochemical and nervous stimuli are automatically activated, these stimuli modify the intensity of the physiological processes performed by the aforementioned systems.

Following a physical approach, we identify the appropriate physiological parameters that allow the evaluation of the individual physical performance. The chosen parameters operate in a limited range of variability depending on the wear state of apparatuses (elderly subjects) or the disease's degree or therapeutic intervention (subjects with cardiovascular or respiratory diseases).

In this chapter we will briefly describe the basic anatomy and physiology of the cardiovascular, respiratory, musculoskeletal and autonomic nervous systems, in order to understand and quantify the mechanisms that occur in the resting state or during a mild, moderate or intense physical activity.

1.1 Cardiovascular system

The cardiovascular system is an organ system that guarantees blood perfusion to the tissues, it permits blood to circulate and transport nutrients (such as amino acids and electrolytes), oxygen, carbon dioxide, hormones, and blood cells to and from the cells in the body to provide nourishment, stabilize temperature and pH, and maintain homeostasis. The circulation ensures the survival of the micro-organism and the metabolism of each individual cell of the body, provides the chemicals and maintains the physiological properties. The blood transports oxygen from the lungs to the cells and carbon dioxide in the opposite direction.

The cardiovascular system consists of the heart, the propeller motor, and blood vessels that branch out and progressively reduce in diameter; depending on thickness, blood vessels are divided in arteries, arterioles, capillaries, useful for the oxygen's transport to the tissues, and in venules and veins that carry blood in the opposite direction from the tissues to the heart.

The blood circulatory system is seen as having two components, a systemic circulation and a pulmonary circulation.

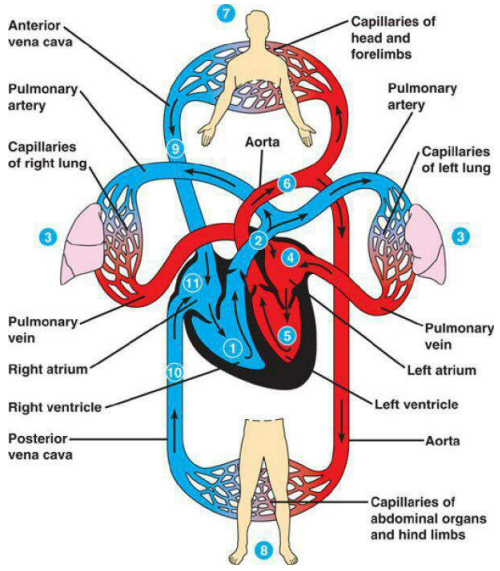

Figure 1.1: Blood's path through the cardiovascular system.

1.1.1 The heart

The heart is the propelling organ of the blood and constitutes the central element of the circulatory system, because it pumps the blood through the entire bloodstream. The pumping function is performed by the contractile activity of the heart muscle, the myocardium, whose fibers have peculiar characteristics of both the smooth muscle (located mainly in the walls of hollow organs such as stomach, bladder or blood vessels) and the skeletal muscle (which accounts for most of the muscles of the body, about 40% of body weight). It is a striated muscle (characteristic of skeletal muscle), the striations appear because each myofibril consists of numerous contractile and elastic proteins including myosin and actin. It also has a rapid contraction that ensures the right blood supply to all organs and tissues (characteristic of skeletal muscle).

The heart is divided into two cavities through a intraventricular septum: the left one pumps the arterial oxygenated blood to the various districts of the body, and the right one receives the venous and desaturated blood from the peripheral tissues and sends it to the lungs to be oxygenated. Each cavity includes an upper and a lower part: the atria and the ventricles. The atria have thin walls and receive blood from the veins, while the ventricles have thicker walls and are responsible for pumping blood in the arteries.

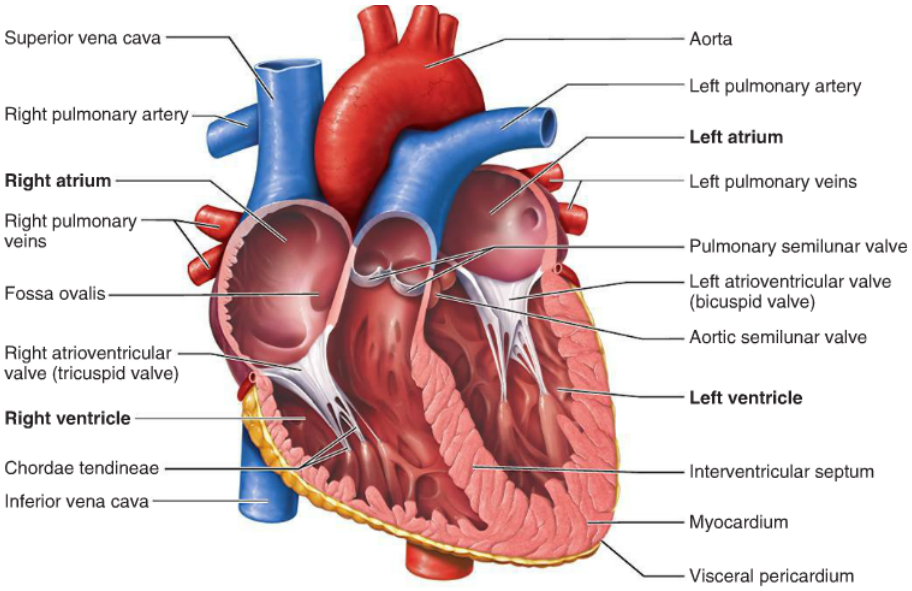

Figure 1.2: Heart's frontal section showing its anatomy.

Each atrium is divided by a valve from the corresponding ventricle, the deoxygenated blood from the veins is collected in the atria and then flows into the ventricles through the opening of the appropriate valves, then the ventricles direct the blood flow by pumping the blood towards the arteries.

There are four heart valves :

- tricuspid valve;
- bicuspid or mitral valve;
- aortic valve, structured in the form of swallows with three semi-moonary cusps, has the task of regulating the blood flow from the left ventricle to the aorta and therefore to the entire systemic circulation;
- pulmonary valve with three semi-moonary cusps regulates the blood's passage from the right ventricle to the left pulmonary artery.

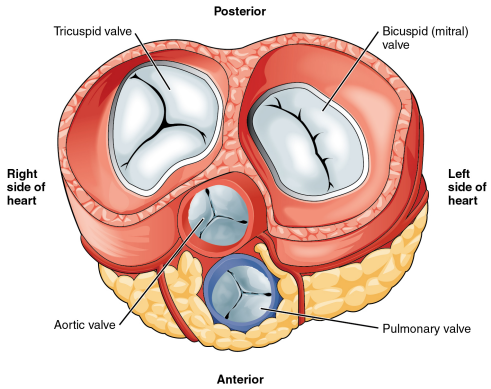

Figure 1.3: Heart's cross section seen from above showing the four heart valves.

All four cardiac valves consist of thin, flexible but durable tissue-embroidery valves, coated with endothelium and firmly attached to the fibrous valve rings. The cardiac valves' orientation ensures the unidirectionality of the blood flow through the heart; in addition, the opening and closing of the valves is entirely linked to intracardiac pressure variations. In fact, there is no type of nervous or muscular control over the valves' activity, which are simply driven by the very blood flow. The main task of heart valves is to prevent, guaranteeing effective and passive resistance, the blood reflux towards

the atria during the systolic phase or "ventricular contraction" (tricuspid and bicuspid valves) or towards the ventricles during the diastolic phase or "ventricular release" (semi-moon valves).

Laplace law: cardiac compensation and scompensation

From a mechanical standpoint, the heart works as a pump, i.e. an elastic wall cavity, and the internal pressure is linked to the wall's tension, which is therefore subject to deformation. Considering the local curvature of the wall, it is possible to identify two radii of orthogonal curvatures and establish the relationship between the wall elastic tension and the pressure gradient, so one obtains the Law of Laplace:

$$P_i - P_e = \tau \left(\frac{1}{r_1} + \frac{1}{r_2} \right) \tag{1.1}$$

When we talk about heart cavities, the intrathoracic external pressure can be considered to be zero, therefore we can consider the pressure variation is approximately equal to the internal pressure ($P_i - P_e \approx P_i = P$). Assuming the cavity to be approximately spherical ($r_1 \approx r_2$) and indicating with P the pressure between the interior and the outside of the room, one obtain:

$$P = \frac{2\tau}{r} \tag{1.2}$$

The elastic tension τ is due to the wall deformation and generally increases with the deformation (stress-strain curve); so if we consider the variation of local elastic tension in relation to the wall thickness, one obtain the local stress (wall stress) expresses in N/m^2:

$$\sigma = \frac{\tau}{d} \tag{1.3}$$

Replacing the value of elastic tension in Laplace's law (1.1) :

$$\sigma = \frac{Pr}{2d} \tag{1.4}$$

The equation (1.4) is important to understand the heart compensation and decompensation mechanisms in response to an effort: indeed in normal conditions, the wall stress adjusts to the elastic tension values to mantain a constant stress throughout the cavity. In addition, myocardial oxygen consumption and mechanical efficiency depend on the

effort, so compensation mechanisms come into play to keep the effort within acceptable limits, otherwise if the effort exceeds the breaking load, the wall laceration occurs.

We consider the case where you have an increase in vascular resistance R, remembering the Hagen−Poiseuille's law $P_1 - P_2 = Q \cdot R$, as the flow rate Q remains unchanged, there will be an increase in the pressure generated by the ventricle. The effort will tend to increase and consequently there will be an increase in the wall thickness to compensate the increased effort and allow the stress normalization.

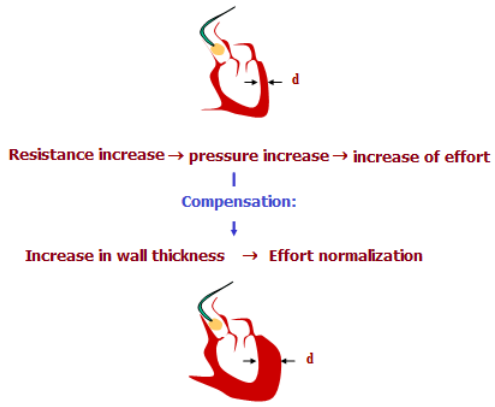

Figure 1.4: Cardiac compensation mechanism aimed at normalizing the effort.

We apply the Laplace Law to a heart of increased size (r major). If the heart size increases as a result of sporting activity (non-pathological condition), the increasing effort would be compensated by a thickening of the ventricular wall (d major). In heart failure, the increasing cavity size is not matched by an increasing wall thickness. This tends to decrease. Therefore the effort increases progressively and the heart muscle comes to operate in unfavorable conditions (increased oxygen consumption).

Figure 1.5: Heart of athlete and heart failure.

Electrical conductivity of the heart

Unlike the other muscles of the body whose activity depends on the brain and spinal cord ('voluntary' musculature that is controllable by our will), the heart is self-sufficient because it has its own stimulator that generates the electrical impulse that causes the heart contraction (beat). The stimulus that generates the contraction has an elettrical nature and originates involuntarily from the control centers located in the central nervous system in the brain and spinal cord. It is transported from the central nervous system to the heart through the efferent parasympathetic and sympathetic pathways.

The electrical conduction system of the heart consists of four basic units which regulate the cardiac tissue depolarization and repolarization: the sinoatrial node (SA node), the atrio-ventricular node (AV node), the His bundle and the Purkinje fibers.

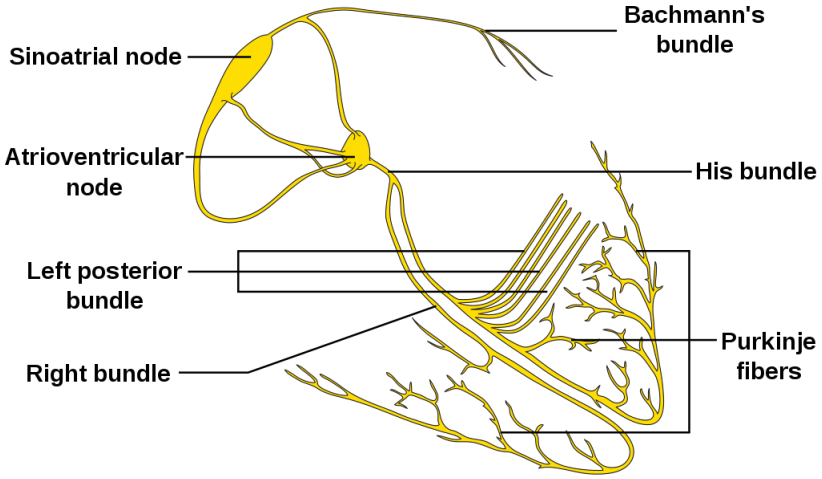

Figure 1.6: Overview of electrical conduction system of the heart.

The sino-atrial node is located near the junction between the superior vena cava and the right atrium, it consists of abundant connective tissue surrounding small myocardial cells, called pacemaker cells. These cells are characterized by a typical self-generated transmembrane action potential and have the very important function of regulating both the heart rate (about 1 Hertz, i.e. 60 bpm, for an adult man), and the force of atrial contraction.

The self-generated depolarization wave propagates below, until it reaches the atrio-ventricular node, from which the nodal fibers gradually join with His bundle. Ventricular conduction starts from the His bundle, consisting of two main branches that, in turn, are

divided into a complex network of conduction fibers distributed on the subendocardial surface of both ventricles (Purkinje fibers). These fibers (in which you have the highest conduction speed), extend to the papillary muscles and the ventricular walls.

It should be noted that the epicardial wall of the right ventricle is activated before that of the left ventricle, because the thickness of the first is much smaller than that of the second and, consequently, the stimulus propagates more quickly.

Depolaritation and ripolaritation of cellular membrane

In order to understand the electrical signal propagation on cardiac tissue, we consider the simplest case of the potential generated by a polarized cell surface.

The potential at the external point will depend on the distributed charge density ϕ, the surface area S, on its orientation $Scos\theta$, on the distance from the point R , i.e. on the solid angle Ω of the observation surface from the point considered $\Omega = \frac{Scos\theta}{R^2}$.

Since the cell surface is closed, the effects of two opposite charge layers (dipoles) are added in each external point far enough from the cell and the effects cancel out in terms of electric potential; therefore the resting cell membrane does not determine any detectable potential in the surrounding space.

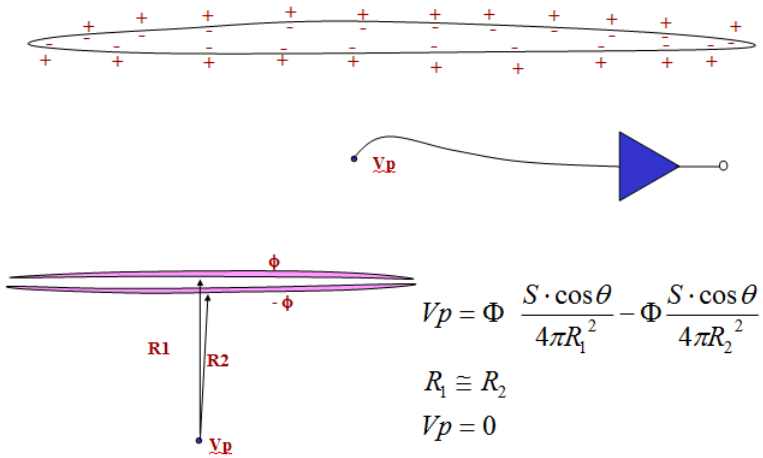

Figure 1.7: Potential V_P of cell surface closed.

We consider a long polarized muscle fiber and observe the polarization front that proceeds along the surface. Through a process of mathematical modelling the intermediate situation can be considered as the sum of two particular conditions: a completely

polarized closed surface plus a bipolarized layer inversely polarized to the surface, which moves with the depolarization front (Figura 1.8).

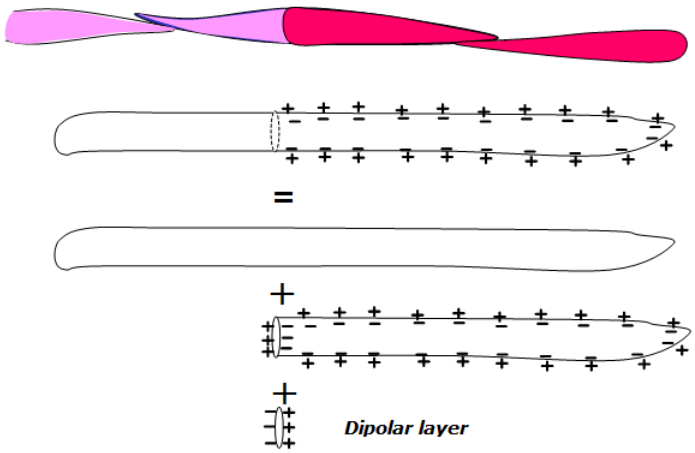

Figure 1.8: Mathematical modelling of the polarization front along the polarized muscle fiber.

The bipolar layer can be represented by a dipole that moves with the depolarization front and generates in the point concerned an instantaneous potential depending on the charge, distance and angle. When the excitation activates the depolarization, the angle is very close to zero, the cosine close to the unit, but the distance r is great and the potential has a very low value. As the face approaches, the distance decreases and the potential tends to increase, but also the angle increases leading to a progressive decrease of $cos\theta$ and a corresponding decrease of the potential that is cancelled when the depolarization face is on the observation point's normal. The further progression of the face is associated with a negative θ's cosine and the reversal of the potential. In practice detecting the instantaneous electric potential in a point close to a surface that is depolarizing, one observes an increase of the positive potential in the phase of approach of the depolarizing face followed by a decrease and the potential's reversal in the phase of estrangement (Figure 1.9).

If each cell in the depolarization phase is modelled as a dipole, the entire fibrous muscle tissue can be considered formed by these cells that constitute the resulting dipole, which changes continuously in the process and generates a variable electric field (Figure 1.10).

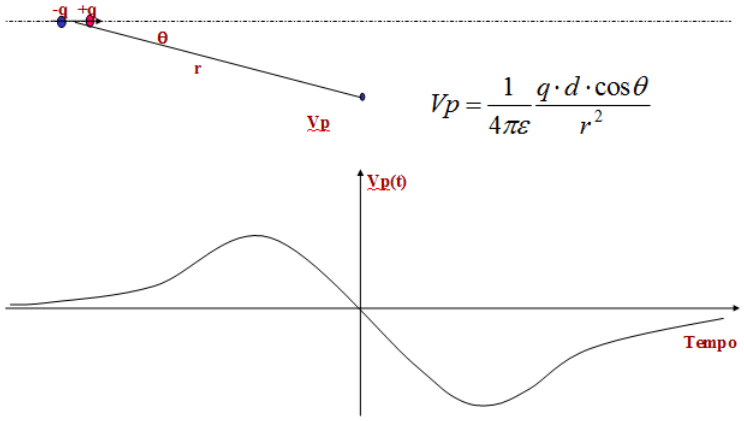

Figure 1.9: Potential V_P of a single dipole.

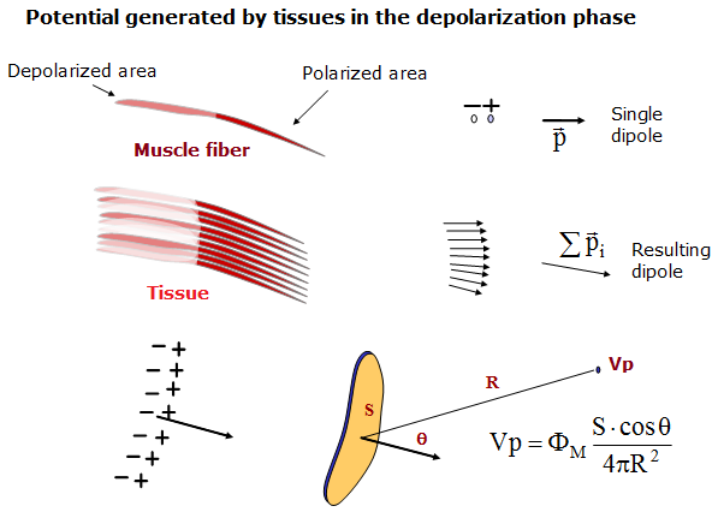

Figure 1.10: Polaritation front generated by muscle fibre tissue.

All human cells have a resting membrane potential originated by an ionic concentration gradient between the inside and the outside of the cell structure; this gradient induces the diffusion of some ions through the cell membrane (selectively permeable), until a steady condition is reached, in which a d.d.p. of about $-90mV$ is detected between the inside and the outside of the cell (negative towards the inside). This condition, defined as "polarization" is mainly associated with the ionic potassium diffusion. If the cell is stimulated (mechanically or electrically), the membrane becomes permeable to other ions (particularly sodium), which diffuse in the opposite direction and cancel out

the previous polarization: in this step, called "depolarization", the cell manifests its contractile function or the electrical stimulus's transmission.

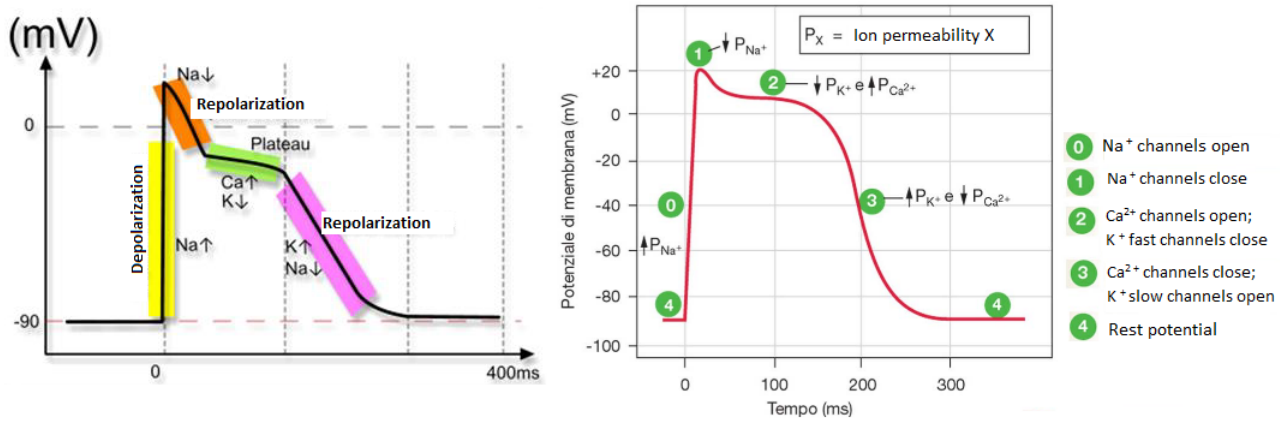

Figure 1.11: Action potential of the heart muscle.

The speed at which pacemaker cells depolarize determines the rate at which the heart contracts, i.e. the heart rate. The time interval between the action potentials can be modified by altering the membrane permeability to different ions: the increasing permeability to sodium and calcium accelerates the depolarization phase and thus the heart rate, while the decreasing permeability to calcium slows it down.

Electrocardiogram ECG

Electrocardiography (ECG) is the recording process of the heart's electrical activity over a time period using electrodes placed over the skin. These electrodes detect the tiny electrical changes on the skin that arise from the heart muscle's electrophysiologic pattern of depolarizing and repolarizing during each heartbeat. The potential differences detected by the electrodes are small, about 1 mV, so the signal is appropriately amplified before recording. ECG is very commonly performed to detect any cardiac problems.

The heart's polarization and repolarization front's displacement is described by means of 3 electrodes placed on the frontal plane and 6 electrodes placed on the transversal plane near the organ.

The 3 frontal electrodes are placed respectively on the right shoulder, left shoulder and groin and allow the sampling of signals I, II, III, aVR, aVL, aVF.

The 6 electrodes that describe the motion on the transversal plane, at the heart's level, are positioned equidistant from the chest, starting from an area very close to the sternum up to the line that corresponds to the vertical of the patient's left armpit. The 6 electrodes allow the collection of electrical potentials V1, V2, V3, V4, V5, V6.

An electrode is also placed on the right leg to connect the patient with a reference to the ground. Then a total of 10 electrodes are used, through which it is possible to detect 12 potential values that vary over time periodically showing the phases of the cardiac cycle.

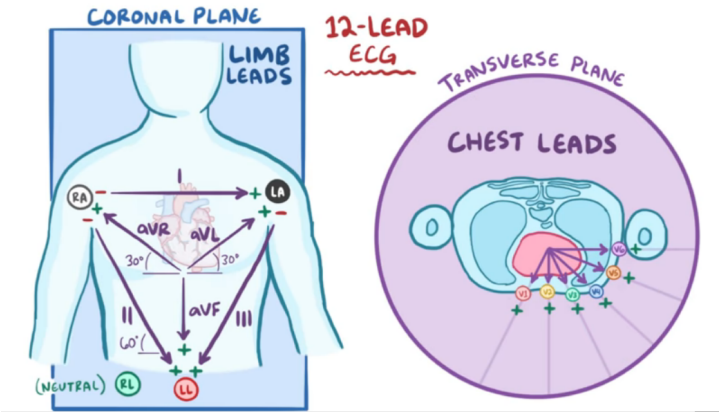

(a)

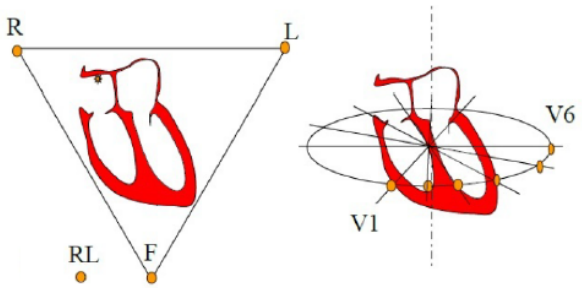

(b)

Figure 1.12: Placement of 10 electrodes for recording the 12 leads electrocardiographic signal.

The 12 measured potential values are called electrocardiogram derivations and are divided into:

- 3 differential leads (indicated by roman numerals I, II, III) so called because the

signal is picked up between two electrodes;

$$I = V_L - V_R \qquad II = V_F - V_R \qquad III = V_F - V_L$$

- 9 unipolar leads (aVR, aVL, aVF, V1, V2, V3, V4, V5, V6) that pick up the signal from a single electrode, compared to a reference assumed as zero. The 3 verses on the frontal plane $\vec{R}$, $\vec{L}$, $\vec{F}$ indicate the observation directions of the right arm, left arm and groin, and the local potential V_R, V_L, V_F will be represented by the scalar product of these verses for the vector $\vec{P}$. On the transverse plane the observation directions are indicated by verses $\vec{V_1}$, $\vec{V_2}$, $\vec{V_3}$, $\vec{V_4}$, $\vec{V_5}$, $\vec{V_6}$.

$$V_R = \vec{R} \cdot \vec{P} \qquad V_L = \vec{L} \cdot \vec{P} \qquad V_F = \vec{F} \cdot \vec{P}$$

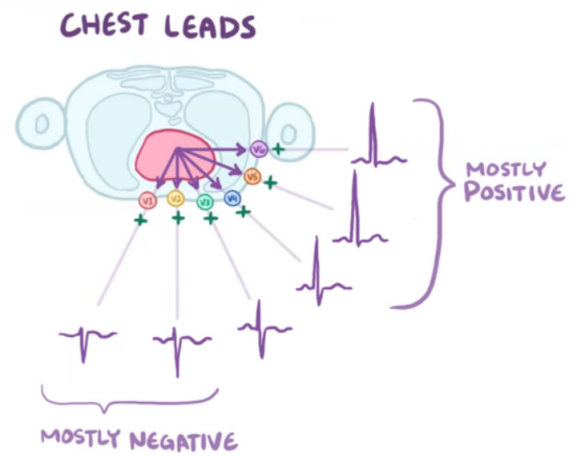

$$V_1 = \vec{V_1} \cdot \vec{P}$$
$$V_2 = \vec{V_2} \cdot \vec{P}$$
$$V_3 = \vec{V_3} \cdot \vec{P}$$
$$V_4 = \vec{V_4} \cdot \vec{P}$$
$$V_5 = \vec{V_5} \cdot \vec{P}$$
$$V_6 = \vec{V_6} \cdot \vec{P}$$

Figure 1.13: The six potential value picked up on the transverse plane.

The vector $\vec{P}$ is reconstructed starting from at least two differential derivations on the frontal plane: the observation directions I, II, III are parallel to the equilateral triangle's sides having as vertices the right and left shoulder and the groin, the three derivations will have an amplitude proportional to the vector projection on the 3 sides of the triangle, so by measuring at a certain moment at least 2 of the 3 derivations, it is possible to reconstruct the amplitude and the direction of the global vector $\vec{P}$ (see Figure 1.14).

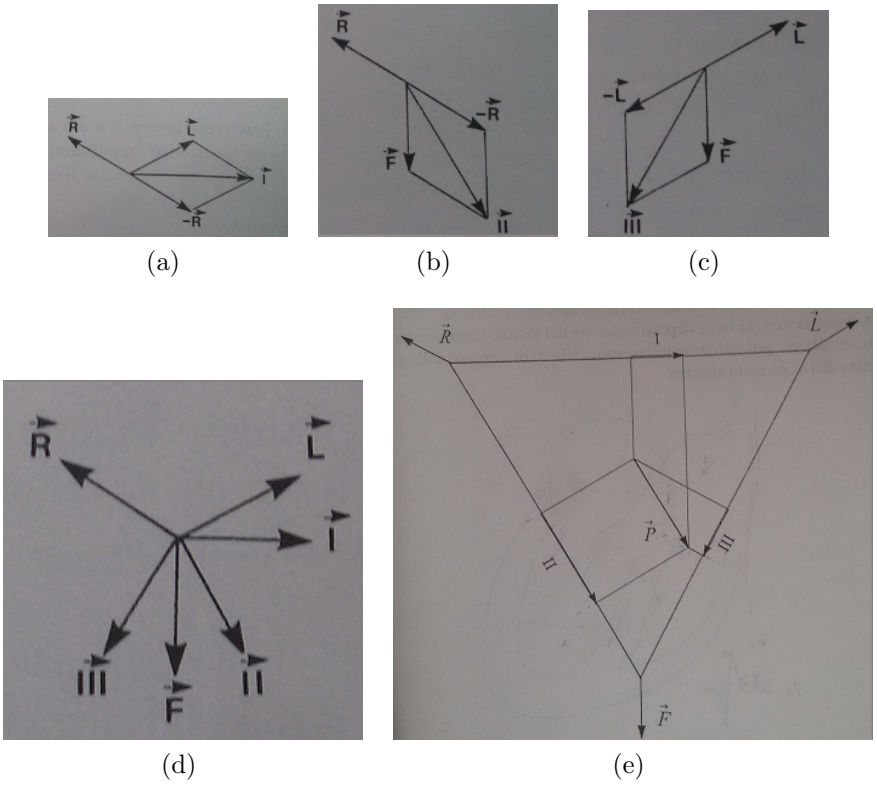

Figure 1.14: Observation directions for ECG leads on the frontal plane (a) ,(b) ,(c) ,(d) and reconstruction of the $\vec{P}$ vector from at least two differential derivations on the frontal plane (e) .

Initially all cardiac tissue is polarized and the pontential is null at the detection point, subsequently the self-generated potential from the pacemaker cells causes the depolarization membrane that propagates from the atria up to the ventricles, while the repolarization front proceeds in the opposite direction, from the ventricles to the atria. The detected periodic signal consists of three waves:

- P WAVE : atrial depolarization phase, activated by pacemaker cells (potential self-generated) placed in the right atrium, which can last about 100 ms. In this phase the number of muscle fibers involved is low due to the limited thickness of the walls: the resulting dipole will have limited amplitude, it will be directed towards the relief point and the detected potential will be positive and small amplitude ($\approx 0.1mV$).

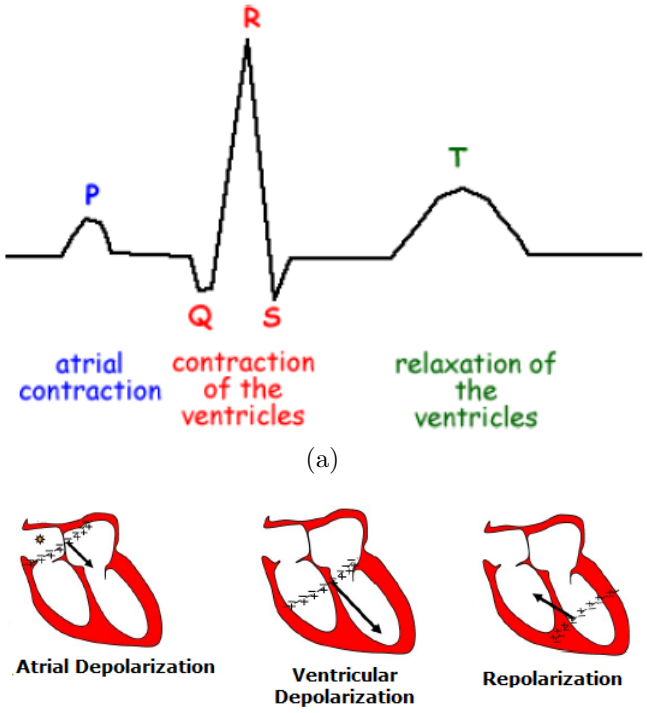

Figure 1.15: Phases of the ECG electrocardiogram.

- QRS COMPLEX: ventricular depolarization phase. When the depolarization front reaches the base of the atria, muscle tissue is lacking and the front reaches the ventricles through the fibres of the AV node and the His Beam. This electrical signal conduction phase to the ventricles lasts from 100 to 200ms, the signal detected will be close to zero at the external point, because there is no muscle fiber. As soon as the depolarization affects the ventricular tissue, the number of elementary dipoles increases enormously, the resulting dipole takes on a considerable amplitude and moves rapidly to the relief point and then move away: the result is a wide potential initially positive, then negative. The complex is formed by three waves that represent the depolarization wave's progression in the ventricles. The Q wave, due to the interventricular septum's depolarization, is negative and small; instead the R wave is characterized by a large positive peak; the S wave, caused by depolarization of the ventricular basal and posterior region, is negative.

- WAVE T: ventricular repolarization phase. Once the atrial and ventricular depolarization that causes the contraction of all the cardiac muscle fibers has been completed, the cellular membranes return impermeable to sodium and the repolarization process is activated. While the atria repolarize at the same time as the ventricular depolarization, the ventricular tissues, that have depolarized last, are repolarized first, generating a repolarization front in the opposite direction and with different speeds compared to the original depolarization front. The result is an inverted repolarization dipole that moves in the opposite direction, generating a potential of the same sign as that detected in the depolarization phase. This phase lasts about 400 ms,so the cycle repeats again starting from the atria.

Moreover, the electrocardiographic signal's study is carried out through the schematization in segments and intervals: the segments are line traits between two waves, while the intervals are a combination of waves and segments; among these we remember the interval PR (which corresponds to the atrio-ventricular conduction time), the interval QT (which corresponds to the time of depolarization-ventricular repolarization) and the interval ST (which is the period in which the ventricular cells are all depolarized and therefore no electrical movements are detectable) (see Figure 1.16). It is very important that the ST interval does not deviate by more than 1 mm above or below the isoelectric line, otherwise you would be in the presence of a myocardial infarction or ischemia. The PR interval indicates the atrioventricular node's delay; indeed the electrical activity of the AV node and His beam is not visible on the surface electrocardiogram and is included in the PR interval; during the interval TP the ventricles relax and fill up.

A "normal" complex is characterized by a wave P, a narrow QRS, a T wave, constant duration. The succession of normal complexes is called "sinus rhythm", while "non-normal complex" is defined as "arrhythmia". Because cardiac electrical activity induces cardiac mechanical activity, abnormal electrical patterns are typically accompanied by abnormal contractile activity. Therefore, the analysis of ECG traces can provide useful information on the heart's state. The main deviations from the norm that can be determined by ultrasound are: (1) abnormalities of heart rate; (2) abnormalities of heart rhythm; (3) myocardial diseases: impaired blood perfusion, electrolyte imbalance or cell death (heart attack).

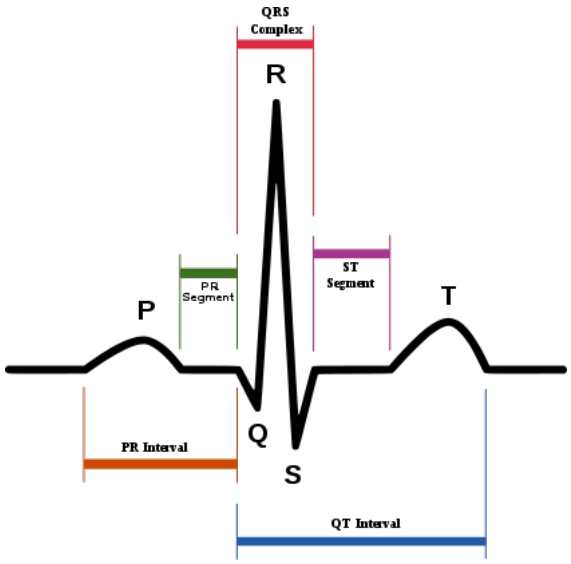

Figure 1.16: Electrocardiographic signal schematization in segments and intervals.

1.1.2 Pulmonary circulation

Pulmonary circulation is the transport system that shunts de-oxygenated blood from the heart to the lungs to be re-saturated with oxygen before being dispersed into systemic circulation. In the first phase, all the oxygen-poor blood flows to the right atrium through the lower and upper hollow veins; from here, when the tricuspid valve opens, the blood passes into the right ventricle, which pushes the blood into the left pulmonary artery, starting the small circulation. During this first phase, the blood is free from carbon dioxide and oxygenates through exchange phenomena; once this process is over, the blood reaches the left atrium through the pulmonary veins.

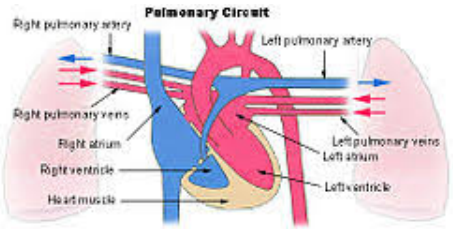

Figure 1.17: Pulmonary circulation.

1.1.3 Systemic circulation

The systemic circulation provides the functional blood supply to all body tissue. It carries oxygen and nutrients to the cells and picks up carbon dioxide and waste products. Systemic circulation carries oxygenated blood from the left ventricle, through the arteries, to the capillaries in the tissues of the body. From the tissue capillaries, the deoxygenated blood returns through a system of veins to the right atrium of the heart.

The coronary arteries are the only vessels that branch from the ascending aorta. The brachiocephalic, left common carotid, and left subclavian arteries branch from the aortic arch. Blood supply for the brain is provided by the internal carotid and vertebral arteries. The subclavian arteries provide the blood supply for the upper extremity. The celiac, superior mesenteric, suprarenal, renal, gonadal, and inferior mesenteric arteries branch from the abdominal aorta to supply the abdominal viscera. Lumbar arteries provide blood for the muscles and spinal cord. Branches of the external iliac artery provide the blood supply for the lower extremity. The internal iliac artery supplies the pelvic viscera.

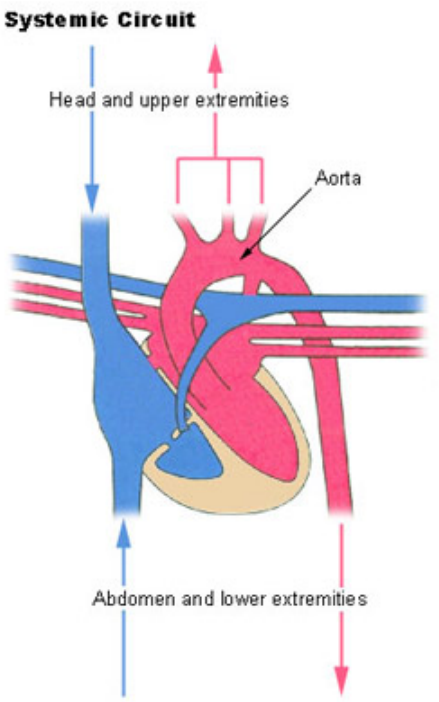

Figure 1.18: Systemic circulation.

1.1.4 Blood vessels

The blood vessels are part of the circulatory system and function to transport blood throughout the body. The most important types, arteries and veins, carry blood away from or towards the heart, respectively.

All blood vessels have the same basic structure: the inner lining is the endothelium and is surrounded by subendothelial connective tissue; around this there is a layer of vascular smooth muscle, which modifies the elastic behaviour of the structure when it is active. Finally, there is a further layer of connective tissue known as the tunica adventitia, which contains nerves that supply the muscular layer, as well as nutrient capillaries in the larger blood vessels.

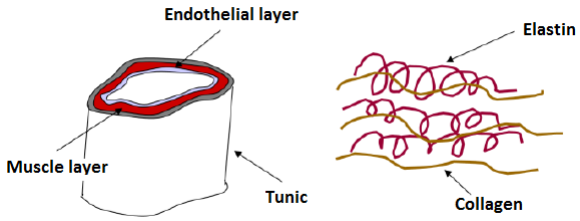

Figure 1.19: Internal and external structure of a blood vessel

The particular behaviour of the stress strain curve of the vascular wall is due to the coexistence in the vessel's outer layer (tunic) of filaments of collagen and elastin. Elastin is widely deformable and intervenes due to small intensity stresses. For greater stresses, when the elastin is completely elongated, the collagen filaments take over, which are very rigid and cause the curve to pry . The vascular wall has a typical elastomeric behavior, i.e. it increases its Young's modulus Y (slope of a stress-strain curve) with deformation, since the modulus Y is an index of wall stiffness and determines the slope of a stress-strain curve ($\sigma = Y\epsilon$). Initially the vascular wall is very compliant, then it becomes gradually more rigid (Figura 1.20 a). The curve changes with the subject's age, because the continuous stress of the elastin filaments determines the breakage and the progressive intervention of those of collagen (Figura 1.20 b).

The change of the aorta's elasticity, due to age or pathology (arteriosclerosis, hypertension), causes evident changes in the pulse of arterial pressure and the load of the heart pump. The pressure pulse in the aorta is determined by the introduction of a blood volume from the ventricle (cardiac output). In the Figure 1.21 it is represented

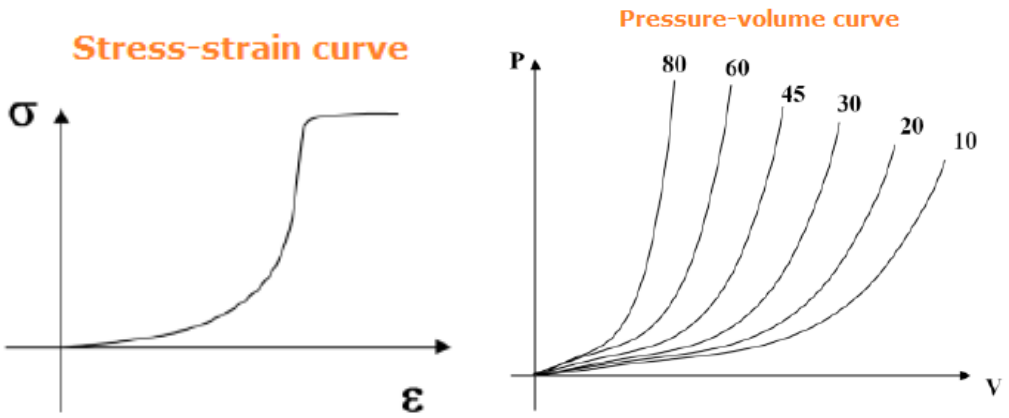

(a) (b)

Figure 1.20: Stress-strain curve of the vascular wall (a) and pressure-volume curve that pry with increased age of subject (b).

as the same stroke volume (x axis), with two aortas of different elastic curve, determine different amplitude of the arterial pulses : the one with the most rigid artery is wider.

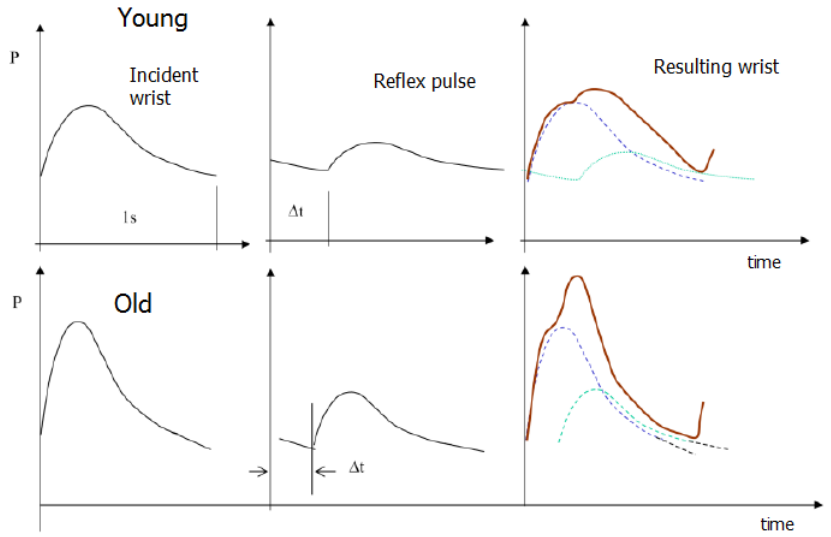

Figure 1.21: Pressure pulse in the aorta of young and elderly subject.

The greater or lesser arterial wall stiffness also has another effect, in fact a more rigid wall determines a greater speed of the wrist towards the periphery and a wider reflection by the peripheral bifurcations (iliac bifurcation). The reflex pulse, wider than

normal, returns to the ventricle in advance and overlaps with what the ventricle is still generating. In a young man, the reflex pulse, of just amplitude, arrives in the ascending aorta at the end of the ventricular ejection and helps to maintain high pressure in the diastolic phase, when coronary perfusion occurs. In a senior, the pulse returns to the ascending aorta when the ventricle is still pumping and forcing it to additional work. Moreover, in the diastolic phase, the pressure decreases very quickly penalizing coronary perfusion.

1.2 Respiratory system

The respiratory system (also ventilatory system) is an apparatus consisting of specific organs and structures used for gas exchange. Indeed, respiratory function includes all those physiological activities aimed at:

- ensuring an adequate supply of oxygen (O_2) to the tissues;
- ensure the disposal of carbon dioxide (CO_2) produced by the metabolism of cells.

The anatomy of a respiratory system is the respiratory tract which is divided into an upper and a lower respiratory tract. The upper tract includes the nose, nasal cavities, sinuses, pharynx and the part of the larynx above the vocal folds. The lower tract includes the lower part of the larynx, the trachea, bronchi, bronchioles and the alveoli.

The alveoli are microscopic dead-end air-filled sacs, where gas exchange occurs: a very thin membrane (called the blood-air barrier) separates the blood in the alveolar capillaries (in the alveoli's walls) from the alveolar air in the sacs.

Air is brought to the alveoli in small doses (called the tidal volume), by breathing in (inhalation) and out (exhalation) through the respiratory airways, a set of relatively narrow and moderately long tubes which start at the nose or mouth and end in the alveoli of the lungs in the chest. Air moves in and out through the same set of tubes, in which the flow is in one direction during inhalation, and in the opposite direction during exhalation.

During each inhalation, at rest, approximately 500 ml of fresh air flows in through the nose. It is warmed and moistened as it flows through the nose and pharynx. By the time it reaches the trachea the inhaled air's temperature is $37°C$ and it is saturated

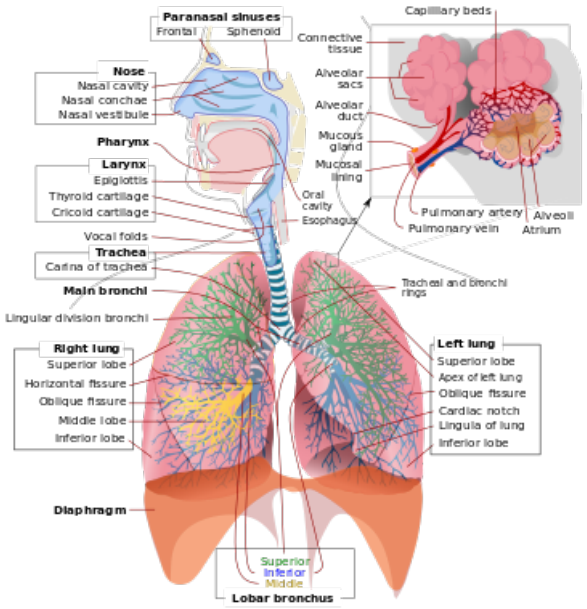

Figure 1.22: Respiratory system.

with water vapor. On arrival in the alveoli it is diluted and thoroughly mixed with the approximately $2,5$–$3,0L$ of air that remained in the alveoli after the last exhalation. This relatively large volume of air that is semi-permanently present in the alveoli throughout the breathing cycle is known as the functional residual capacity (FRC).

At the beginning of inhalation the airways are filled with unchanged alveolar air, left over from the last exhalation. This is the dead space volume, which is usually about $150ml$. It is the first air to re-enter the alveoli during inhalation. Only after the dead space air has returned to the alveoli does the remainder of the tidal volume ($500ml - 150ml = 350ml$) enter the alveoli. The entry of such a small volume of fresh air with each inhalation, ensures that the composition of the FRC hardly changes during the breathing cycle. A highly diagrammatic illustration of the process of gas exchange in the lungs, emphasizing the differences between the gas compositions of the ambient air, the alveolar air (light blue) with which the alveolar capillary blood equilibrates, and the blood gas tensions in the pulmonary arterial (blue blood entering the lung on the left) and venous blood (red blood leaving the lung on the right).

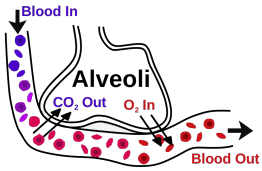

Figure 1.23: Gas exchange through the alveoli's walls.

1.3 Skeletal muscle system

The musculoskeletal system is the set of bone, joint and muscular structures that support and defend the body and allow its movements. It is the most voluminous apparatus of the human body, in fact it represents about 80 % of the total weight. Muscle is not a rigid body and it is not rigorous to treat it as such, but it has two important functions. The first is to protect the bone, the second is to "load" it in order to compensate the bending stress. Mechanically, the muscle modifies its behavior according to the activation state and can be very rigid or very compliant. the muscles are used to generate the forces and movements resting on levers and fulcri. When the muscles contract, they urge the bones in compression and counteract the rupture. In the area not covered by the muscle and therefore more exposed to breaking the bones are thicker and have a greater radius, also to better withstand the torsion.

1.4 Autonomic nervous system

The autonomous nervous system (ANS), also known as the vegetative or visceral nervous system, is that set of cells and fibers that innervate the internal organs and glands, controlling the so-called vegetative functions, i.e. those functions that are generally outside the voluntary control, which is why it is also called "involuntary autonomous system". The SNA is part of the peripheral nervous system. The autonomic nervous system consists of anatomically and functionally distinct portions, but synergistic among them:

- the sympathetic (or orthosympathetic) nervous system,
- the parasympathetic nervous system,

- the enteric (or metasympathetic) nervous system, nerve fibres that innervate the viscera.

It has the regulating function of the body's homeostasis and is a neuromotor system that cannot be influenced by the will that operates with precisely autonomous mechanisms, relating to peripheral reflexes under central control.

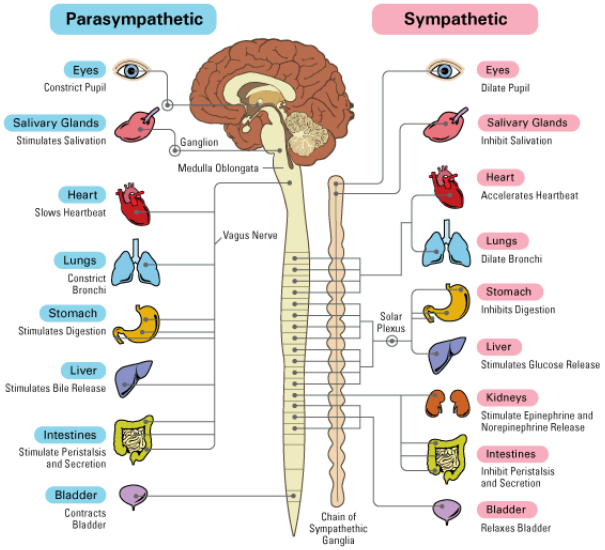

Figure 1.24: The main stimuli of the sympathetic and parasympathetic nervous system.

1.4.1 Heart Rate Variability (HRV) and vegetative stimulation

Resting heart rate (HR) varies widely in different individuals. During various physiological stresses, particularly exercise, it can increase up to three-fold. Heart rate is dependent on the level of physical fitness; highly trained endurance athletes, for example, have resting levels of HR wich, in some people, might indicate the need of pacemaker implantation. The maximum level of HR achieved during physical exeercise is dependent on the subject's age , with 20-year olds typical able to achieve rates of 200 beats per minute (bpm) compared with maximum levels of 20 to 30 bpm less in older people. Heart rate is normally determined by the rate of depolaritation of the cardiac pacemaker. Pacemaker tissue is found in the sinuatrial node, the AV node , and the Purkinje tissue. Howeever, because the rate of depolaritation of the sinuatrial node is faster than that of

other pacemaker tissue and the depolarizing impulse spreads via the heart's conducting mechanism to other pacemakers before they spontaneously depolarize, it is the sinuatrial node wich normally determines the rate. If, for any reason, the normal pacemaker fails to generate an impulse, pacemaker tissue elsewhere usually takes over. The intrinsic HR, in absence of any neurohumoral influence, is about 100 to 120 bpm. In the intact, unblocked individual, the HR at any time represents the net effect of the parasympathetic (vagus) nerves wich slow it and the sympathetic nerves wich accelerate it. In resting conditions, tonically active with the vagal effects dominant.

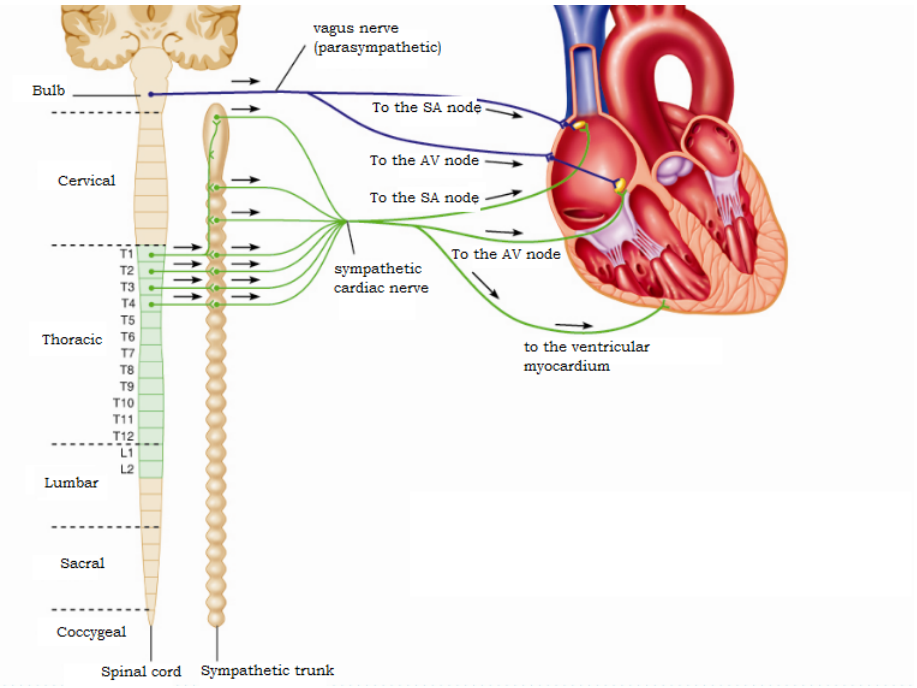

Figure 1.25: The main vegetative stimuli at the heart come from the parasympathetic vagus nerve and the sympathetic heart nerve. Myocardial nerve fibres are carried to the SA and AV nodes and to the ventricular myocardium, parasympathetic fibres are carried mainly to the nodes.

The motor neurons forming the vagus nerves originate in the dorsal motor nucleus and in the nucleus ambiguus. They run down the neck alongside the carotid arteries into the thorax. Sympathetic nerves originate in the intermediolateral column of the spinal cord in the upper thoracic region. White rami synapse in the sympathetic gangli and the grey rami run with the preganglionic vagal fibers over the mediastinum, forming a plexus of cardiac nerves and parasympathetic ganglia, wich supply the various parts of

the heart, as well as many extracardiac structures. There is abudant evidence that both the vagal ans sympathetic nerves carry not only efferent nerves including those to the heart, but also many afferent fibers wich subserve various reflex functions. [9]

1.4.2 Vagal interactions

The vagal nerve innervate the sinuatrial node, the AV conducting pathways, and the atrial muscle. Parasympathetic stimulation hyperpolarizes the membrane potential of the autoritmic cell and slows down the depolarization speed, resulting in a reduction in heart rate. The speed of spontaneous depolarization decreases and there will be a hyperpolarization of the membrane, with consequent removal of the membrane potential from the threshold level for the onset of the action potential.

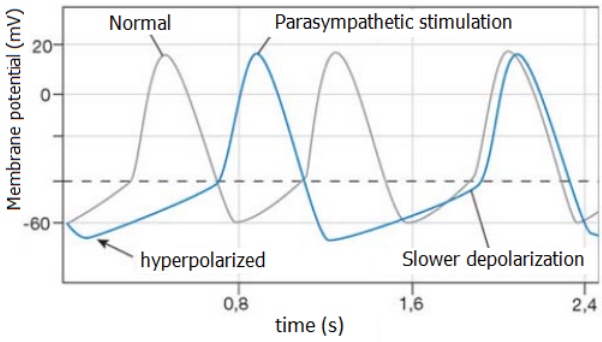

Figure 1.26: Membrane potential of the autoritmic cell subjected to parasympathetic stimulation.

1.4.3 Sympathetic interactions

Sympathetic postganglionic fibers innervate the entire heart, including the sinuatrial node, the AV conducting pathways, and the atrial and ventricular myocardium. Increased activity in the sympathetic nerves results in increases in both HR and the force of contraction. In addition, the rate of conduction through the heart of the cardiac impulse is increased and duration of contraction shortened. An increase in sympathetic activity forms the principal method of increasing HR above the intrinsic level generated by the sinuatrial node (about 110 bpm) to the maximal levels achieved, that may be

about 200 bpm in a young person. The sympathetic stimulation depolarizes the autoritmic cells and increases the speed of depolarization, resulting in an increase in heart rate.

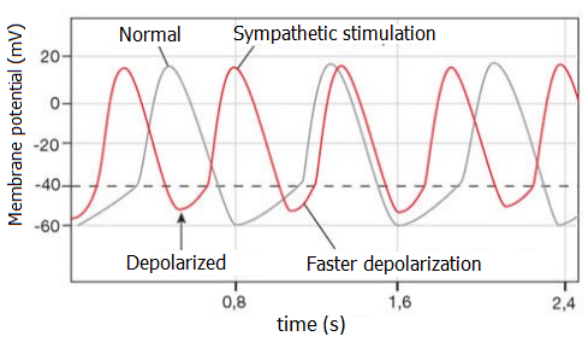

Figure 1.27: Membrane potential of the autoritmic cell subjected to sympathetic stimulation.

There will be an increase in the speed of spontaneous depolarization and a decrease in the level of repolarization so that the threshold for the onset of the action potential is reached more rapidly.

Chapter 2

Cardiopulmonary exercise testing

Cardiopulmonary exercise testing (CPET) provides assessment of the integrative exercise responses involving the pulmonary, cardiovascular, haematopoietic, neuropsychological, and skeletal muscle systems, which are not adequately reflected through the measurement of individual organ system function. This non−invasive, dynamic physiological overview permits the evaluation of both submaximal and peak exercise responses, providing the doctor with relevant information for clinical decision making. [4]

The cardiopulmonary test is a complement to the normal exercise test, the so-called exercise electrocardiogram; indeed while the latter can be used to check the patient's electrocardiographic behaviour under stress, the cardiopulmonary test can also assess the metabolic aspect. The cardiopulmonary test has been in use for some years, but it has become a routine test recently. Today, a good hospital with a cardiology department cannot ignore having it.

Gas exchange measurements during exercise have been demonstrated to enhance the decision-making process in several clinical settings, and cardiopulmonary exercise testing indications entail functional capacity assessment, prognostic stratification, training prescription, treatment efficacy evaluation, diagnosis of causes of unexplained reduced exercise tolerance, and exercise pathophysiology evaluation in an extremely wide spectrum of clinical pictures. In this way, you can have an overall picture of the physiological state of the patient with the measured parameters.

2.1 Procedure and methodology

Cardiopulmonary exercise test can be performed using incremental or constant work rate protocols, according to work rate progressive increase or constancy during the test, respectively. Incremental tests are aimed at maximally stressing the O_2 transport and use system and are routinely used in the clinical setting, whereas constant work rate tests are usually performed at submaximal effort intensities and mainly used for research purposes. Among incremental protocols, the ramplike ones are preferred to conventional incremental tests whenever possible (Figure 2.1). Ramp protocols are characterized by a gradual increase of work rate, evenly distributed within each minute of the exercise phase. For example, on a cycle ergometer, a 10 W/min ramp protocol (which is frequently used in the clinical setting) increases the work rate by 1 W every 6 seconds.

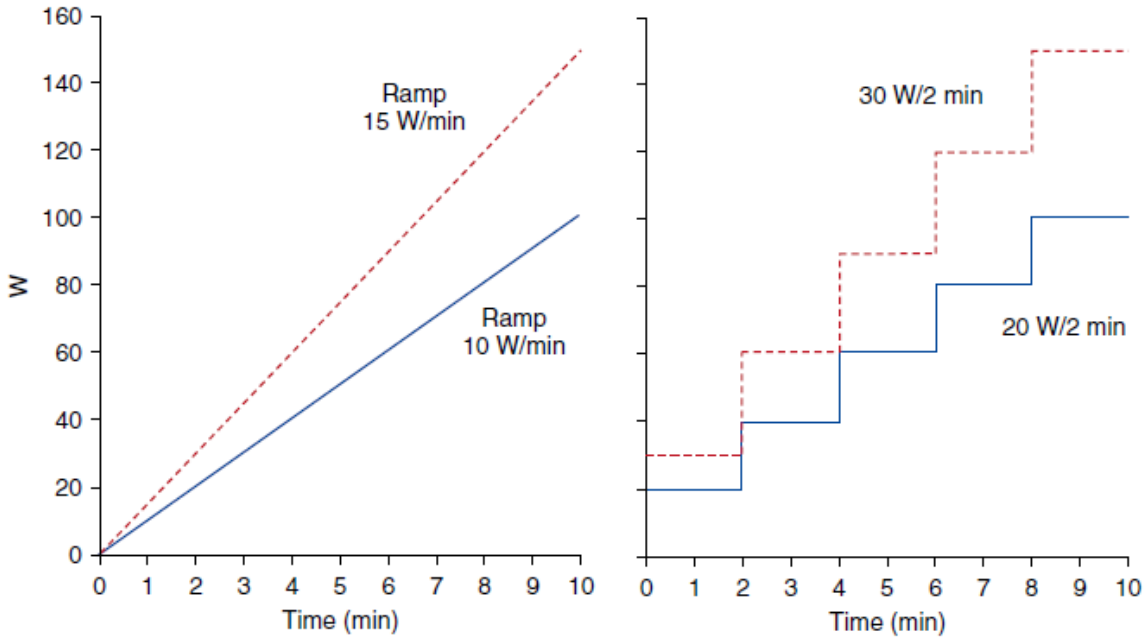

Figure 2.1: Ramp incremental (left panel) abd 2-minute incremental (right panel) protocols for cycle ergometry [3].

Several ramp grades are commonly used for patients, with 5 W/min, 7 W/min, 10 W/min, and 15 W/min the most popular. The choice of ramp protocol steepness should be tailored to the subject's exercise tolerance, aiming at a test duration ranging between 8 and 12 minutes.

The advantage of ramp protocols is twofold:

1. the work rate increase is devoid of brisk step increases typical of step protocols (e.g. 25 W every 3 minutes);

2. the trend of parameters changes over time is not affected by protocol steps, making physiological responses linear and more readable for the operators.

Cardiopulmonary exercise test can be performed on different kinds of ergometers (i.e., cycle ergometer or treadmill), the pros and cons of which are summarized in Table 2.1. Of note, ramp incremental protocols are much easier to implement when a cycle ergometer is used. Cardiopulmonary exercise testing systems contain flow meters and gas analyzers that allow for breath-by-breath measurement of ventilation and the $\dot{V}_{O_2}$ and $\dot{V}_{CO_2}$. Ventilation parameters and respiratory gases can be collected using a face mask or a mouthpiece, with the choice between the two more linked to a given laboratory's habits than to specific advantages. A face mask allows patient swallowing, which a mouthpiece does not. On the other hand, some patients may feel uncomfortable using a face mask because of lack of air sense. In any case, every laboratory should give patients a choice between a face mask and a mouthpiece, according to their preferences. As flow meters and gas analyzers are prone to drift, all systems should be calibrated immediately before each test, and the test should not be performed if proper calibration is not confirmed. Response times of the analyzers and transport delay between sampling point and analyzers must be systematically checked as well. In addition, because ambient conditions affect the concentration of oxygen in the inspired air, temperature, barometric pressure, and humidity should also be taken into account. Calibration procedures are automatically performed by all commercial cardiopulmonary exercise testing software. [3]

2.2 CPET equipment

The type of equipment that is used to perform the cardiopulmonary stress test allows you to measure ventilation, oxygen consumption and carbon dioxide production during exercise. The equipment consists of an ergometer, an electrocardiograph with 12 standard leads, a pneumotachograph (used to measure lung ventilation) combined with a

Variable	Cycle	Treadmill
Peak oxygen content (PV_{O_2})	Lower	Higher
Work rate measurement	Yes	No
Blood gas collection	Easier	More difficult
Noise and artefacts	Less	More
Safety	Safer	Less safe
Weight bearing in obese subjects	Less	More
Degree of leg muscle training	Less	More
More appropriate for	Patients	Active normal subjects

Table 2.1: Variables of exercise equipment that show the pros and cons of the cyclergometer or treadmill. Adapted from ATS/ACCP Statement on Cardiopulmonary Exercise Testing. [4]

gas analyzer (oxygen and carbon dioxide), all managed by a software. The patient is connected to this equipment by means of a mouthpiece with a breath detector. This instrument transmits, analyzing breath by breath, the trend of oxygen consumption and the production of carbon dioxide. The equipment allows you to build a graph consisting of curves that illustrate the person's metabolism.

2.3 CPET protocols

Many different protocols are used for functional testing. The purpose of the test and the functional capabilities of the patient determine the choice of protocol. In evaluating patients with chronic heart failure (CHF), both bicycle and treadmill protocols have been used. The rate of workload progression is somewhat arbitrary, although it has been suggested that optimal exercise duration for functional assessment on the bicycle is between 8 and 17 minutes.

Bicycle work is quantified in Watts (W) or in kilopod/metres/min (kpm/min) and we remember that 1 W $\approx$ 6 kpm/min. The initial workload with patients with CHF is usually 20–25W and increased by 15–25W every 2 minutes until maximal exertion is reached. Alternatively, the workload can be computer controlled for electronically braked bicycle ergometers, and a ramp protocol (eg, 10 W/min) is often used. The modified Naughton protocol is recommended for treadmill exercise testing in patients with heart failure. This protocol is designed to increase the workload by approximately 1 MET (3,5

ml O_2 kg/min) for each 2−minute stage.

Treadmill exercise testing has several advantages over cycle ergometry and for most people, treadmill walking is a more familiar activity than cycling. It involves a larger muscle mass and more work against gravity. Consequently, PV_{O_2} is, on average, 5–10% higher on the treadmill than on a cycle ergometer. Holding onto the treadmill handrails usually decreases the metabolic cost of treadmill walking and should be discouraged if possible. A cycle ergometer is less prone to induce noise artefacts with better quantification of the metabolic cost. Generally it is less expensive and requires less space than the treadmill. [4]

2.4 Healthy subjects and patients with limitated performance

The cardiopulmonary test is mainly used in cases of cardiopathic and/or bronchopneumatic patients. In particular, it is aimed at three types of patients:

1. ischaemic heart patients,
2. the cardiopathic and/or chronic bronchial patients,
3. patients with more or less severe chronic heart failure.

The first type concerns patients for whom it is necessary to verify the coronary reserve. For example, patients operated on coronary by-pass, for whom the evaluation of the test serves to check for the presence of residual stress ischaemia.

The second type concerns patient who is carrying out a rehabilitation programme.

The third type concerns cardiac patient who is continuously subjected to an evaluation test to consider to be submitted for cardiac transplantation. For people suffering from respiratory diseases, for example those suffering from emphysema or chronic bronchitis, this test can provide important information on the severity of the disease, its evolution and assess the possible therapeutic-rehabilitative approach.

In addition, the cardiopulmonary test can be used to assess the physiological conditions of healthy people, but also of athletes or sportsmen with a history of cardiovascular diseases of very slight entity for which a return to sporting activity can be assumed, trying

to give the subject the opportunity to recover their skills to 100%. It is also particularly recommended for middle-aged people who want to understand what is their limit and what are the margins for improvement from the cardio-respiratory standpoint, especially for those who practice aerobic sports, i.e. cycling, cross-country skiing, marathon, etc.

2.5 Physiology of exercise: the Fick equation

Peak exercise capacity is defined as "the maximum ability of the cardiovascular system to deliver oxygen to exercising skeletal muscle and of the exercising muscle to extract oxygen from the blood".

Consequently, exercise tolerance is determined by three factors:

1. pulmonary gas exchange;
2. cardiovascular performance, including the peripheral vascular tree;
3. and skeletal muscle metabolism. [3]

The Fick equation expresses the dependence of oxygen consumption on parameters such as heart rate, systolic volume; it permits to appreciate the utility of functional exercise testing.

At rest, the Fick equation states that oxygen uptake (V_{O_2}) equals cardiac output times the arterial minus mixed venous oxygen content:

$$V_{O_2} = (SV \cdot HR) \cdot (C_aO_2 - C_vO_2) \tag{2.1}$$

where SV is the stroke volume, HR is the heart rate, C_aO_2 is the arterial oxygen content, and C_vO_2 is the mixed venous oxygen content. Oxygen uptake is often normalised for body weight and expressed in units of O_2 ml/kg/min. One metabolic equivalent (MET) is the resting oxygen uptake in a sitting position and equals 3,5 ml/kg/min.

At maximal exercise, the Fick equation is expressed as follows:

$$V_{O_2}^{max} = (SV^{max} \cdot HR^{max}) \cdot (C_aO_2^{max} - C_vO_2^{max}) \tag{2.2}$$

Maximum oxygen uptake ($V_{O_2}^{max}$) obtained at peak exercise reflects the maximal ability of a person to take in, transport and use oxygen. It defines that person's functional aerobic

capacity, therefore it is a global indicator of the performance and relative importance of the patient's lungs, pulmonary circulation, heart, peripheral circulation (large and small vessels), muscles and motivation during exercise (Figura 2.2) . This allows us to assess the entire cardiopulmonary system from top (mouth) to bottom (muscle) in one simple measure (i.e., the rate of oxygen flowing through the various subsystems that allow exercise to proceed). [3]

$V_{O_2}^{max}$ has become the preferred laboratory measure of cardiorespiratory fitness and is the most important measurement during functional exercise testing.

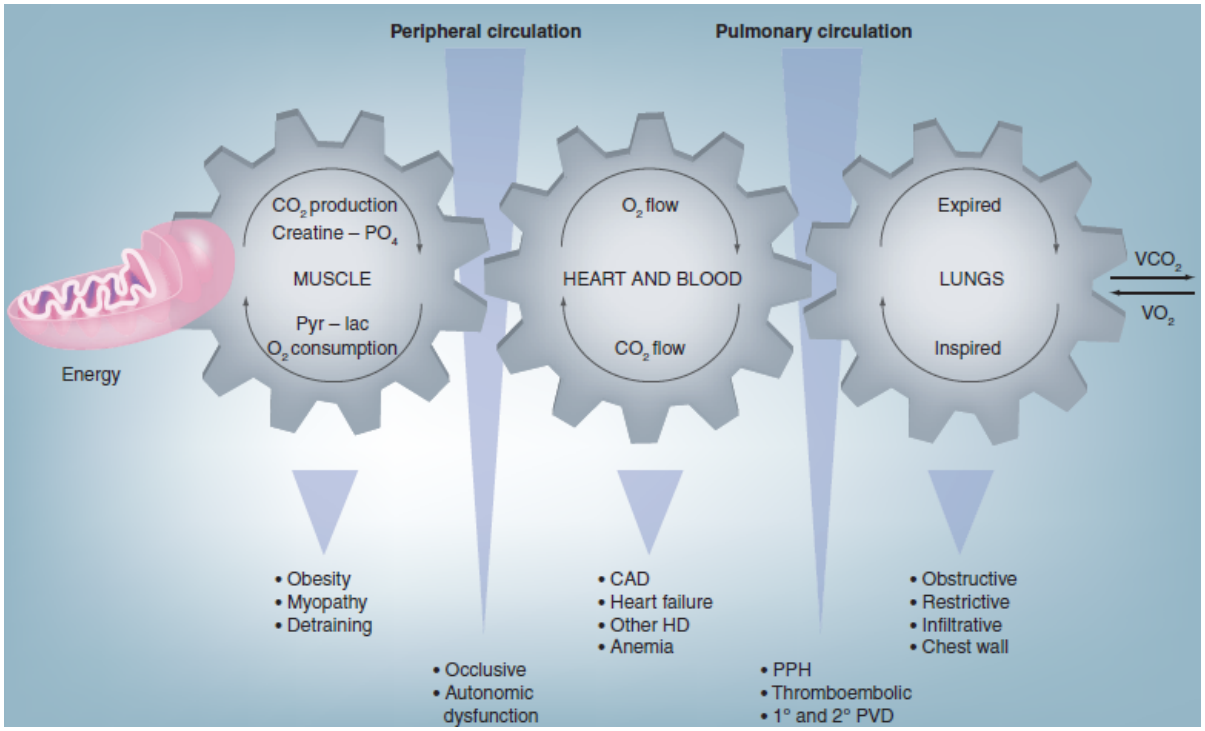

Figure 2.2: Respiratory gas flow from mouth to mitochondria. CAD: Coronary artery disease; HD: Heart disease; PPH: Primary pulmonary hypertension; PVD: Peripheral vascular disease. [7]

In healthy people, a V_{O_2} plateau occurs at near maximal exercise. This plateau in V_{O_2} has traditionally been used as the best evidence of $V_{O_2}^{max}$. It represents the maximal achievable level of oxidative metabolism involving large muscle groups. However, in clinical testing, a clear plateau may not be achieved before symptom limitation of exercise. Consequently, peak V_{O_2} (PV_{O_2}) is often used as an estimate of $V_{O_2}^{max}$. [4]

2.6 Performance parameters

Cardiopulmonary exercise testing joins ventilation and volume of oxygen uptake (V_{O_2}) and exhaled carbon dioxide (V_{CO_2}) to routine physiological and performance parameters measured during incremental exercise testing, such as heart rate, blood pressure, work rate, and exercise duration. Therefore, this methodology markedly increases the amount of information obtainable from conventional exercise testing, furnishing an all-around vision of the systems involved in both O_2 transport from air to mitochondria and its use during exercise.

2.6.1 Peak oxygen uptake

Oxygen uptake (V_{O_2}) is determined by cellular O_2 demand up to some level that equates to maximal rate of O_2 transport, which then is determined by that maximal rate of transport. As V_{O_2} increases with increasing external work, one or more of the determinants of V_{O_2} approach limitations (eg, stroke volume, heart rate, or tissue extraction), and V_{O_2} versus work rate may begin to plateau. This plateau in V_{O_2} has traditionally been used as the best evidence of $V_{O_2}^{max}$. V_{O_2} is measured in liters or milliliters of oxygen per minute(l/min o ml/min) or in milliliters per kilogram of body weight per minute ($ml/kg/min$) and is defined by the Fick principle (2.1), in which cardiac output $CO = SV \cdot HR$ is multiplied with the arteriovenous oxygen content difference $C_{(a-v)}O_2$. Peak oxygen uptake (PV_{O_2}) is a parameter describing the maximal amount of energy obtainable by aerobic metabolism per unit of time (aerobic power) at peak incremental exercise and is defined as the highest volume of V_{O_2}, averaged over a 20 to 30 second period, achieved at presumed maximal effort during an incremental cardiopulmonary exercise test. PV_{O_2} is known to describe patient exercise tolerance far more reliably than performance descriptors obtainable by conventional exercise testing, such as exercise duration or peak work rate. Peak V_{O_2} declines on average by 10% per decade after the age of 30, due to decreasing maximal heart rate, stroke volume, blood flow to skeletal muscle, and skeletal muscle aerobic potential with decreasing age. In addition, Peak V_{O_2} is 10% to 20% greater in men than in women of comparable age , because of higher hemoglobin concentration and greater muscle mass and stroke volume in men. All pathophysiological states impairing oxygen transport from air to mitochondria and its use during exercise will determine some degree of reduction of $V_{O_2}^{max}$ with respect to predicted values ac-

cording to age and sex. This is commonly observed not only in several different organ and system diseases, such as chronic heart failure, chronic obstructive pulmonary disease, amyotrophic lateral sclerosis , mitochondrial myopathies ,and so forth but also in bed-rest deconditioning. Of note, $C(a–v)O_2$ increases linearly with work rate progression during incremental exercise, and its value is relatively fixed at peak effort in both normal subjects and patients. Accordingly, peak CO is indirectly determinable according to the Fick principle using estimated peak $C(a–v)O_2$ and measured Peak V_{O_2}.

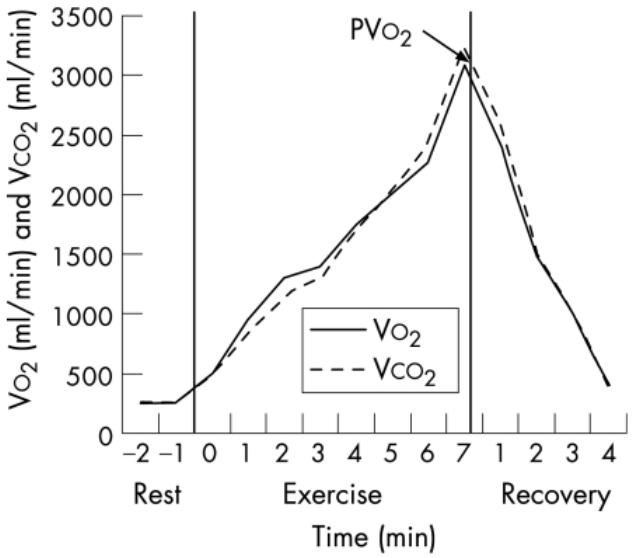

Figure 2.3: VO2 and VCO2 in function of time measued during cardiopulmonary exercise testing in a healtly 49-year-old man using the Bruce protocol [4].

2.6.2 Ventilatory Thresholds

During incremental exercise, an energy requirement is reached above which anaerobic metabolism is activated, with blood lactate concentration increasing above baseline level at a progressively steeper rate. Almost all hydrogen ions generated in the cell from lactic acid dissociation are buffered by bicarbonate, yielding an excess carbon dioxide amount that makes the V_{CO_2} versus V_{O_2} relationship become steeper. By measuring at the mouth gas exchange modifications induced by these metabolic changes, the so-called first ventilatory threshold can be identified by analyzing the slope of V_{CO_2}/V_{O_2} relationship (plotted on equal scales) during ramp incremental exercise. Accordingly,

the first ventilatory threshold is the transition point of the slope from less than 1 to greater than 1 (Figure 2.5a), occurring in the vast majority of subjects and patients between 40% and 60% of PV_{O_2}.

With increasing exercise intensity above the first ventilatory threshold, a point in time is reached when intracellular bicarbonates are no longer able to adequately counteract exercise-induced metabolic acidosis. Hyperventilation thus develops through a ventilation increase in excess of V_{CO_2}, which is termed the second ventilatory threshold or "respiratory compensation point" (Figure 2.5b) and is usually attained at around 70% to 80% of PV_{O_2}.

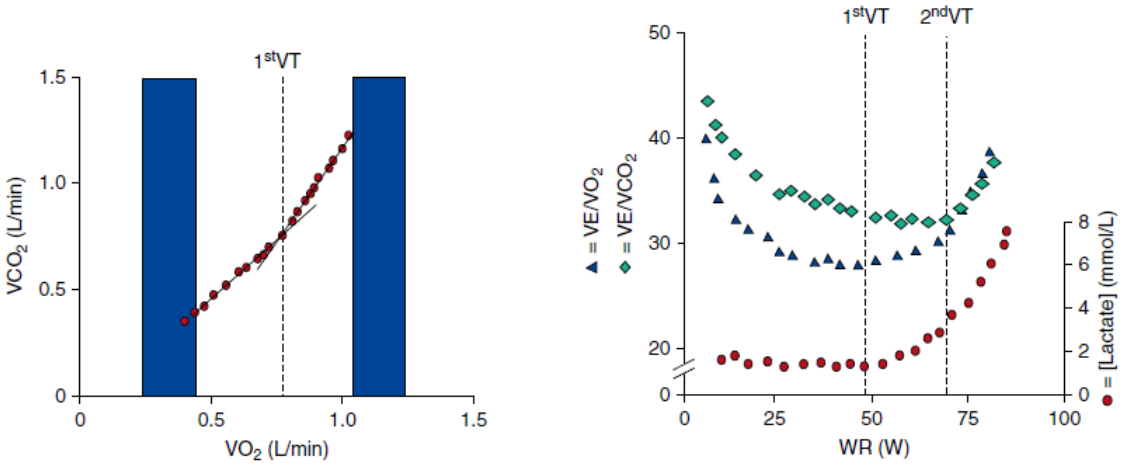

(a) (b)

Figure 2.4: Volume of exhaled carbon dioxide (VCO_2) as a function of volume of oxygen uptake (VO_2) during incremental exercise, the initial and final phases of exercise (blue rectangles) are usually excluded so represent possible hyperventilation (Left panel (a)). Ventilatory equivalents for oxygen and carbon dioxide as a function of work rate (WR) during ramp incremental exercise. The nadir of the ventilatory equivalent for oxygen (VE/VO_2) identifies the first ventilatory threshold $1^{st}VT$. The nadir of ventilatory equivalent for carbon dioxide (VE/VCO_2) identifies the second ventilatory threshold $2^{nd}VT$ (Right panel (b)).

The first and second ventilatory threshold are important parameters for aerobic training intensity prescription over a wide spectrum of exercise capacities, ranging from top-level athletes to patients with severely reduced exercise performance. As a multitude of different (and somewhat confusing) terms are found in the literature describing the

two thresholds, the term "ventilatory" thresholds is preferred. This is because those two transitions are detected using incremental exercise-induced changes in ventilation related parameters and not in direct descriptors of metabolic homeostasis alteration (e.g., lactic acid). Finally, ventilatory thresholds are not always clearly identifiable in patients with severely reduced exercise tolerance, and inability to identify the first ventilatory threshold plays an important negative prognostic role in patients with advanced chronic heart failure.

In summary, there are two methods of identifying separately the ventilatory anaerobic threshold (VAT) :

1. the ventilatory equivalent method (Figure 2.5a): the VAT is the V_{O_2} at which the ventilatory equivalent for O_2 (VE/V_{O_2} ratio) and end−tidal oxygen tension (PET_{O_2}) begin to increase systematically without an immediate increase in the ventilatory equivalent for CO_2 (VE/V_{CO_2}) and end−tidal CO_2 tension (PET_{CO_2}). [3]

2. the V-slope method (Figure 2.5b): the VAT is defined as the V_{O_2} at which the rate of increase in V_{CO_2} relative to V_{O_2} increases in the absence of hyperventilation. The VAT determined by this method is a more reproducible estimate. [3]

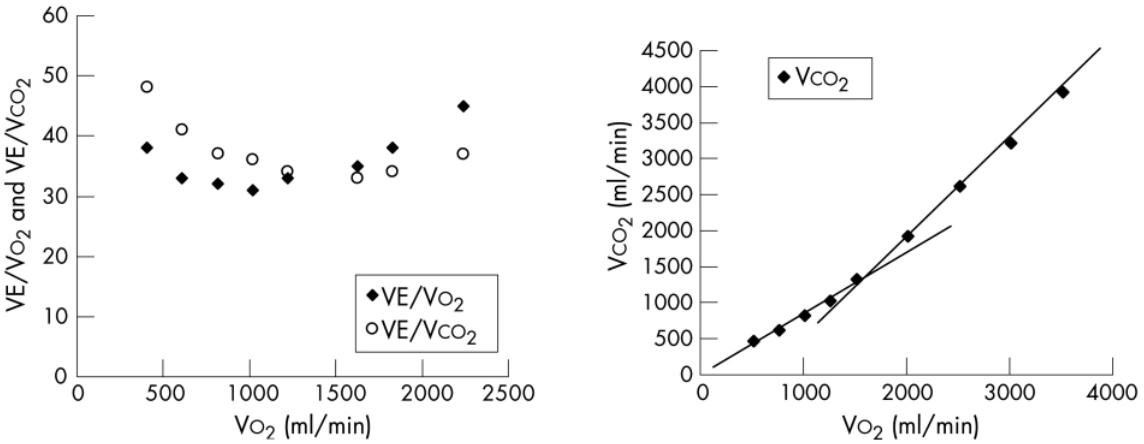

(a) (b)

Figure 2.5: Determination of the VAT by the ventilatory equivalents method, the VAT is $VO_{2=1400ml}$(a). Determination of the VAT by the V-slope method, the VAT is $VO_2 = 1,5$l/min or 49 % of PV_{O_2}(b).

2.6.3 Respiratory Exchange Ratio

The respiratory exchange ratio is the ratio between V_{CO_2} and V_{O_2}. As discussed above, with increasing exercise intensity, lactic acid buffering generates an excess V_{CO_2}, which increases the respiratory exchange ratio numerator at a faster rate than the denominator. Therefore, a respiratory exchange ratio higher than $1,00$ implies significant anaerobic metabolism activation above the first ventilatory threshold and is further increased by hyperventilation occurring past the second ventilatory threshold. This physiological response to exercise is consistent across healthy subject and patient populations, which makes peak respiratory exchange ratio an objective descriptor of maximal effort attainment and subject motivation (i.e., of a crucial issue to guarantee reliable and clinically meaningful V_{O_2} peak values). Of note, even though a peak respiratory exchange ratio of higher than 1.10 is generally considered to describe a significant exercise-induced whole-body stress, it must not be considered an indication for test interruption. On the other hand, achievement of a peak respiratory exchange ratio lower than 1.00 in the absence of ECG or hemodynamic abnormalities generally reflects submaximal cardiovascular effort. It must be borne in mind, however, that patients with severely impaired exercise tolerance can attain skeletal muscle strength exhaustion even earlier than central hemodynamic and ventilatory factors become limiting, interrupting exercise at peak respiratory exchange ratio values even lower than 1.00. Another possibility for lack of an adequate respiratory exchange ratio increase during incremental exercise is severe chronic obstructive lung disease, wherein lung hyperinflation can hinder hyperventilation past the first ventilatory threshold.

2.6.4 Oxygen Pulse

Oxygen pulse is the V_{O_2}/heart rate ratio and reflects the amount of oxygen consumed per heartbeat (i.e., stroke volume SV multiplied by $C_{(a-v)}O_2$). During incremental exercise, the relative contribution of stroke volume to CO is dominant during the initial and intermediate phases of exercise. Thus, oxygen pulse expressed as a function of work rate has a typical hyperbolic profile, with a rapid increase during the initial stages of exercise and a slow approach to an asymptotic value at the end of exercise. A flattening or downward displacement of oxygen pulse kinetics during incremental exercise likely reflects peripheral vascular perfusion or extraction or central cardiogenic performance

limitations. Among the latter, the development of exercise-induced myocardial ischemia can be present when a flattening or even decrease of both the oxygen pulse versus work rate (Figure 3) and V_{O_2} versus work rate relationships occur at the same time. However, it is important to understand that these abnormal responses are nonspecific and can also be seen in other conditions that might impair CO on response during exercise.

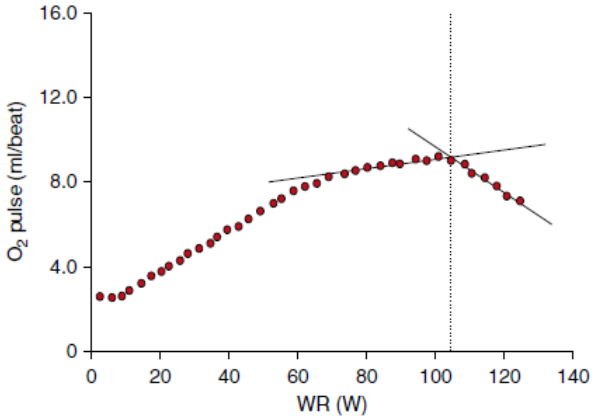

Figure 2.6: Oxygen pulse as a function of work rate (WR) during ramp incremental exercise in a patient with coronary artery disease. The red dotted line shows the transition from a typical hyperbolic profile to a decrease in oxygen pulse. [3]

2.6.5 Ventilation VE and Slope of the VE/VCO2 Relationship

From a physiological standpoint, ventilation is equal to

$$V_E = 863 \cdot \frac{V_{CO_2}}{Pa_{CO_2}\left(1 - \frac{V_D}{V_T}\right)} \tag{2.3}$$

where V_{CO_2} is the volume of exhaled carbon dioxide, Pa_{CO_2} is the partial pressure of arterial carbon dioxide, and VD and VT are pulmonary dead space and tidal volume, respectively. When plotting ventilation as a function of V_{CO_2} during incremental exercise, the slope of such a relationship (V_E/V_CO2 slope) describes the patient's ventilatory efficiency (i.e., the amount of air that must be ventilated to exhale 1 L of carbon dioxide) (Figure 2.7). The physiological meaning of V_E/V_{CO2} slope is described by rearranging

the above equation as follows:

$$V_E/V_{CO_2} = \frac{863}{Pa_{CO_2}\left(1 - \frac{V_D}{V_T}\right)} \tag{2.4}$$

.

Accordingly, V_E/V_{CO_2} slope will increase when PaCO2 is reduced by hyperventilation and when VD/VT (i.e., wasted ventilation) is high. Another proposed cause of increased V_E/V_{CO_2} slope is effort-induced muscle ergoreflex overactivation. Normal values of V_E/V_{CO_2} slope show a progressive increase with increasing age.

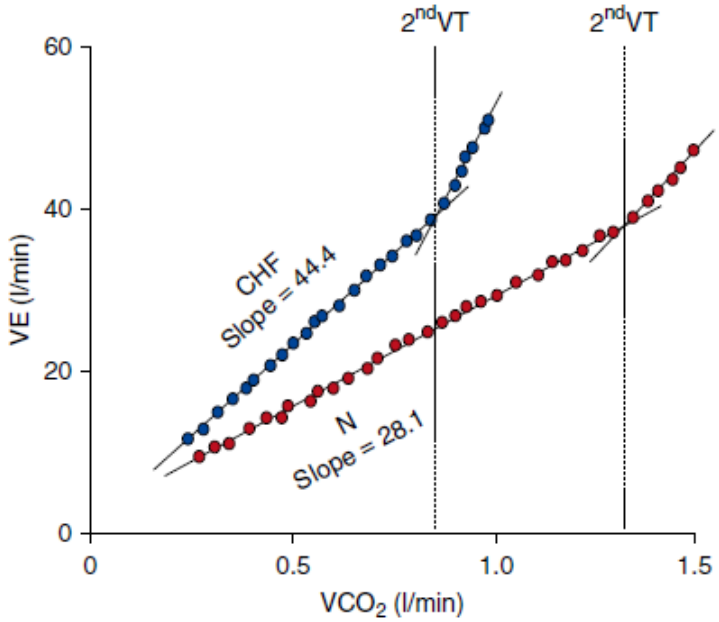

Figure 2.7: Ventilation (VE) as a function of volume of exhaled carbon dioxide (VCO_2) during ramp incremental exercise in a normal subject and a patient with chronic heart failure. A reduced ventilatory efficiency is present in chronic heart failure, as witnessed by a steeper VE/VCO_2 slope when compared with that of a normal subject. [4]

A higher than normal V_E/V_{CO_2} slope may be of undeterminable origin (i.e., primary hyperventilation) or due to respiratory or cardiac diseases that induce a mismatch of ventilation to perfusion. An increased V_E/V_{CO_2} slope is classically observed in patients with chronic heart failure and in those with pulmonary hypertension of different etiologies, with values progressively higher with increasing disease severity. Conversely, a

downward displacement of the V_E/V_{CO_2} slope occurs when the PaCO2 set point is raised (i.e., in primary alveolar hypoventilation).

2.6.6 Exercise Oscillatory Ventilation

Oscillatory ventilation during exercise is a slow, prominent, consistent (rather than random) fluctuation of ventilation (Figure 2.8) that may occur in different patterns (i.e., be present during the entire duration of the exercise phase or only during early or peak exercise).

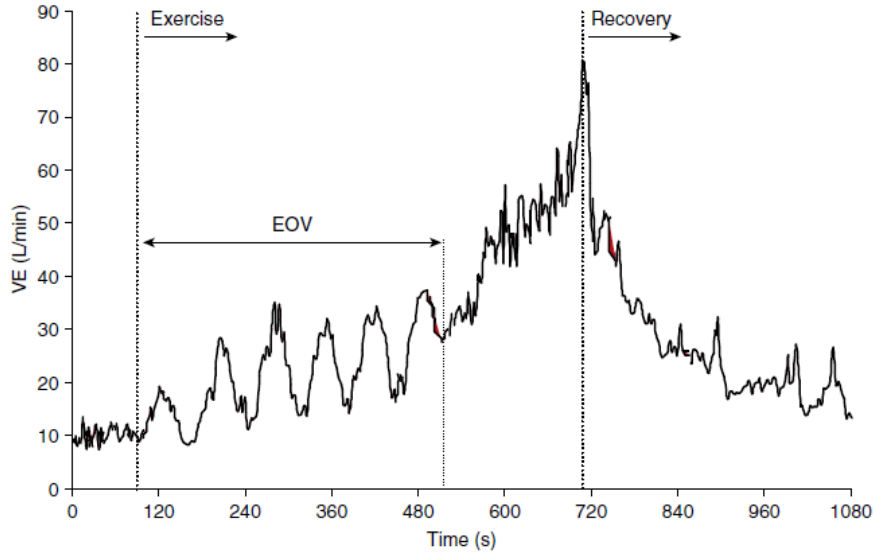

Figure 2.8: Ventilation (VE) as a function of time during ramp incremental exercise in a patient with chronic heart failure. EOV = exercise oscillatory ventilation.

Several pathophysiological determinants of this phenomenon have been proposed, which may be grouped into ventilatory (i.e., instability in the feedback ventilatory control system) and hemodynamic (i.e., pulmonary blood flow fluctuations). The criteria used to identify oscillatory ventilation during exercise suffer from lack of standardization, with the most often adopted being those recommended by the American Heart Association (i.e., persistence of an oscillatory ventilation pattern for at least 60% of exercise duration at an amplitude higher than 15% of the average value of ventilation at rest). Among patients with cardiac disease, exercise oscillatory ventilation is specifically detected in those with chronic heart failure and associated with cyclic changes in arterial oxygen

and carbon dioxide tensions. Of note, in this population, exercise oscillatory ventilation is often associated with nocturnal periodic breathing [3].

2.6.7 Partial Pressure of End-Tidal Carbon Dioxide

The partial pressure of end-tidal carbon dioxide in exhaled air (PET_{CO_2}) is commonly derived in mm Hg units by cardiopulmonary exercise testing instrumentation (Figure 2.9). Normal values at rest range between 36 and 42 mm Hg, increase from rest to first ventilatory threshold and then decrease as maximal effort is approached. Several investigations have demonstrated a significant direct relationship between resting PETCO2 and CO. The PET_{CO_2} measured at first ventilatory threshold during incremental exercise has also been correlated with CO in patients with chronic heart failure and found to mirror disease severity in this population. However, caution is required in interpreting PET_{CO_2} values in individual patients, as they may be affected by acute hyperventilation, increased dead space due to emphysema or other lung diseases, or rapid and shallow breathing patterns, all of which will reduce the PETCO2 independently of cardiac function. In patients with pulmonary hypertension, PET_{CO_2} at rest and first ventilatory threshold is related to pulmonary pressures and can thus provide a noninvasive picture of disease severity.Changes in PETCO2 may also be of help in the detection of exercise-induced right-to-left shunting, as testified by (1) an abrupt and sustained increase in partial pressure of end-tidal oxygen with a simultaneous sustained decrease in partial pressure of end-tidal carbon dioxide, (2) an abrupt and sustained increase in the respiratory exchange ratio, and (3) an associated decline in pulse oximetry saturation [3] .

2.6.8 Metabolic Equivalent

1 MET is equivalent to an oxygen use of 3.5 mL O_2/kg/min. Simple household activities, or light work, require 1.5-4 METs of energy to perform. Moderate work usually requires 3-6 METs, whereas heavy work and high-energy sports require 5-15 METs. [6]

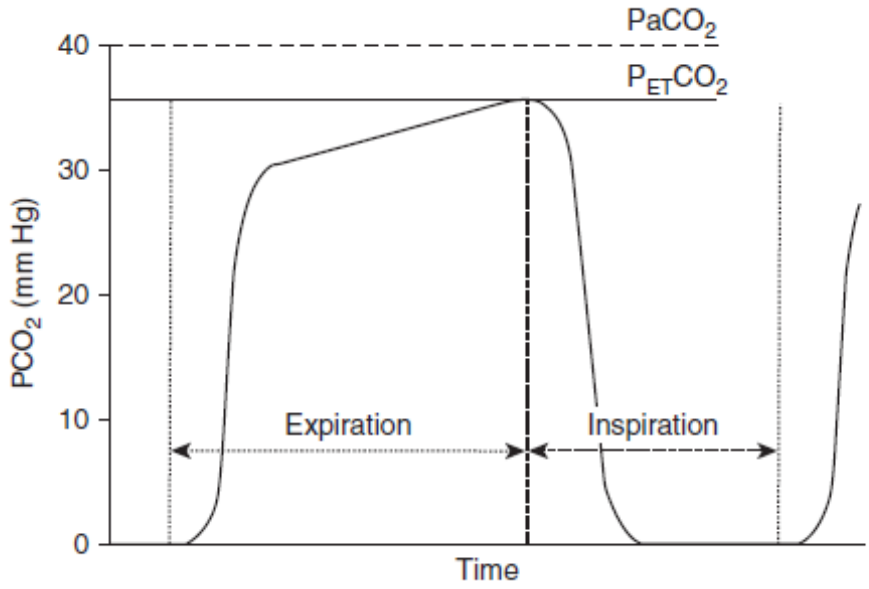

Figure 2.9: Partial pressure of end-tidal carbon dioxide (PET_{CO_2}) in breathed air during a respiratory cycle as a function of time.

2.7 Advantages and disadvantages of Cardiopulmonary testing

Standard ECG treadmill testing can provide information on heart rate, blood pressure, ECG changes suggestive of ischemia or arrhythmias, and an estimation of the metabolic rate in metabolic equivalents (METs; as a proxy for actual metabolic rate). The CPET is advantagous as it can provide additional information to assist in diagnosis, including precise data on gas exchange and metabolic data (oxygen uptake V_{O_2}, carbon dioxide output V_{CO_2}, gas exchange anaerobic threshold [GE_{LAT}], minute ventilation V_E, ventilatory equivalents for oxygen [VE/V_{O_2}] and carbon dioxide [VE/V_{CO_2}]), oxygen pulse (O_2 pulse), oxygen saturation via pulse oximetry (O_2 Sat), end tidal O_2 and CO_2 values, and a quantifiable and reproducible work rate in watts (see Figure 2.10).

The main disadvantage of the cardiopulmonary test is the use of masks or mouthpieces to collect expired air, these masks are uncomfortable for the patient and reduce the exercise tolerance, limiting the diagnostic value of the test. For this reason, it is appropriate to develop a new type of test to improve patient comfort and performance.

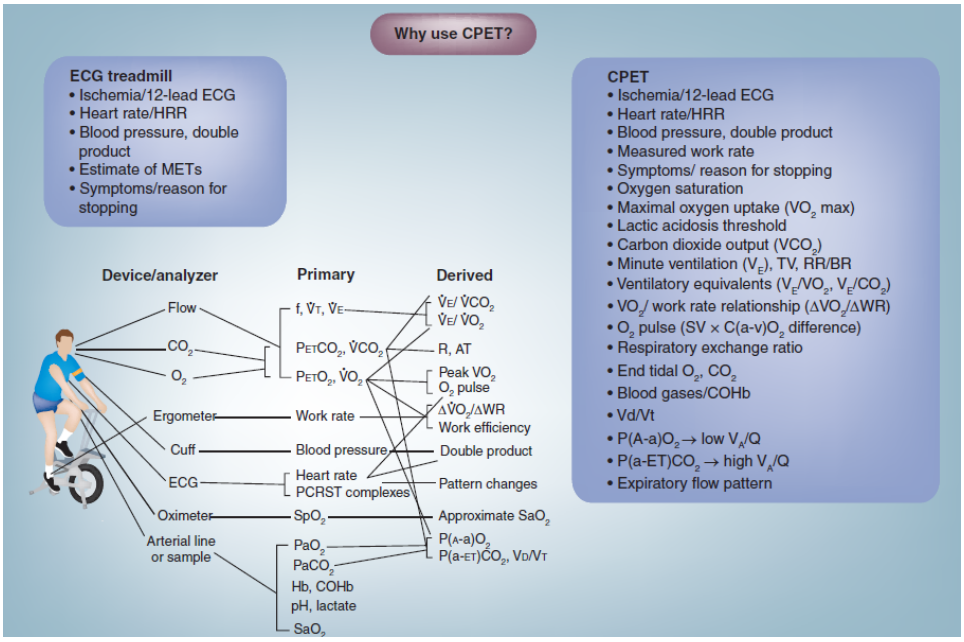

Figure 2.10: Multiple advantages of cardiopulmonary exercise testing over ECG treadmill exercise testing. COHb: Carboxyhemoglobin; CPET: Cardiopulmonary exercise testing; HRR: Heart rate reserve; MET: Metabolic equivalent; RR/BR: Respiratory rate/breathing reserve; SV: Stroke volume; TV: Tidal volume; WR: Work rate

Chapter 3

Test of Performance

The cardiopulmonary test offers a complete evaluation of the patient through the parameters acquisition that reveals the functioning of the respiratory and cardiovascular system without neglecting the metabolic component. This test is very efficient in healthy patients, but it is inadequate for subjects with a limited cardiac, ventilatory and musculoskeletal performance range. The Test of Performance represents a valid alternative to the standard procedure and provides for the development of an instrumentation suitable for subjects with limited performance.

The Figure 3.1 shows the diseases or pharmacological therapies that may limit the cardiovascular, respiratory and musculoskeletal system respectively. This test's purpose is to acquire the physiological parameters by subjecting the patient to very limited workloads so as not to induce him to exhaustion. Furthermore, the test of perfomance can also be used in rehabilitation programs that involve the patient's training submitted to small periodic changes in the workload, i.e. the subject's performance is assessed before and after the moderate increase in workload.

The adaptation of physiological parameters to small changes in loading can be seen by comparing the results obtained before and after a gradual training program. Therefore the test of perfomance offers a possibility of improving performance depending on the individual body's ability to adapt to increasingly heavy workloads.

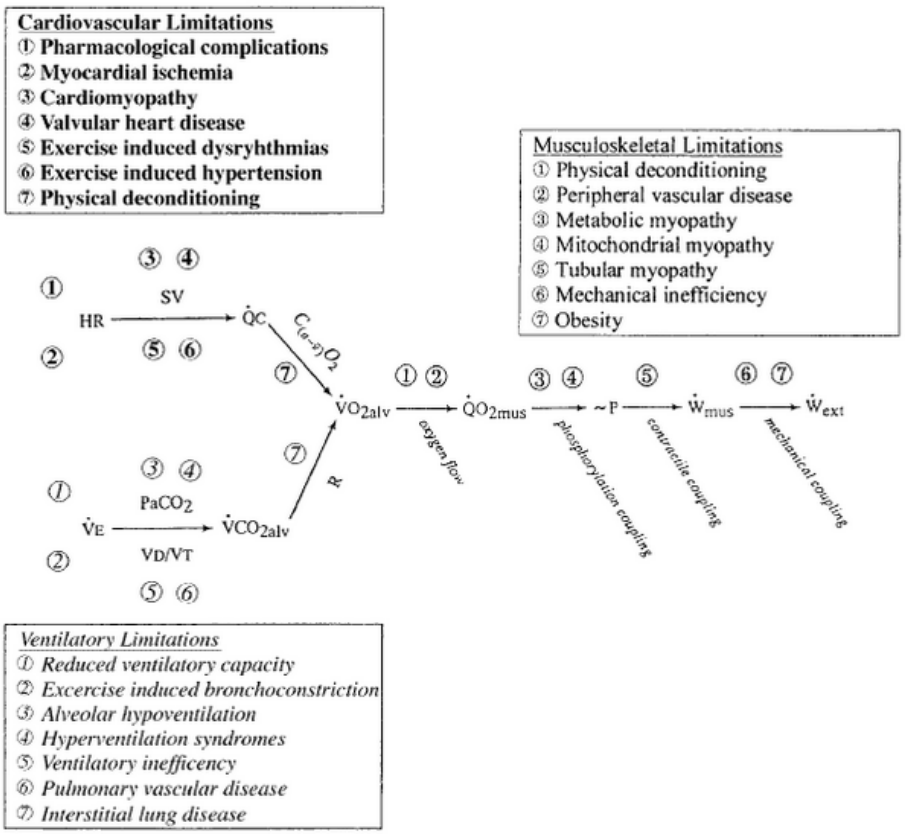

Figure 3.1: Cardiovascular, ventilatory and musculoskeletal limitations which affect the performance of external work.

3.1 ECG signal recorded during the execution of exercise testing

The test of performance aims to facilitate the patient during the execution of the test by avoiding the use of masks and mouthpieces to collect expired air, to not limit its already compromised physical performance. To this end, the ECG signal was recorded during the exercise test performed according to a previously established experimental protocol.

The ECG signal allows to evaluate the following aspects:

- the single heartbeat consisting of a P wave, a QRS complex and a T wave to check for any premature ventricular beats, any slimming of the isoelectric features (eg an over-segmentation of the ST segment is an infarct index of the myocardium) and

alterations of the various electrical waves that may indicate morphological changes in the heart chambers.

- Rhythmicity of the cardiac action, place the sinus rhythm defined as the succession of normal complexes, we evaluate the possible presence of arrhythmias, not normal electrocardiographic complexes, that can be generated at the atrial level, in excitation points different from the sinus node, at the atrio-ventricular or intraventricular conduction tissue level at the ventricular tissue level. [6]

- Heart rate useful for assessing each patient's ability to adapt to the effort. In particular, the increase and decrease of the heart rate has been considered in relation to the different workloads to which the subject is submitted.

3.2 Heart beat period and QRS detection

The aim in HRV analysis is to examine the sinus rhythm modulated by the autonomic nervous system. Therefore, one should technically detect the occurrence times of the SA-node action potentials. This is, however, practically impossible and, thus, the fiducial points for the heart beat is usually determined from the ECG recording. The nearest observable activity in the ECG compared to SA-node firing is the P-wave resulting from atrial depolarization (see Figure 3.2) and, thus, the heart beat period is generally defined as the time difference between two successive P-waves. The signal-to-noise ratio of the P-wave is, however, clearly lower than that of the strong QRS complex which results primarily from ventricular depolarization. Therefore, the heart beat period is commonly evaluated as the time difference between the easily detectable QRS complexes. A typical QRS detector consists of a preprocessing part followed by a decision rule. Several different QRS detectors have been proposed within last decades. [14]

3.3 Heart rate variability during tilt test

Heart rate variability (HRV) describes the variations between consecutive inter-beat-intervals (IBIs). Both sympathetic and parasympathetic branches of the ANS are involved in the regulation of heart rate (HR). Sympathetic nervous system (SNS) activity

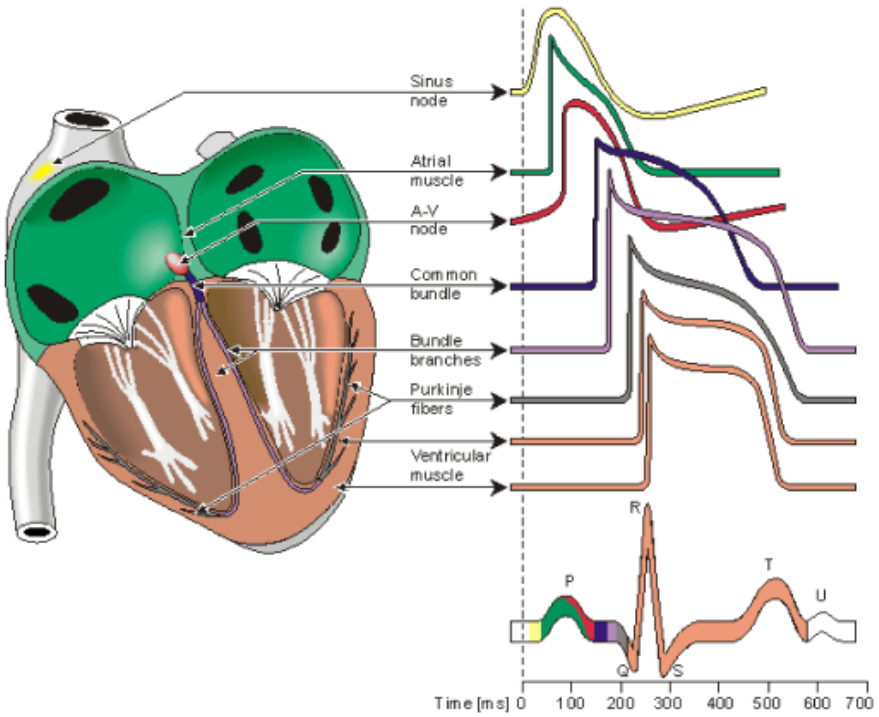

Figure 3.2: Electrophysiology of the heart: the different waveforms for each of the specialized cells found in the heart are shown. The latency shown approximates that normally found in the healthy heart.

increases HR and decreases HRV, whereas parasympathetic nervous system (PNS) activity decreases HR and increases HRV. The control of the autonomic output involves several interconnected areas of central nervous system, which form the so-called central autonomic network. In addition to this central control, arterial baroreceptor reflex as well as respiration are known to induce quick changes in heart rate. The baro reflex is based on baroreceptors which are located on the walls of some large vessels and can sense the stretching of vessel walls caused by pressure increase. Both sympathetic and parasympathetic activity are influenced by baroreceptor stimulation trough a specific baroreflex arc (Figure 3.3).

Typically, the most conspicuous oscillatory component of HRV is the respiratory sinus arrhythmia (RSA), where the vagus nerve stimulation is being cut-off during inhalation, and thus, HR increases during inhalation and decreases during exhalation.

Heart rate variability (HRV) is a commonly used tool when trying to assess the

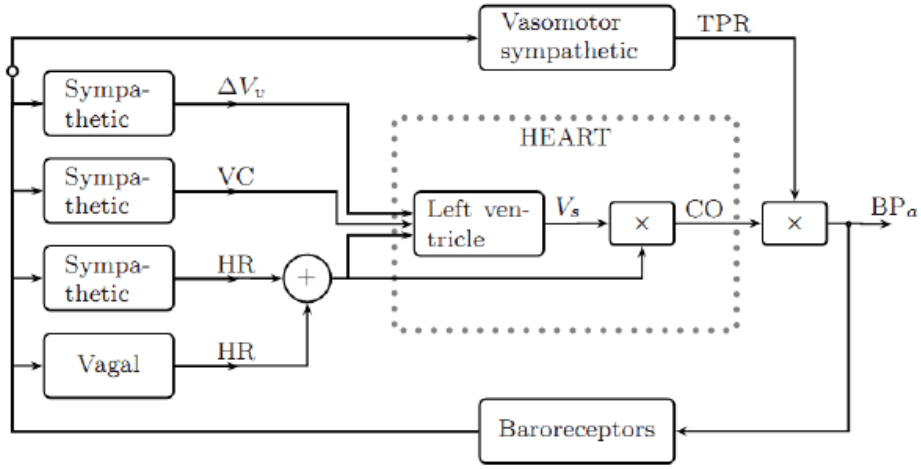

Figure 3.3: The four baroreflex pathways (redrawn from [47]). Variation in venous volume (ΔVv), left ventricular contractility (VC), sympathetic and parasympathetic (vagal) control of heart rate (HR), stroke volume (Vs), cardiac output (CO), total peripheral resistance (TPR), and arterial blood pressure (BPa). [14]

functioning of cardiac autonomic regulation. It has been used in multitude of studies, related to cardiovascular research and different human wellbeing applications, as an indirect tool to evaluate the functioning and balance of the autonomic nervous system (ANS). One of the main clinical scenarios where HRV has been found valuable include the risk stratification of sudden cardiac death after acute myocardial infarction. In addition, decreased HRV is generally accepted to provide an early warning sign of diabetic cardiovascular autonomic neuropathy, the most significant decrease in HRV being found within the first 5-10 years of diabetes. Besides these two main clinical scenarios, HRV has been studied with relation to several cardiovascular diseases, renal failure, physical exercise, occupational and psychosocial stress, gender, age, drugs, alcohol, smoking and sleep. The term HRV refers, in general, to changes in heart beat interval which is a reciprocal of the heart rate. This is also the case here. The starting point for HRV analysis is the ECG recording from which the HRV time series can be extracted. In the formulation of the HRV time series, a fundamental issue is the determination of heart beat period. [14]

Chapter 4

Materials and methods

This chapter describes the instrumentation used to collect the measurements, the procedure used to execute the performance evaluation test, i.e. the experimental protocol has been defined by identifying the parameters to be monitored. In the test of performance the protocol is aimed at optimizing the measurement acquisition process taking into account the possible limitations of the patient.

The subjects on which the test was carried out were presented, reporting their age, weight, height and weekly sports activity. In fact these factors affect the evaluation of the electrocardiographic signal, as they condition the shape of the cardiovascular system and, therefore, of the individual performances.

Finally, this chapter describes the methods by which the different parts of the ECG signal is analyzed and elaborated, in particular an analysis of the first part of the signal, corresponding to the execution of the tilt test, in the time and frequency domain. Next, the heart rate trend was assessed during the top test by focusing on the adaptive response of the ECG signal at the addition or removal of the mild or moderate workload, respectively.

4.1 Strumentation

It is reported below the tools that are used for the acquisition of the ECG signal briefly describing their characteristics, the method with which they were used and their purpose.

Electrocardiograph

The electrocardiograph is a device for monitoring heart electrical activity. During the test a Click ECG Cardioline electrocardiograph is used (Figure 4.1) and the signals are taken from the R, L, N, F cables (Figure 4.2) positioned respectively on the right shoulder, left shoulder, on the right leg, on the left leg.

Figure 4.1: Electrocardiograph Click ECG Cardioline.

(a) *Cable R* (b) *Cable L* (c) *Cable F* (d) *Cable N*

Figure 4.2: The four cables R, L, N, F.

The electrocardiograph is a digital device equipped with a recording voltmeter and electric wires, which connect the device to the patient using electrodes applied to the skin. Finally, a monitor allows you to graphically display the path. The electrodes are metallic suckers that apply to the patient skin, in the execution of a ECG track. There are a total of 10 electrodes, 4 apply to the limbs, 6 in the thorax, in the precordial region. These electrodes register 12 leads, ie 12 signals that describe the heart electrical activity from different positions.

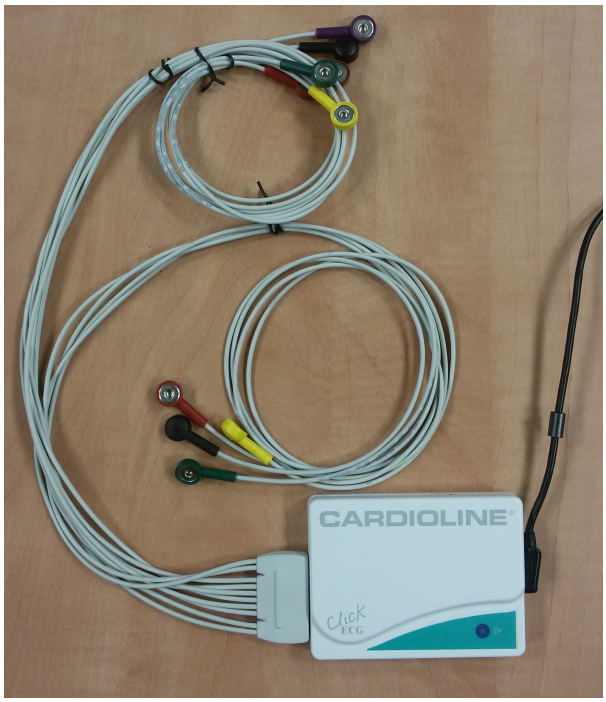

Figure 4.3: Electrocardiograph Cardioline with 12 electric cables and electrical connection wire to the computer.

The electrocardiogram can be performed with patient at rest or under stress. In the first case the patient is lying on the bed, the electrodes are applied to the skin that pick up the electrical signals of the heart and transmit them through the electric wires to the electrocardiograph that processes them and reproduces them graphically on the monitor. The exercise test is performed while the patient is pedaling in an exercise bike.

Electrodes

During the execution of the ECG signal test 4 electrodes are applied to the patient's skin, the electrodes are metallic suckers connected to the R, L, F, N cables at the limbs, respectively on the right, left shoulder, and at the bottom of the chest in the direction of the right and left leg. The electrodes used are shown in Figure 4.4.

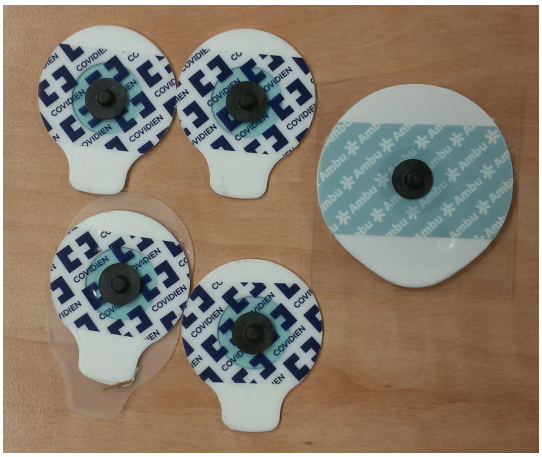

Figure 4.4: Electrodes.

Cyclergometer

The TOP test was performed on upright bike RHC400 Air Machine. The seat of the bike has been adjusted according to the patient's height. It is possible through the Air Machine display to monitor the patient's pedaling speed and adjust the load to which it is submitted, referring to the difficulty of the exercise. The cyclergometer is shown in Figure 4.5.

Computer

The recorded ECG signal is displayed on the monitor of a computer via the Anscovery System software, then it is processed and the tacogram is extracted. Below, starting from the tacogram, the analysis of the ECG signal taken during the tilt test in the time and frequency domain is carried out using the Kubios software.

Software

1) Anscovery System

The ECG signal is displayed on the computer monitor using Anscovery System software (Sparkbio srl). It is necessary to specify that initially there are more signal dispaly channels and the signal with less noise is chosen. Through the Anscovery software it is possible to carry out a first processing of the ECG signal by searching for the R-waves on the entire track. The search for R-waves is based on a derivative method, that is, on

Figure 4.5: Cyclergometer RHC 400 Air Machine.

the derivative of the entire track. The time distance between a heartbeat and the next is called time R-R and is expressed in milliseconds (ms). After detecting the R waves of the QRS complex, the tachogram track is added, by placing the sequence of heart beats on the abscissa and their length in ordinate, normally calculated from the peak of the R wave taken into consideration at the peak of the next R (see Figure 4.7). In this way it is possible to have a precise indication regarding the trend of the heart rate [15].

2) Kubios HRV

Kubios HRV is an advanced tool for studying the variability of heart beat intervals. The first versions of the Kubios HRV were developed as part of academic research work carried out at the Department of Applied Physics, University of Eastern Finland, Kuopio, Finland.

The Kubios software performs pre-processing operations such as:

- QRS detector for accurate detection of beat-to-beat RR intervals from ECG data;
- Artefact correction methods like threshold based RR correction algorithm, automatic RR correction algorithm, ECG based R-wave correction.

The software has the following analysis options:

- Time-domain parameters: Mean RR and STD RR, Mean HR and STD HR, min/max HR,
- Frequency-domain parameters: VLF, LF and HF band powers (in absolute, relative and normalised units), peak frequencies and LF/HF ratio.
- Spectrum estimation methods: Welch's periodogram and AR spectrum estimate.

After the analysis of the signal has been carried out, it is possible to export reports and results:

- HRV reports (PDF reports) including time-domain, frequency-domain results;
- ECG print (PDF report) showing the raw ECG trace for selected time period;
- HRV analysis results exported to PDF file, Text file.

4.2 Choice of subjects

For the execution of the physical performance evaluation test, 6 subjects were chosen, 2 males and 5 female. The Table 4.1 shows for each subject the data of interest that affect the physical performance, such as age, sex, weight, the level of sporting activity carried out on an indicative scale divided into 5 levels.

4.3 TOP Protocols

The preliminary phase of the test involves the preparation of the subject lying on the bed for the application of the 4 electrodes on the limbs for the detection of the ECG signal. Once the respective R, L, N, F cables have been assembled with the electrodes, the electrocardiograph is connected to a computer monitor to visualize the signal. The

Name and Surname	Age	Sex	Weight	Height	Smoker	Sporting activity
R.Z.	70	M	75 kg	1.73 m	No	1
M.F.M.	25	F	58 kg	1.81 m	No	4
M.Z.	20	F	47 kg	1.60 m	No	1
S.C.	24	F	49 kg	1.57 m	Yes	1
A.L.	39	M	62 kg	1.63 m	Yes	4
A.M.	29	F	65 kg	1.67 m	Yes	3

Table 4.1: Subjects chosen for the performance test whose age, sex, weight, smoking habits, level of sport activity are indicated. Level of sport activity: 1-sedentary, 2-occasional, 3-one time a week, 4-more than one time a week, 5-agonism.

height of the cyclergometer' seat is adjusted and the test is carried out. The experimental protocol provides for the ECG signal to be taken during the execution of the entire test, divided into two phases, respectively:

- **First phase** in which tilt test takes place, it is also called passive orthostatic stimulation test and the patient goes from clinostatism to orthostatism. This test is one of the most effective tests for the diagnosis of syncope.
- **Second phase** in which the patient performs the exercise test on the cycle ergometer, submitting the subject to two different workloads, initially a mild one and then a moderate one.

The patient is asked to keep the pedaling speed constant, around the value of 50 Ped/min. In particular, the procedure is carried out according to the following order and the respective timing:

- **TILT TEST**

  - **CLINO PHASE**, patient lying on the bed for 5 minutes,

  - **ORTO PHASE**, patient standing for 5 minutes.

- The patient is moved to the cyclergometer and carries out the **TOP TEST**

  - **WARM UP PHASE**, the patient pedal on the bicycle for 2 minutes maintaining the pedaling speed v = 50 Ped/min and reaches the workload of 10 W;

  - **STEP 1**, the patient is submitted to the first workload of 50 W for a period of 4 minutes;

- **DEFACTING**, the patient stops pedalling and stays on the cycle-ergomenter in a passive recovery phase lasting 5 minutes.

- **WARM UP PHASE**, the patient starts pedaling again on the bicycle for 2 minutes maintaining the pedaling speed v = 50 Ped/min and reaching the workload of 10 W again;

- **STEP 2**, the patient is submitted to the second workload, higher than the first one, equal to 70 W for a period of 4 minutes;

- **DEFACTING**, the patient stops pedalling and stays on the cyclergomenter in a passive recovery phase lasting 5 minutes.

At the end of the test, the ECG signal recorded by the Anscovery System software is saved in a .dat file that contains the entire ECG track acquired during all phases of the exercise.

4.4 Sygnal analysis methods

The ECG signal recorded by the Anscovery System software during the test execution is saved in a .dat file that is associated with an .ini file, containing the configuration settings. The whole track of the ECG signal is contained in the .dat file, and the QRS complex is detected for each normal complex.

After the QRS complex occurrence times have been estimated, the HRV time series can be derived. The inter-beat intervals or RR intervals are obtained as differences between successive R-wave occurrence times. That is, the n'th RR interval is obtained as the difference between the R-wave occurrence times $RR_n = t_n - t_{n1}$ (see Figure 4.6).

The tachogram is taken from the RR intervals of the respective ECG signal using the Anscovery System software, it is shown in Figure 4.7.

Once the tachogram is extracted from the ECG signal, the time intervals between consecutive RRs heart rate HR and signal acquisition time are obtained. Once the tachogram is extracted from the ECG signal, the time intervals between consecutive RRs, heart rate HR and signal acquisition time are obtained.

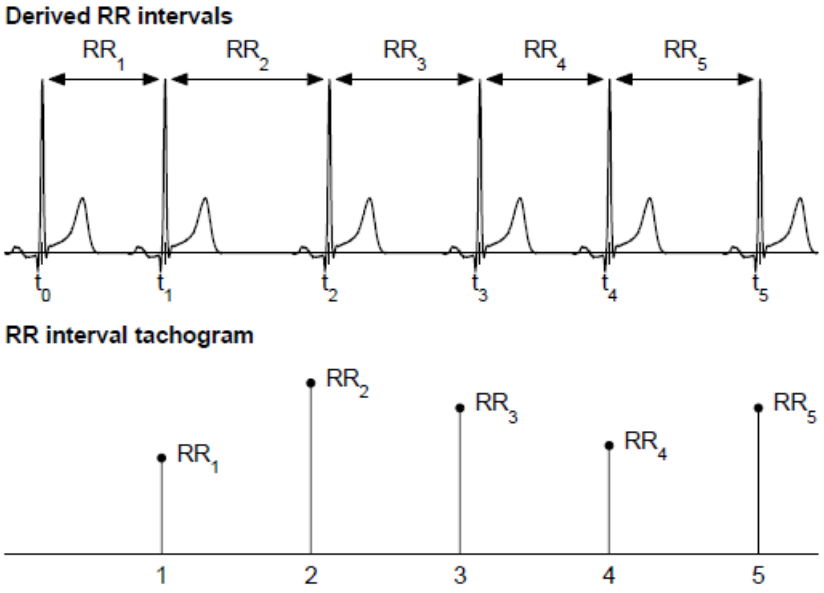

Figure 4.6: RR interval tachogram obtained from the search for R waves by derivative method.

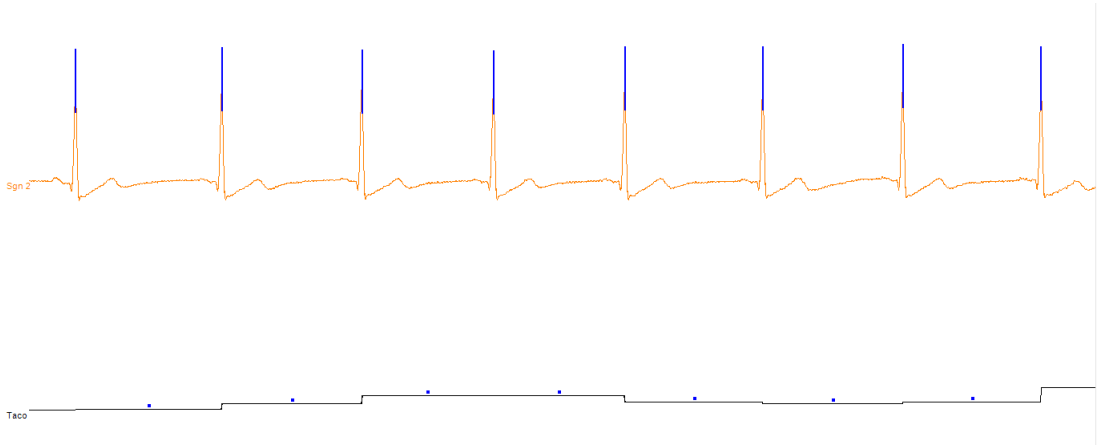

Figure 4.7: Detection of R waves and related tachogram extracted from the time interval R-R.

4.4.1 Sygnal analysis recorded during tilt test

The time series constructed from all available RR intervals contained in RR text file is, clearly, not equidistantly sampled, but has to be presented as a function of time, i.e. as values (tn,RRn). This fact has to be taken into account before frequency-domain

analysis. In general, three different approaches have been used to get around this issue. The simplest approach that have been adopted in, e.g., is to assume equidistant sampling and calculate the spectrum directly from the RR interval tachogram (RR intervals as a function of beat number). This assumption can, however, cause distortion into the spectrum. This distortion becomes substantial when the variability is large in comparison with the mean level. Furthermore, the spectrum can not be considered to be a function of frequency but rather of cycles per beat . Another common approach, adopted in this software, is to use interpolation methods for converting the non-equidistantly sampled RR interval time series (also called the interval function) to equidistantly sampled, see Figure 4.8. One choice for the interpolation method is the cubic spline interpolation. After interpolation, regular spectrum estimation methods can be applied. In our case

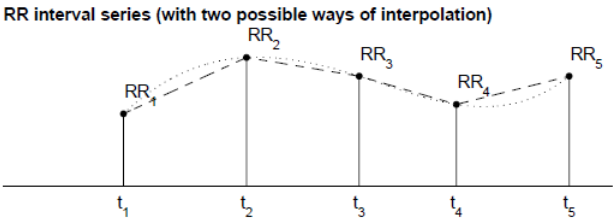

Figure 4.8: Tachogram of RR interval series.

the resampling of the RR intervals was done by cubic spline interpolation at a frequency of 4 Hz. The Figure 4.9 shows the portion of the signal selected by Kubios software for subsequent analysis in the time and frequency domain. [14]

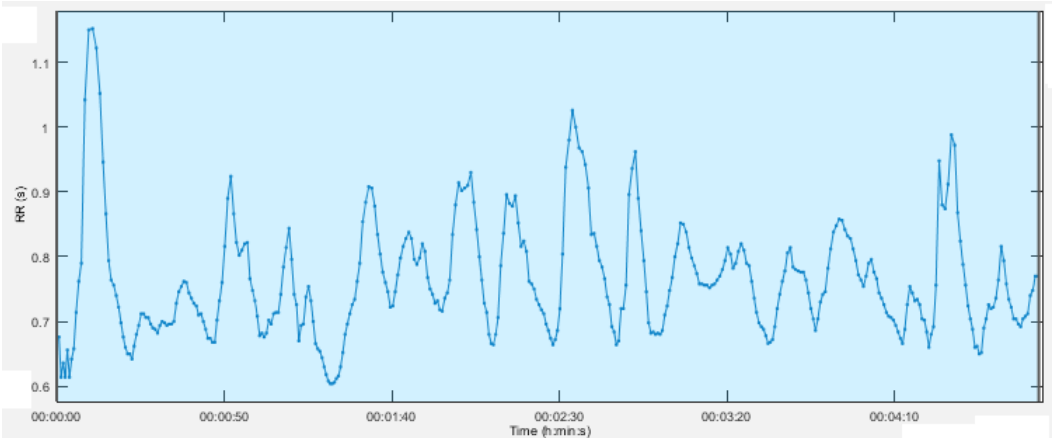

Figure 4.9: Selected resampled sygnal.

The RR interval series may be inadequate due to the presence of missed beat detections, misplaced beats and ectopic beats (e.g. premature ventricular beats), therefore it may be appropriate to apply Artifact correction. The artifact correction options can be used to correct artifacts from a corrupted RR interval series through Threshold correction. The threshold correction simply compares every beat interval against a local mean RR, and identifies the beat as artefact if it exceeds the specified threshold. The threshold should be selected individually, because normal variability in RR intervals can be quite different between individuals, and therefore, a fixed threshold could over-correct the RR data. Figure 4.10 shows the artifact correction applied to the signal via a low threshold.

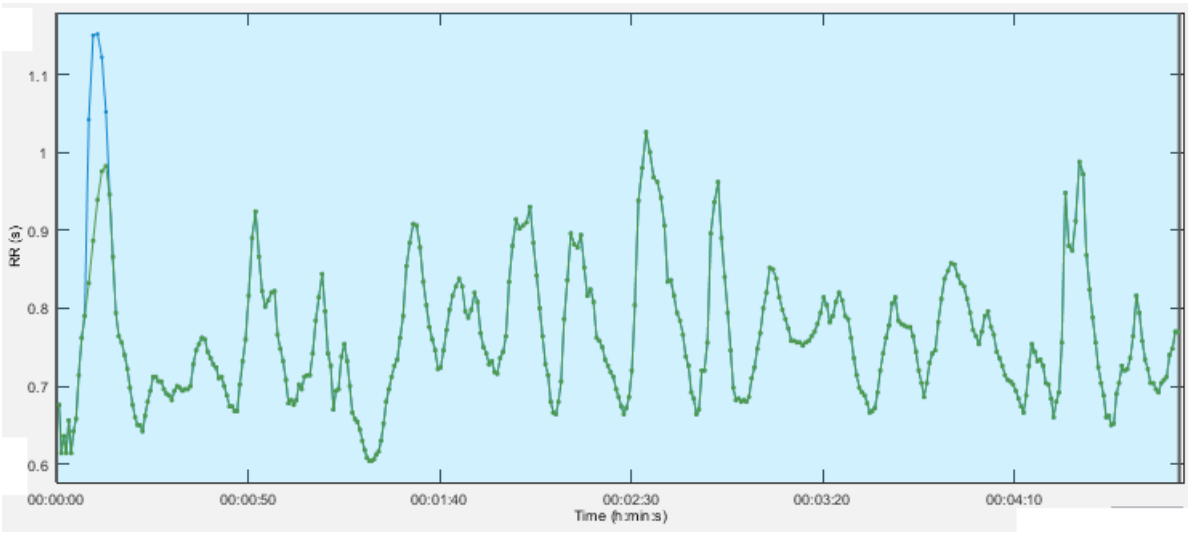

Figure 4.10: Artifact correction obtained by applying a low threshold.

Once the RR interval has been selected and an eventual threshold is applied to eliminate the artifacts, the clino and ortho signal, the 2 phases in which the tilt test is subdivided, are analyzed in the time and frequency domain.

The clino and ortho signals are selected, not considering in the analysis the transition phases in which sympatho-vagal activation changes, therefore it is fundamental the role of the technician/clinician who has to choose the periods of analysis in function of the signal and therefore of the state of the patient as shown in Figure 4.11.

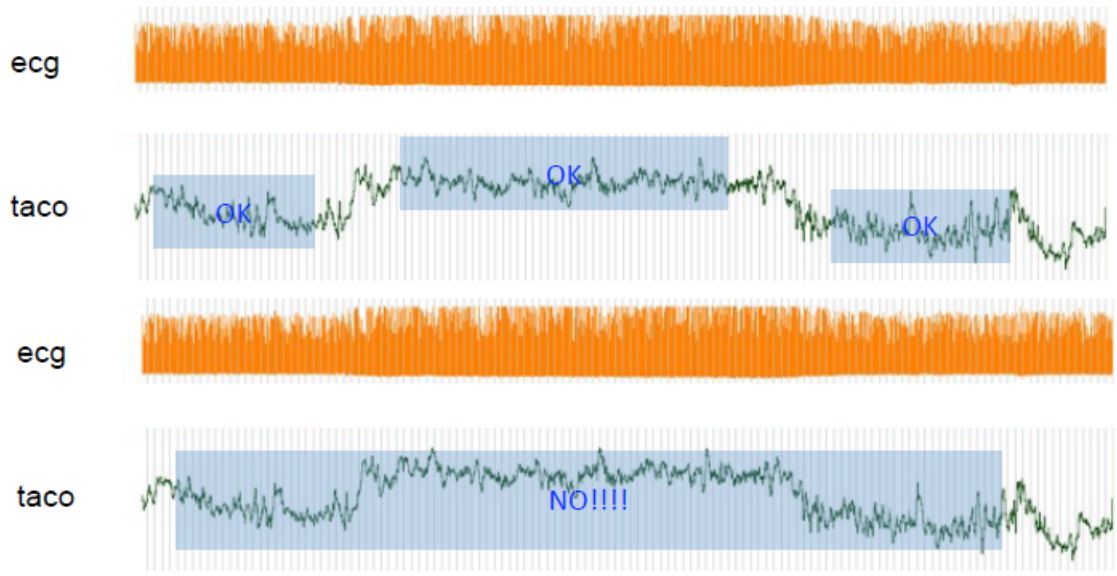

Figure 4.11: Example of a correct and a wrong selection of the ECG signal.

Sygnal analysis HRV in the time domain

Either the heart rate at any point in time or the intervals between successive normal complexes are determined in the time domain methods. In a continuous ECG record, each QRS complex is detected, and the so-called RR intervals (that is, all intervals between adjacent QRS complexes resulting from sinus node depolarizations) or the instantaneous heart rate is determined.

Simple Time domain variables that can be calculated include:

- the mean RR interval and the standard deviation of RR (SDNN) ,

$$MeanRR = \frac{\sum_{i=1}^{NN} RR_i}{NN}$$

$$SDNN = \sqrt{\frac{\sum_{i=1}^{NN}(RR_i - MeanRR)}{NN - 1}}$$

where NN is the total number of intervals RR.

- the mean heart rate HR and the standard deviation of HR ,

$$MeanHR = \frac{\sum_{i=1}^{NN} HR_i}{NN}$$
$$SDHR = \sqrt{\frac{\sum_{i=1}^{NN}(HR_i - MeanHR)}{NN-1}}$$

  where NN is the total number of intervals RR.

- the minimum and maximum HR value.

Geometric Methods

The geometric methods take into account the distribution shape of the differences between contiguous RRs. The Poincaré diagram is shown as a cartesian graph in which the x-axis represents the intervals RR, while the y-axis the intervals RR out of phase of + 1 beats. Then a point is represented at each pair of values (RR_i, RR_{i+1}). The graphical dispersion of this diagram is therefore related to the variability of the heart rhythm. The displayed points are enclosed in an ellipse and the respective dispersion (standard deviations) is calculated. In the Poincaré plot (left hand axis), the successive RR intervals are plotted as blue circles and the SD1 and SD2 variables obtained from the ellipse fitting technique are presented. [14] It is possible to quantify the short and long-term variability by calculating the two SD1 and SD2 beams of the ellipse, which interpolates the set of points on the (RR_{i+1}, RR_i) plane, respectively. By projecting the points along the transverse axis and the bisector, SD1 and SD2 are getted as the standard deviations of the two distributions obtained (see Figure 4.12b). Considering the RR interval series along the x axis and the y axis:

$$x = RR_1, RR_2, RR_3.....RR_N$$
$$y = RR_2, RR_3.....RR_{N+1}$$

the coefficients are calculated:

$$d_{i1} = \frac{|(x_i - \bar{x}) - (y_i - \bar{y})|}{\sqrt{2}}$$
$$d_{i2} = \frac{|(x_i - \bar{x}) + (y_i - \bar{y})|}{\sqrt{2}}$$

from which the two SD1 and SD2 standard deviation values are obtained:

$$SD1 = \frac{1}{N}\sum(d_{i1})^2$$
$$SD2 = \frac{1}{N}\sum(d_{i2})^2$$

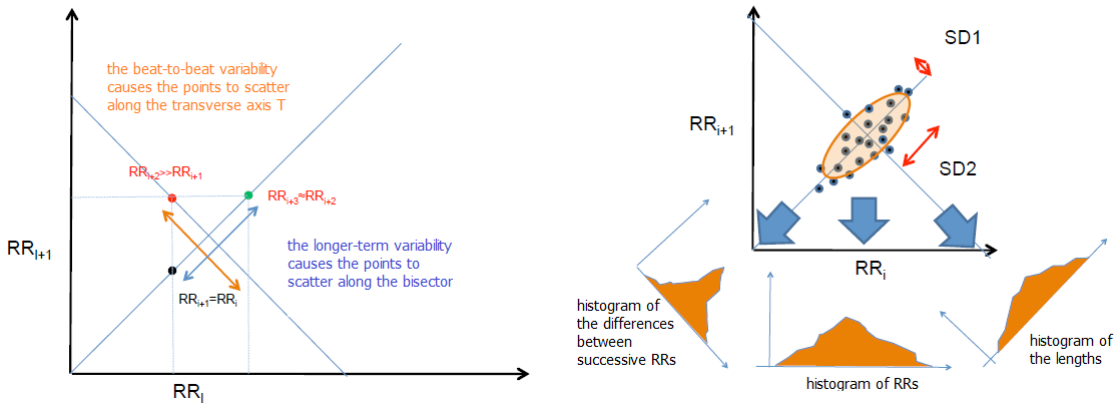

(a) (b)

Figure 4.12: Plot that evaluates the variability of each RR interval compared to the previous one through quantitative parameters SD1 ed SD2.

Sygnal analysis HRV in the frequency domain

Various spectral methods for the analysis of the tachogram have been applied since the late 1960s. Power spectral density (PSD) analysis provides the basic information of how

power (variance) distributes as a function of frequency. Independent of the method used, only an estimate of the true PSD of the signal can be obtained by proper mathematical algorithms.

Methods for the calculation of PSD may be generally classified as nonparametric and parametric. In most instances, both methods provide comparable results. The advantages of the nonparametric methods are

1. the simplicity of the algorithm used (Fast Fourier Transform [FFT] in most of the cases) ,

2. the high processing speed,

while the advantages of parametric methods are

1. smoother spectral components that can be distinguished independent of preselected frequency bands,

2. easy postprocessing of the spectrum with an automatic calculation of low- and high-frequency power components with an easy identification of the central frequency of each component, and

3. an accurate estimation of PSD even on a small number of samples on which the signal is supposed to maintain stationarity.

The basic disadvantage of parametric methods is the need of verification of the suitability of the chosen model and of its complexity (that is, the order of the model).

In addition, you can find settings for the very low frequency (VLF), low frequency (LF), and high frequency (HF) bands limits. The default values for the bands are VLF: 0–0.04 Hz, LF: 0.04–0.15 Hz, and HF: 0.15–0.4 Hz. This high frequency (HF) component of HRV is thus centered at respiratory frequency and is considered to range from 0.15 to 0.4 Hz. Another conspicuous component of HRV is the low frequency (LF) component ranging from 0.04 to 0.15 Hz. The HF component is mediated almost solely by the PNS activity, whereas the LF component is mediated by both SNS and PNS activities and is also affected by baroreflex activity . The origin of the LF oscillations is however considered to be dominated by SNS and the normalized power of the LF component could be used to assess sympathetic efferent activity. The fluctuations below 0.04 Hz,

on the other hand, have not been studied as much as the higher frequencies. These frequencies are commonly divided into very low frequency (VLF, 0.003-0.04 Hz) and ultra low frequency (ULF, 0-0.003 Hz) bands, but in case of short-term recordings the ULF band is generally omitted. These lowest frequency rhythms are characteristic for HRV signals and have been related to, e.g., humoral factors such as the thermoregulatory processes and renin-angiotensin system. [14]

Fourier analysis

Fourier's theorem states that any g(t) function limited in amplitude and periodic can be expressed as an infinite sum of sinusoidal functions:

$$g(t) = \frac{A_0}{2} + \sum_{m=1}^{\inf} \left[A_m cos(2\pi m f_1 t) + B_m sen(2\pi m f_1 t) \right] \qquad f_1 = \frac{1}{T}$$

The signal on which the Fourier analysis is applied is discrete, since the sequence of RR intervals is a discrete signal sampled at variable frequency. It is possible to interpolate the RR intervals using different algorithms, typically polynomials of degree ≥ 2.

Resampling the fixed frequency signal (2-8 Hz) increases the range of frequencies that can be represented on the spectrum and consequently:

- increases the maximum frequency that can be represented on the spectrum,
- the frequency resolution remains unchanged,
- increases the number of RR intervals, including a portion of these non-physiological ones that do not exist in the original sequence.

If you have a discrete function g_k of N points and periodic, with sampling frequency of f_c and higher frequency harmonic limited by the A/D system according to Nyquist-Shannon's theorem [1].

[1]The Nyquist-Shannon theorem states that, given a function whose Fourier transform is nothing outside a certain frequency range (ie a limited bandwidth signal), in its analog-to-digital conversion the minimum sample rate required for avoiding aliasing and loss of information in the reconstruction of the original analog signal (that is, in digital-analog reconversion) must be greater than twice its maximum frequency.

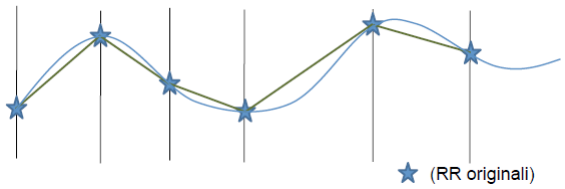

(a)

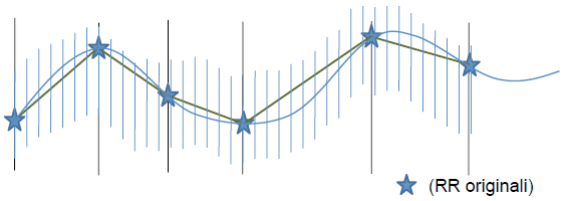

(b)

Figure 4.13: Interpolation and resampling of discrete sygnal of the RR intervals sequence.

$$g(k) = \frac{A_0}{2} + \sum_{m=1}^{\frac{N}{2}-1} \left[A_m cos(2\pi m f_1 k) + B_m sen(2\pi m f_1 k)\right] \qquad f_1 = \frac{1}{T}$$

where mf_1 = harmonic frequency and $m = 1, 2.....N/2$. Knowing that

$$T = \frac{N}{f_c}, \qquad f_1 = \frac{1}{T} = \frac{f_c}{N},$$

the frequency is an integer multiple of the fundamental frequency and can assume the integer values between f_1 and $f_c/2$. Frequency resolution R_f is

$$R_f = \frac{\frac{f_c}{2}}{\frac{N}{2}} = \frac{f_c}{N}.$$

Composing the equations results

$$g(k) = R_0 + 2\sum_{m=1}^{\frac{N}{2}-1} \left(R_m cos(2\pi m f_1 k) + \phi_m\right)$$

$$R_m = \sqrt{A_m^2 + B_m^2} \qquad \phi_m = arctg\left(\frac{B_m}{A_m}\right)$$

The spectrum that is obtained from the Fourier analysis of a discrete signal is discrete,

it is visualized as if it is continuous for legibility and aesthetics reasons.

The sequence of the coefficients R_m defines a discrete function that we can call the Fourier Discrete Transform; then calculating the R_m^2 means performing the Fourier Transform. Then the FFT is introduced to speed up the calculations by reducing the total number of operations to $Nlog_2N$ with the constraint that $N = 2^m$. Having a discrete function consisting of N points, the calculation of the R_m presupposes the execution of about N^2 operations, so the processing times for calculating the discrete fourier transform of a N number of high points are long. The RR sequence is not a periodic signal, therefore it is necessary to consider a sequence long enough to be considered periodic; the longer length, the higher frequency resolution of the spectrum. The purpose of the analysis is to highlight the activation of sympathetic and parasympathetic systems and their relationship. During the analysis period the modulation of the two systems must be constant, the signal must therefore be stationary, the greater length of the signal, the greater likelihood that the activation of the sympathetic and of the vagal will change so that the transitory phases must be neglected, i.e. in which the patient's status changes, for example when the patient passes from the clino phase to the ortho phase as shown in Figure 4.11. Regarding the sequence length to be analyzed, two conditions must be taken into account:

- clinical necessity: signal stability, ie absence of transitory phases,
- technical/clinical necessity: appropriate frequency resolution that allows to correctly highlight the bands of interest that distinguish the very low frequencies VLF, the low frequencies LF and the high frequencies HF respectively. [14]

Autoregressive methods

Autoregressive methods are parametric methods of analysis of heart rate variability in the frequency domain. The self-regression of a data series means to express each point of the series as a linear combination of the previous points, unless an error is so much smaller that the reconstruction is better; that is, the data series can be expressed as:

$$x_t = \sum_{i=1}^{p} a_i x_{t-1} + \epsilon_t$$

The number of points p considered in the reconstruction of the series is the order of the model. The spectral density of the series is obtained by making the fourier transform of the autocorrelation function. Each point in the series is expressed according to the previous ones, so for each point there are p a_i coefficients that bind it to the previous data less than a ϵ error. The autocorrelation of the series thus reconstructed is then made to extract the present periodicity. If the data series contains random noise, then the autocorrelation graph is practically flat. If I have a signal containing waves with its periodicity superimposed to random noise, the autocorrelation eliminates the random noise and highlights the periodic signal present in the initial series. In this way I verify if in the series there are structures that are repeated with which amplitude and which delay one with respect to the other. By extracting the periodicity, then the frequencies and their amplitude of the signal by Fourier analysis, I can therefore obtain the spectrum of the frequencies present in the series. Each band is shown as a bell curve whose area represents the power associated with that given frequency. The sum of the curves relating to all the periodicity found represents the spectrum of the signal (see Figure 4.14). The frequency resolution is much higher than that obtained by Fourier analysis. I can then analyze small pieces of signal by discriminating correctly between the different bands of interest.

Assumptions for applying autoregressive analysis: the signal must be stationary (constant mean and variance) the analysis works correctly if the autoregressione reconstructs the signal without making mistakes. The greater model, the better reconstruction of the signal. the number of periodicity I can extract depends on the order of the autoregressive model I use to reconstruct the signal. If the model has p order, I can extract about p/2 peaks.

If the order of the model is insufficient to correctly reconstruct the signal, I lose the periodicity. If the order of the model is too high, periodicities not identified in the signal are identified.

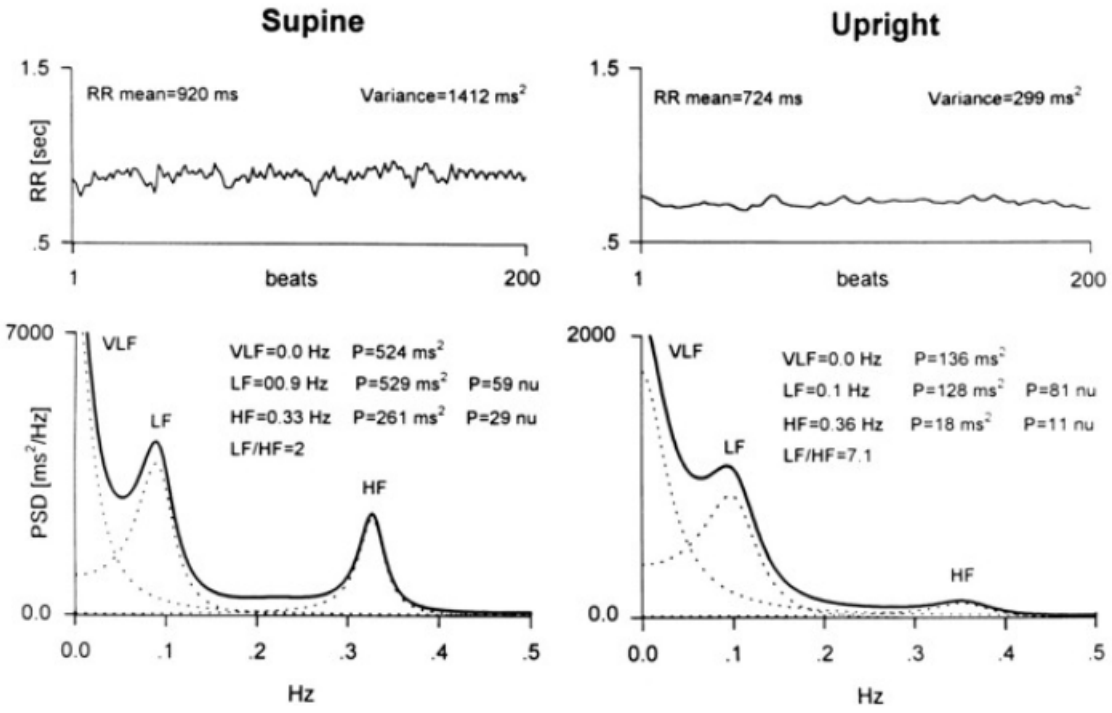

Figure 4.14: Autoregressive analysis od the clinium and ortho phase.

4.4.2 Sygnal analysis recorded during top test

The goal is to monitor the trend of the heart rate during the execution of the top test, in particular we evaluate:

- the ability to adapt to the effort of each subject in the STEP1 and STEP2 phases in which the workload is inserted,
- the passive retrieval capacity of each subject when the workload of STEP1 and STEP2 is removed.

The evaluation of the adaptive capacity to the effort Is made by selecting in the HR vs time curve the signal sections corresponding to the phases of increased heart rate (workload inserted) and passive recovery (workload removed). An exponential interpolation is performed for the selected sections and the coefficients extracted from the fitting are evaluated.

Chapter 5

Results

The following chapter contains the results obtained from the analysis of the ECG signal, ie extracting the tacogram from the series of intervals RR detected by the original signal and carrying out the analysis of the recorded signal.

As described in the previous chapter, for each subject an analysis is carried out in the time and frequency domain for the first part of the signal recorded during the tilt test, while in the second part of the signal recorded during the top test the traits were selected growth and decrease in heart rate related to the addition and removal of a mild or moderate workload, respectively.

The trend of the selected sections has been evaluated, and it has been seen that the exponential curve offers the best interpolation of these data.

5.1 Results of first subject

Figure 5.1 reports the tachogram of the whole recorded signal ECG.

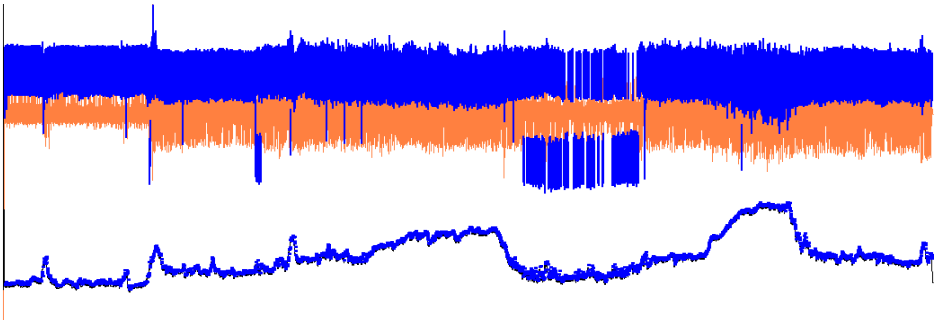

Figure 5.1: Complete tachogram of the signal ECG.

Figure 5.2 shows the heart rate trend during the entire test, both for the tilt test phase and for the top test phase in which the patient is subjected to two different workloads, first a light one (50 W) and then a moderate one (70 W).

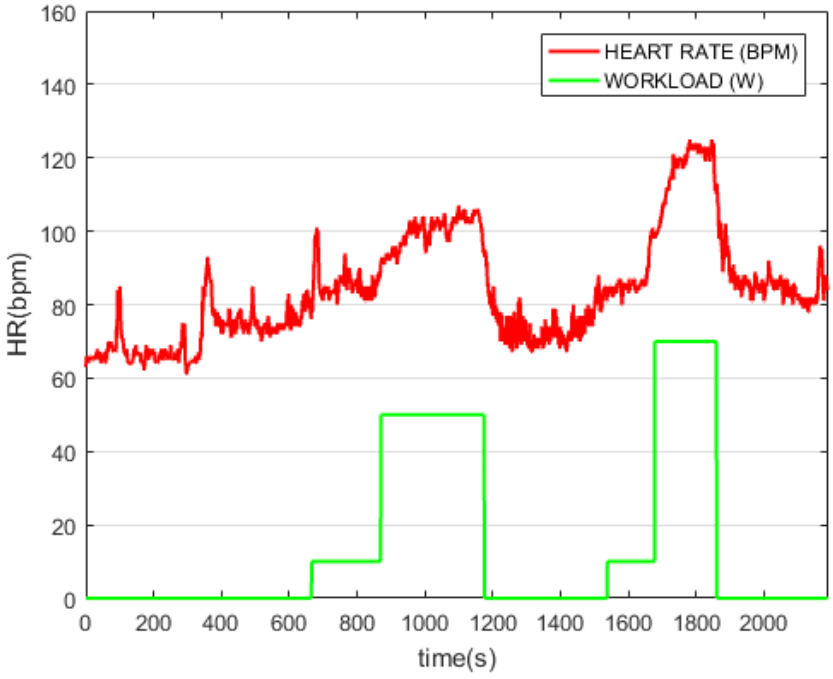

Figure 5.2: Heart rate trend as a function of time.

Figure 5.3 shows the section of the RR intervals, selected through the Kubios software, related to the clinium phase in which the subject is lying on the bed.

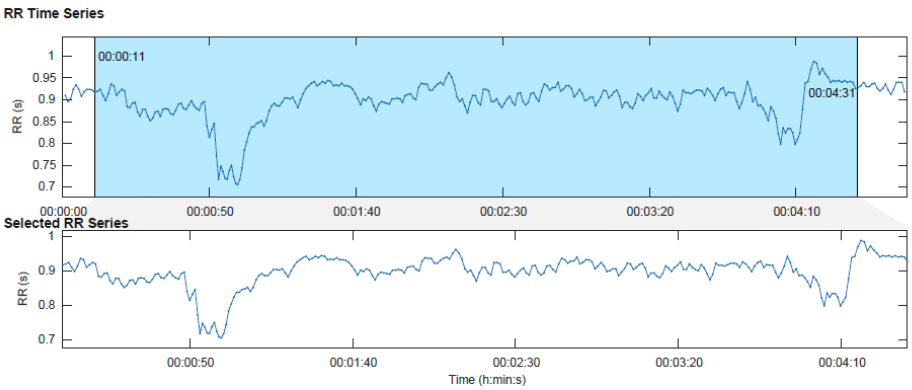

Figure 5.3: Tract of selected RR intervals in the clinium signal for time and frequency domain analysis.

Figure 5.4 shows the distributions of the beat-to-beat RR intervals and the heart rate HR recorded during the clinium phase.

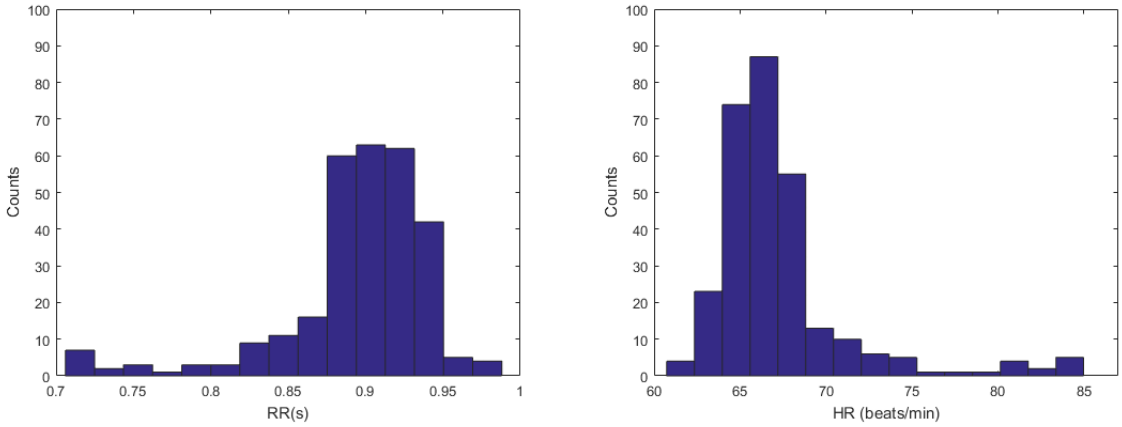

(a) (b)

Figure 5.4: Distributions of the RR intervals (a) and the heart rate HR (b) of the clino phase.

Table 5.1 shows the parameters that quantify the heart rate variability in the time domain.

Time-Domain Results	
Variable	**Value**
Mean RR	894 ms
STD RR	48 ms
Mean HR	67 beats/min
STD HR	1 beats/min
Min HR	62 beats/min
Max HR	83 beats/min

Table 5.1: Variables that quantify HRV during clino phase in the time domain.

Figure 5.5 shows Poincarè plot and the values SD1 and SD2 standard deviations of the distributions along the transverse axis and the bisector.

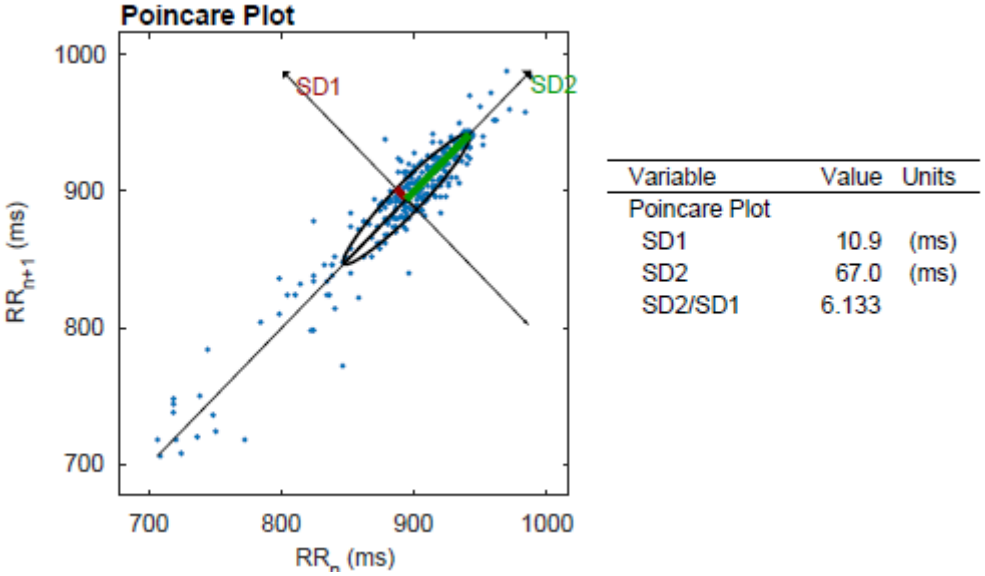

Figure 5.5: Poincarè plot of each RR interval according to the previous one.

Figure 5.6 shows the Fast Fourier Transform (FFT) of the RR intervals, ie the power spectrum is represented, which indicates how the power carried by a signal of a given frequency has been distributed. The Figure 5.7 shows autoregressive methods applied on the RR intervals.

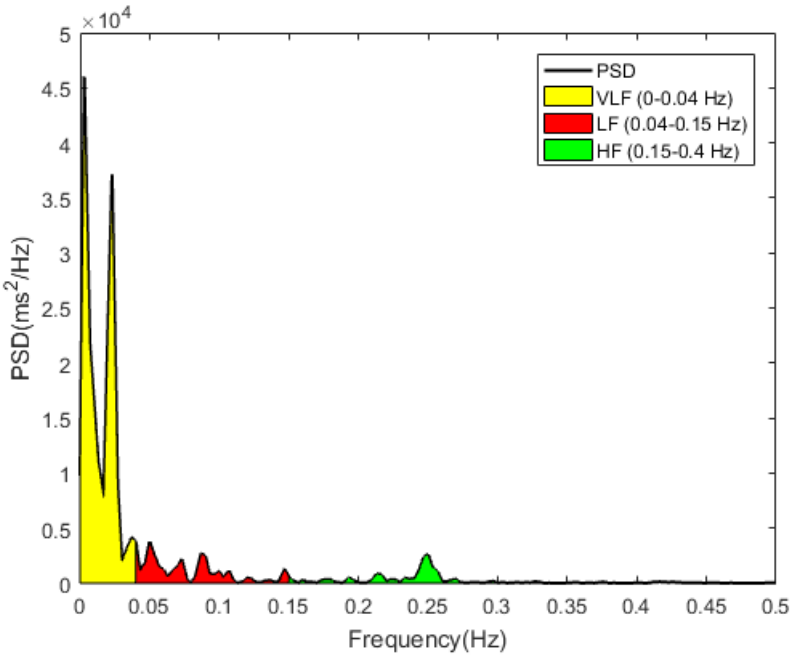

Figure 5.6: Fast Fourier Transform (FFT) of the clinium sygnal.

In the Figure 5.6 and 5.7 it is possible to distinguish three different frequency bands that characterize the sympathetic and vagal activity of the autonomic nervous system.

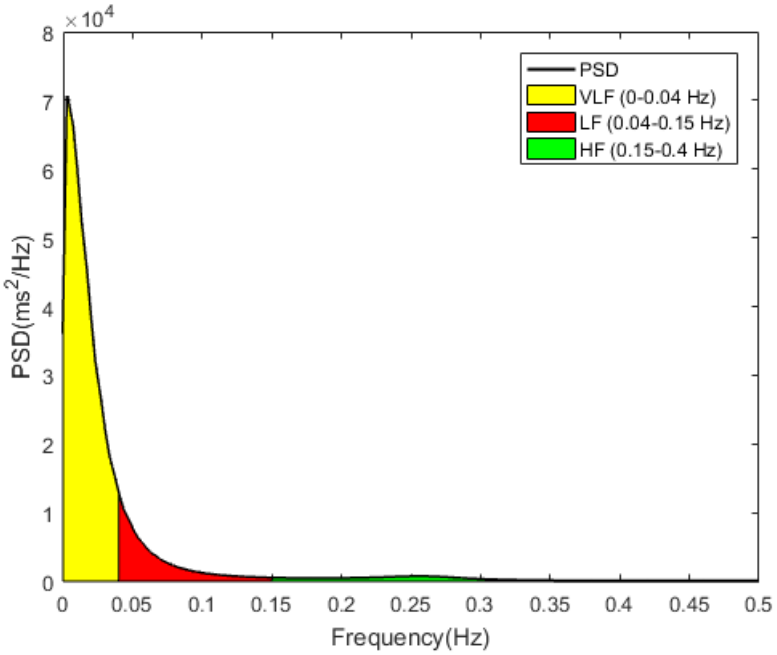

Figure 5.7: Autoregressive analysis of the clinium sygnal.

Table 5.2 shows the parameters that quantify heart rate variability in the frequency domain.

Frequency-Domain Results				
Variable	**VLF**	**LF**	**HF**	**LF/HF**
FFT Results				
Peak (Hz)	0,0033	0,040	0,25	
Power (ms^2)	625,4	114,3	62,4	1,83
Power (%)	77,9	14,3	7,8	
Power (n.u.)		64,7	35,3	
AR Results				
Peak (Hz)	0,0033	0,040	0,26	
Power (ms^2)	1568,5	294,1	86,4	3,41
Power (%)	80,5	15,1	4,4	
Power (n.u.)		77,3	22,7	

Table 5.2: Variables that quantify HRV during clinium phase in the frequency domain.

Figure 5.8 shows the section of the RR intervals, selected through the Kubios software, related to the orthostatic phase in which the subject is standing.

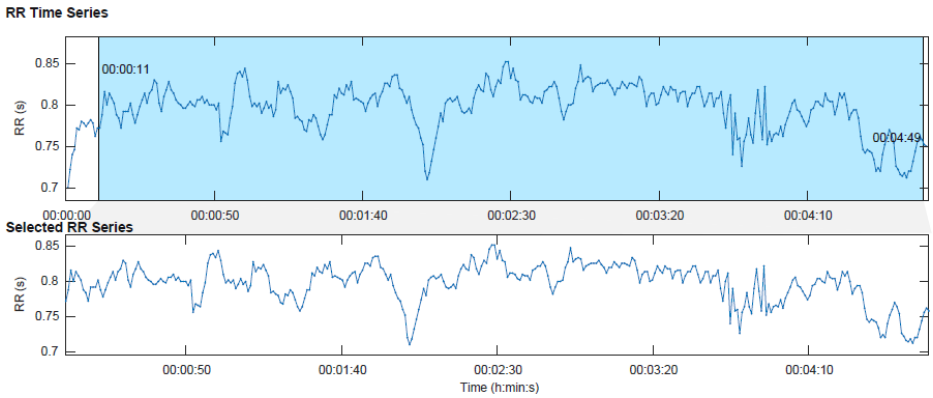

Figure 5.8: Tract of selected RR intervals in the ortho signal for time and frequency domain analysis.

Figure 5.9 shows the distributions of the beat-to-beat RR intervals and the heart rate HR recorded during the ortho phase.

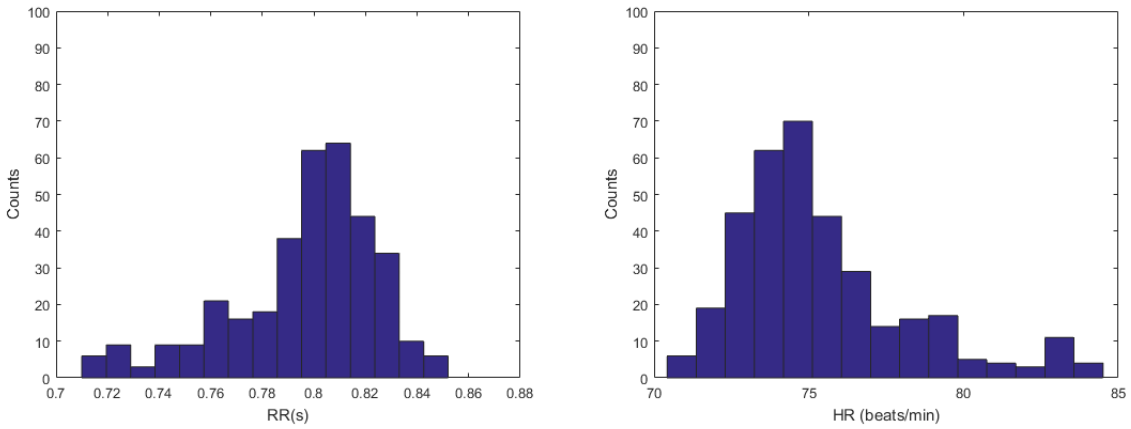

(a) (b)

Figure 5.9: Distributions of the RR intervals (a) and the heart rate HR (b) of the ortho phase.

Table 5.3 shows the parameters that quantify heart rate variability in the time domain.

Time-Domain Results	
Variable	**Value**
Mean RR	797 ms
STD RR	29 ms
Mean HR	75 beats/min
STD HR	1 beats/min
Min HR	71 beats/min
Max HR	84 beats/min

Table 5.3: Variables that quantify HRV during ortho phase in the time domain.

Figure 5.10 shows Poincarè plot and the values of the SD1 and SD2 standard deviations of the distributions along the transverse axis and the bisector.

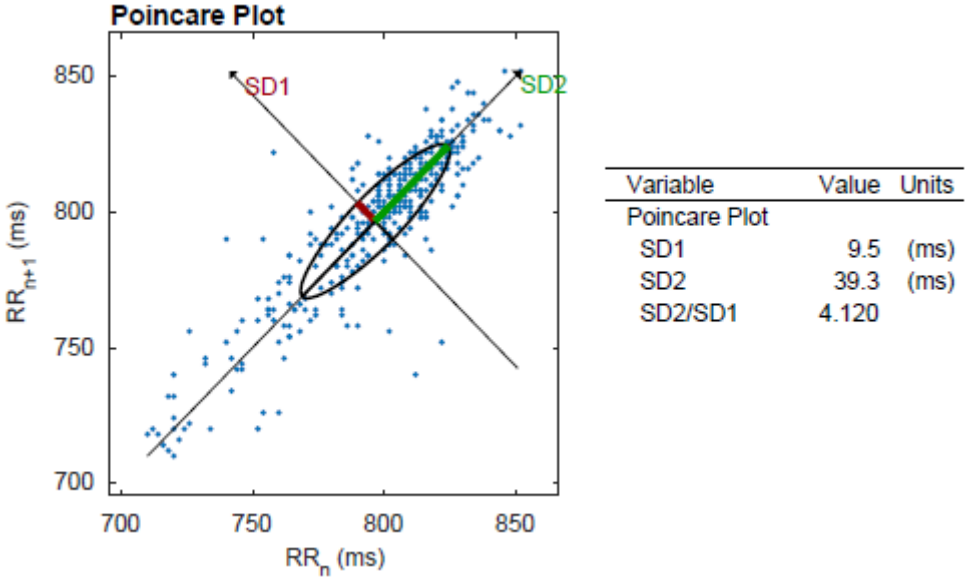

Figure 5.10: Poincarè plot of each RR interval according to the previous one.

Figure 5.11 shows the Fast Fourier Transform (FFT) of the RR intervals of the ortho signal ECG, ie the power spectrum is represented, which indicates how the power carried by a signal of a given frequency has been distributed.

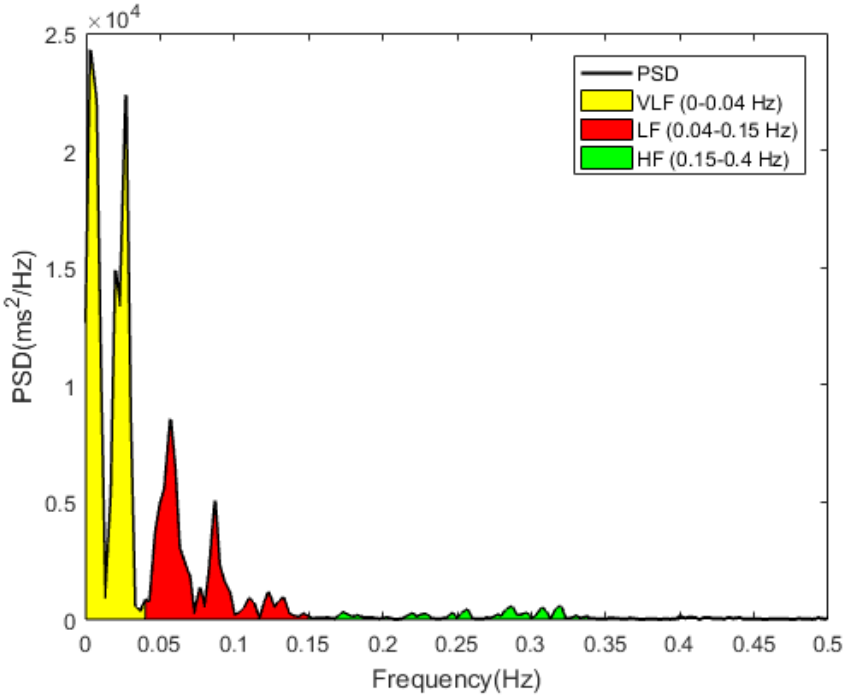

Figure 5.11: Fast Fourier Transform (FFT) of the ortho sygnal.

Figure 5.12 shows analysis of the ortho signal obtained with autoregressive methods.

In the Figure 5.11 and 5.12 it is possible to distinguish three different frequency bands that characterize the sympathetic and vagal activity of the autonomic nervous system.

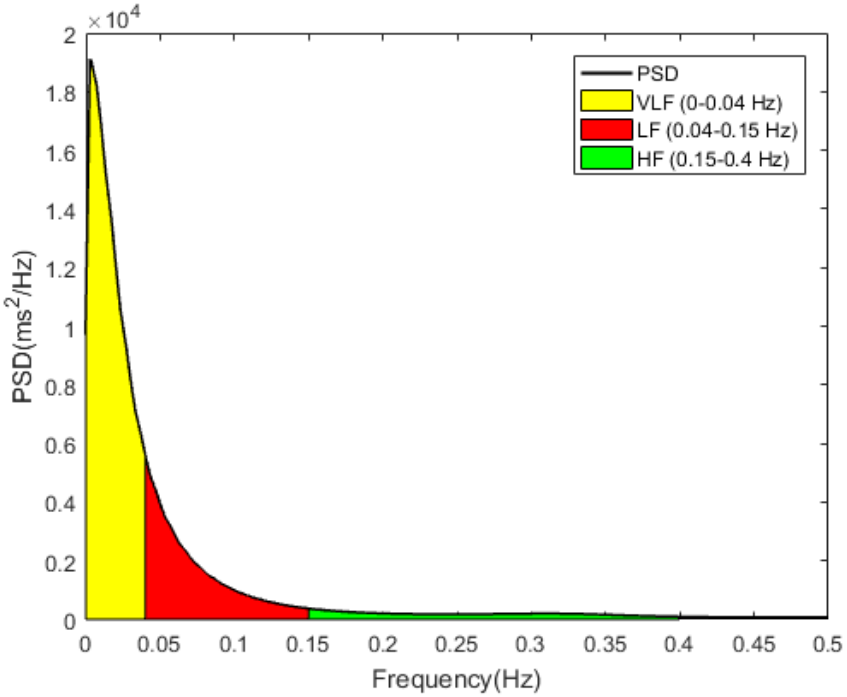

Figure 5.12: Autoregressive analysis of the ortho sygnal.

Table 5.4 shows the parameters that quantify heart rate variability in the frequency domain.

Frequency-Domain Results				
Variable	**VLF**	**LF**	**HF**	**LF/HF**
FFT Results				
Peak (Hz)	0,0033	0,057	0,32	
Power (ms^2)	432,8	197,9	29,0	6,83
Power (%)	65,6	29,9	4,4	
Power (n.u.)		87,1	12,8	
AR Results				
Peak (Hz)	0,0033	0,040	0,15	
Power (ms^2)	479,6	178,6	43,6	4,10
Power (%)	68,3	25,4	6,2	
Power (n.u.)		80,3	19,6	

Table 5.4: Variables that quantify HRV during ortho phase in the frequency domain.

Figure 5.13 shows the ECG signal recorded during the top test execution and the relative tacogram.

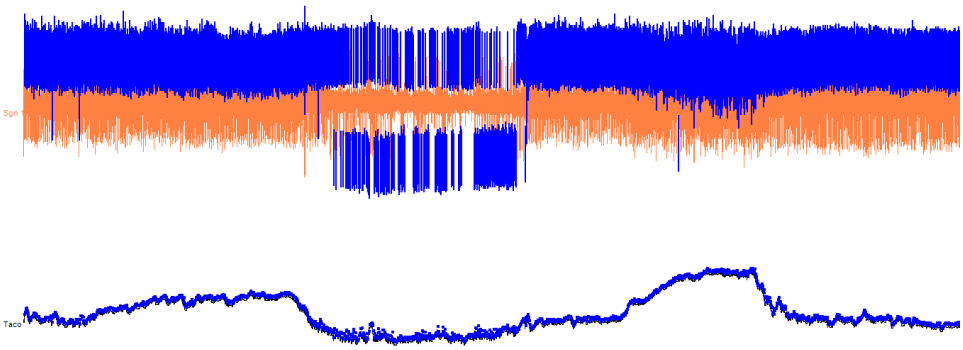

Figure 5.13: Tachogram of the signal ECG recorded during top test.

Figure 5.14 shows the heart rate trend during the top test execution, highlighting in blue the areas where there is a growth and decrease of the frequency in the transition phases in which the workload is added or removed.

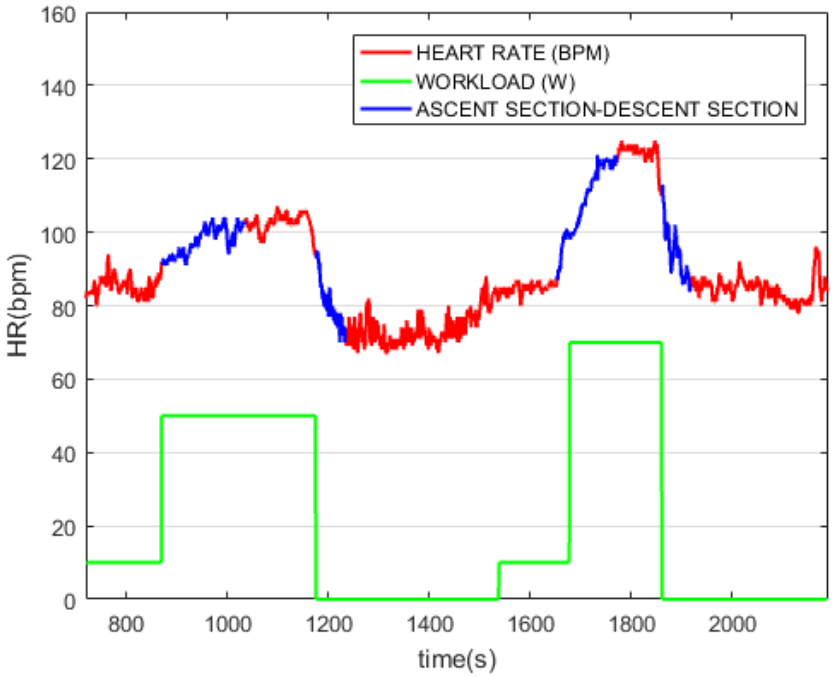

Figure 5.14: Heart rate trend as a function of time during the top test.

Figure 5.15 shows the exponential interpolation in the phase of heart rate increase at the insertion of the first workload (beginning of step 1).

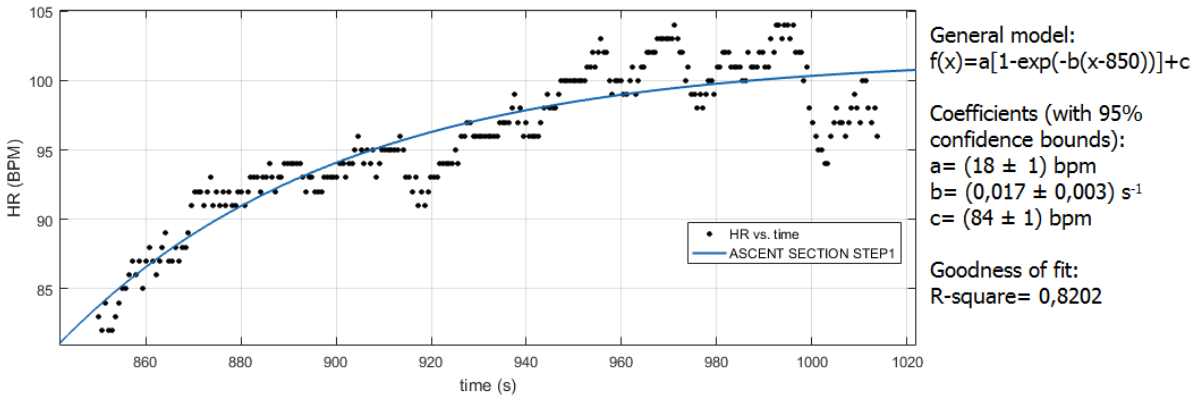

Figure 5.15: Exponential interpolation of the stress adaptation curve in response to the first workload.

Figure 5.16 shows the exponential interpolation in the passive recovery phase in which the heart rate decreases at the removal of the first workload (end of step 1).

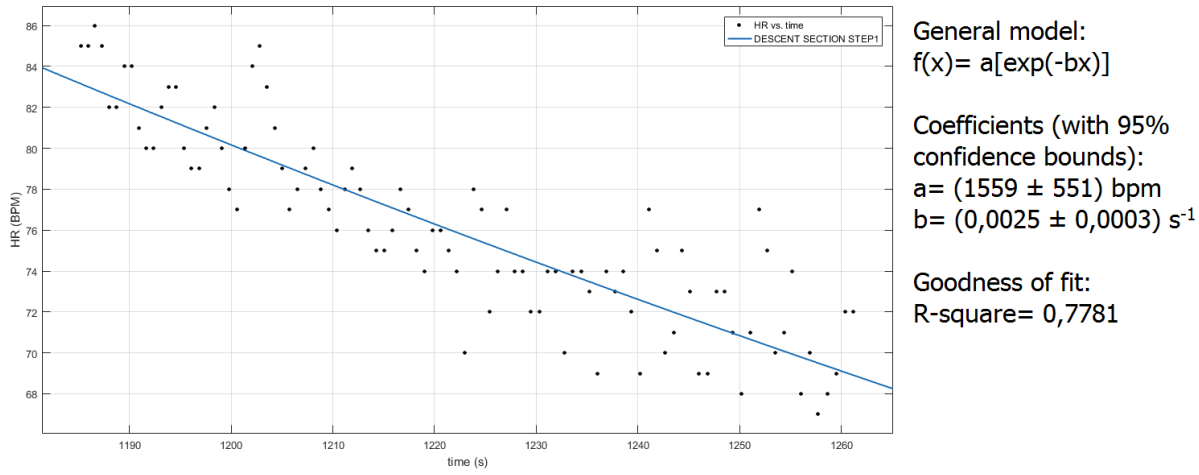

Figure 5.16: Exponential interpolation of the passive recovery curve after removal of the first workload.

Figure 5.17 shows the exponential interpolation in the phase of heart rate increase at the insertion of the second workload (beginning of step 2).

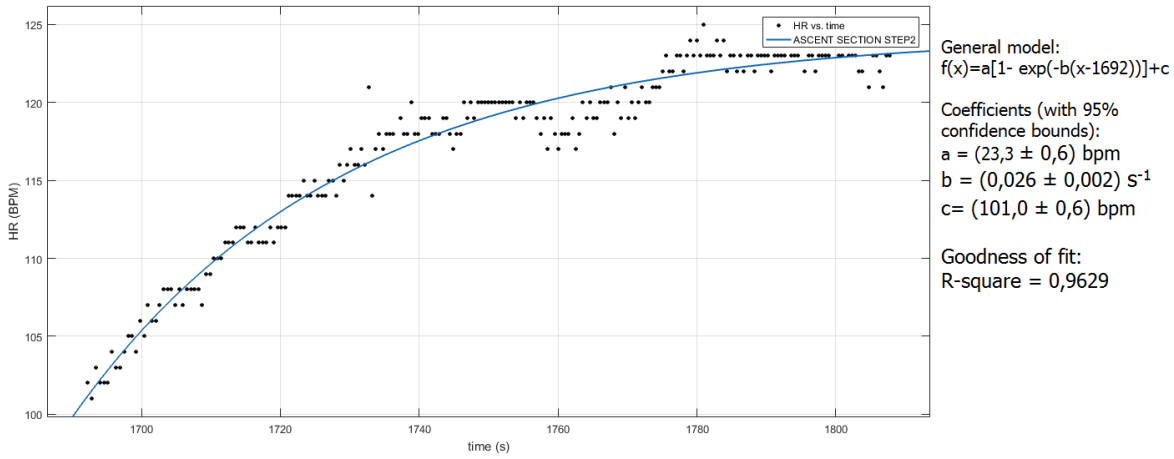

Figure 5.17: Exponential interpolation of the stress adaptation curve in response to the second workload.

Figure 5.18 shows the exponential interpolation in the passive recovery phase in which the heart rate decreases at the removal of the second workload (end of step 2).

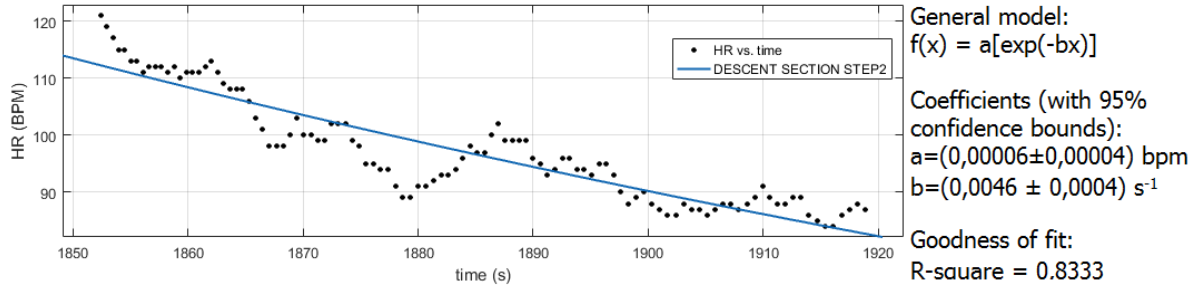

Figure 5.18: Exponential interpolation of the passive recovery curve after removal of the second workload.

5.2 Results of second subject

Figure 5.19 shows the tacogram of the whole recorded signal ECG.

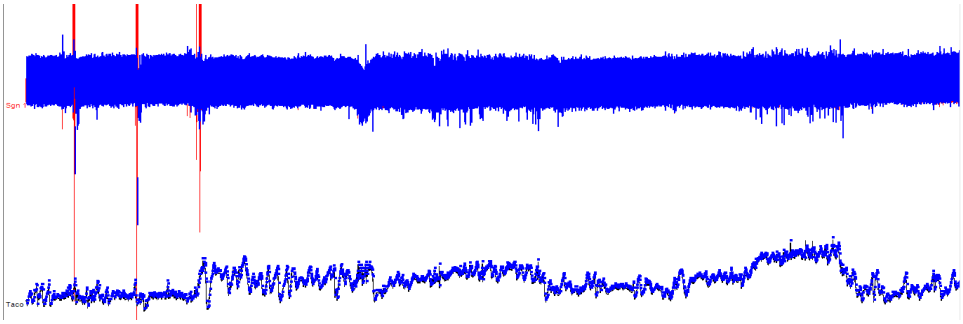

Figure 5.19: Complete tachogram of the signal ECG.

Figure 5.20 shows the trend of the heart rate during the entire test, both for the tilt test phase and for the top test phase in which the patient was subjected to two different workloads, before a light one (50 W) and then a moderate one (70 W).

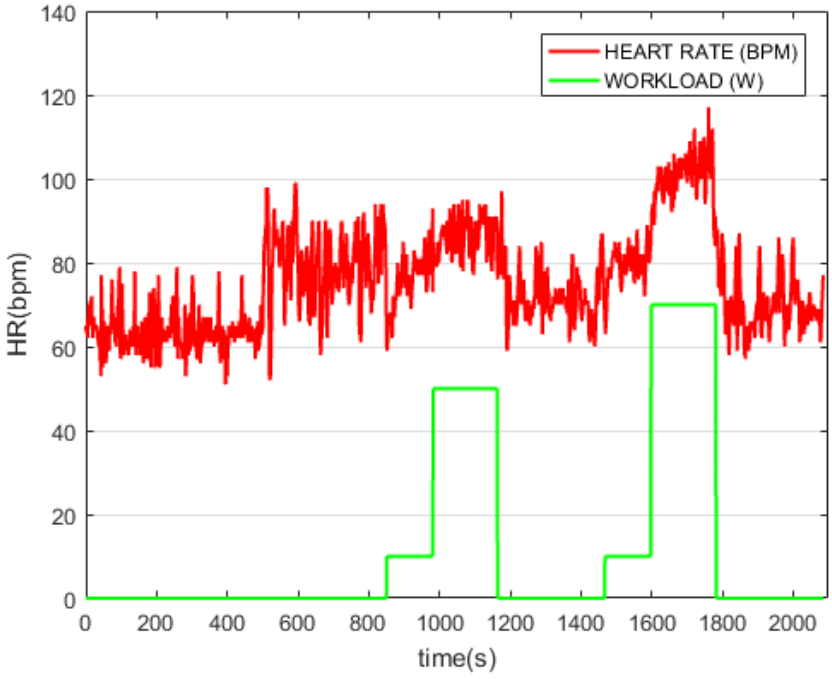

Figure 5.20: Heart rate trend as a function of time.

Figure 5.21 shows the section of the RR intervals, selected through the Kubios software, related to the clinium phase in which the subject is lying on the bed.

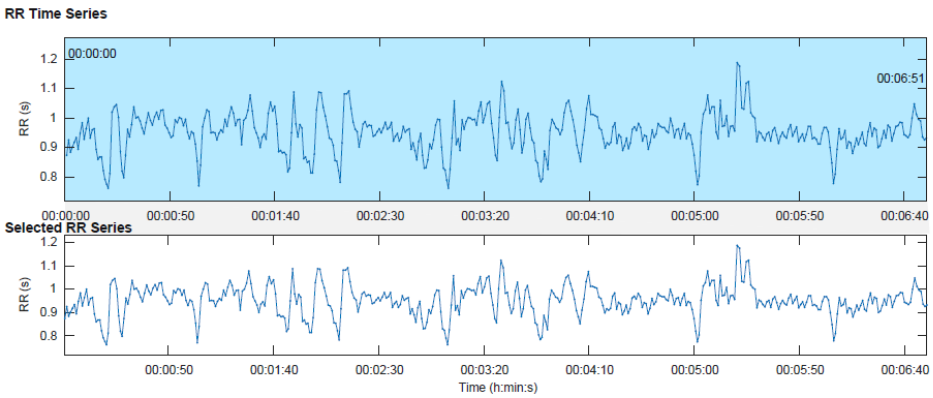

Figure 5.21: Tract of selected RR intervals in the clino signal for time and frequency domain analysis

Figure 5.22 shows the distributions of the beat-to-beat RR intervals and the heart rate HR recorded during the clinium phase.

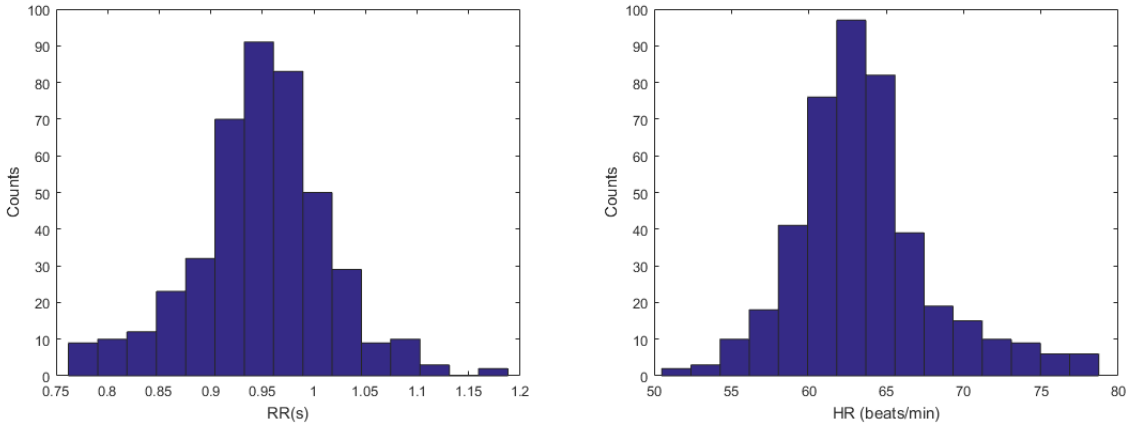

(a) (b)

Figure 5.22: Distributions of the RR intervals (a) and the heart rate HR (b) of the clino phase.

Table 5.5 shows the parameters that quantify the variability of heart rate in the time domain.

Time-Domain Results	
Variable	**Value**
Mean RR	949 ms
STD RR	66 ms
Mean HR	63 beats/min
STD HR	1 beats/min
Min HR	54 beats/min
Max HR	76 beats/min

Table 5.5: Variables that quantify HRV during ortho phase in the time domain.

Figure 5.23 shows Poincarè plot and the values SD1 and SD2 standard deviations of the distributions along the transverse axis and the bisector.

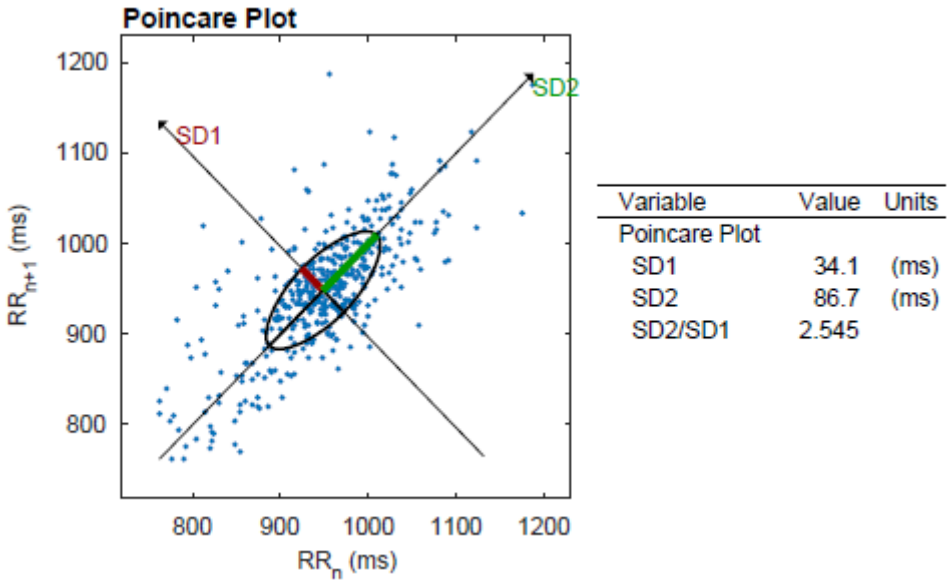

Figure 5.23: Poincarè plot of each RR interval according to the previous one.

Figure 5.24 shows the Fast Fourier Transform (FFT) of the RR intervals of the clino signal ECG, ie the power spectrum is represented, which indicates how the power carried by a signal of a given frequency has been distributed.

The Figure 5.25 shows analysis of the clinium signal obtained with autoregressive methods.

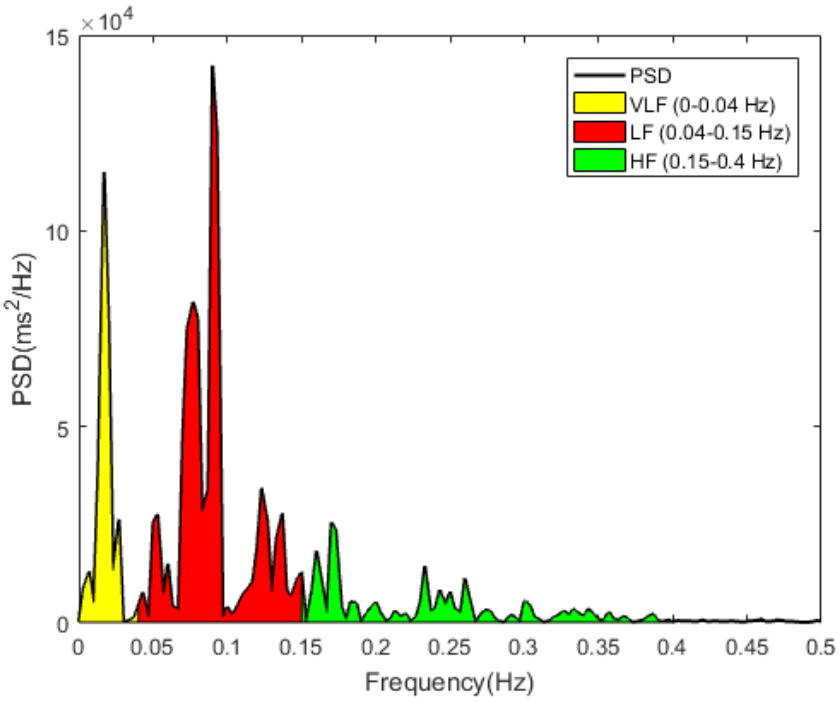

Figure 5.24: Fast Fourier Transform (FFT) of the clinium sygnal.

In the Figure 5.24 and 5.25 it is possible to distinguish three different frequency bands that characterize the sympathetic and vagal activity of the autonomic nervous system.

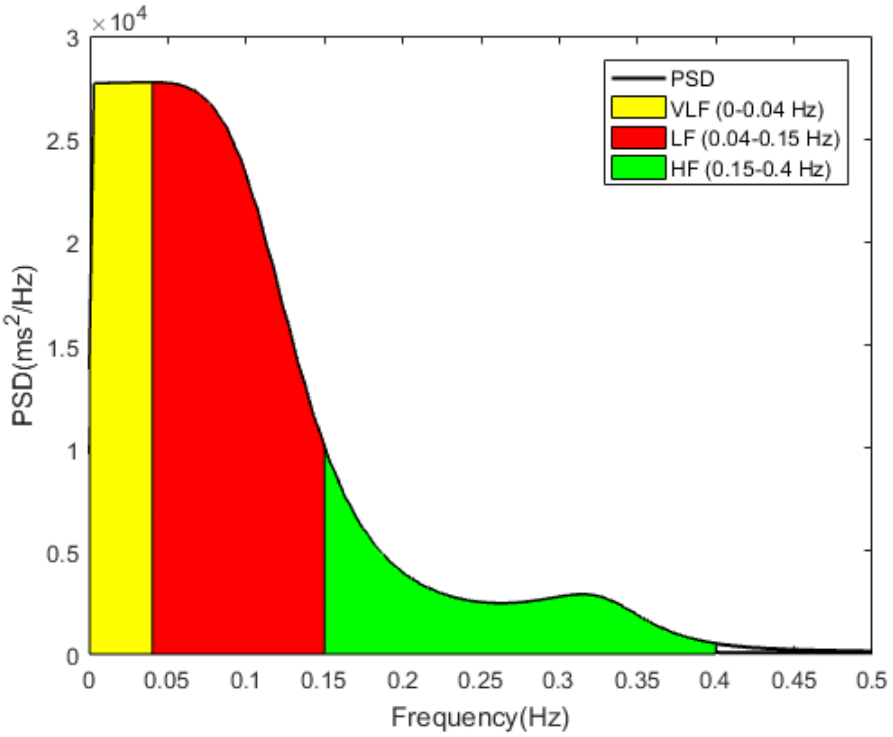

Figure 5.25: Autoregressive analysis of the clinium sygnal.

Table 5.6 shows the parameters that quantify the heart rate variability in the frequency domain.

Frequency-Domain Results				
Variable	**VLF**	**LF**	**HF**	**LF/HF**
FFT Results				
Peak (Hz)	0,017	0,09	0,17	
Power (ms^2)	1005,4	3042,9	883,3	3,44
Power (%)	20,4	61,7	17,9	
Power (n.u.)		77,5	22,5	
AR Results				
Peak (Hz)	0,04	0,04	0,15	
Power (ms^2)	1084,7	2420,5	779,0	3,11
Power (%)	25,3	56,5	18,2	
Power (n.u.)		75,6	24,3	

Table 5.6: Variables that quantify HRV during clinium phase in the frequency domain.

Figure 5.26 shows the section of the RR intervals, selected through the Kubios software, related to the ortho phase in which the subject is standing.

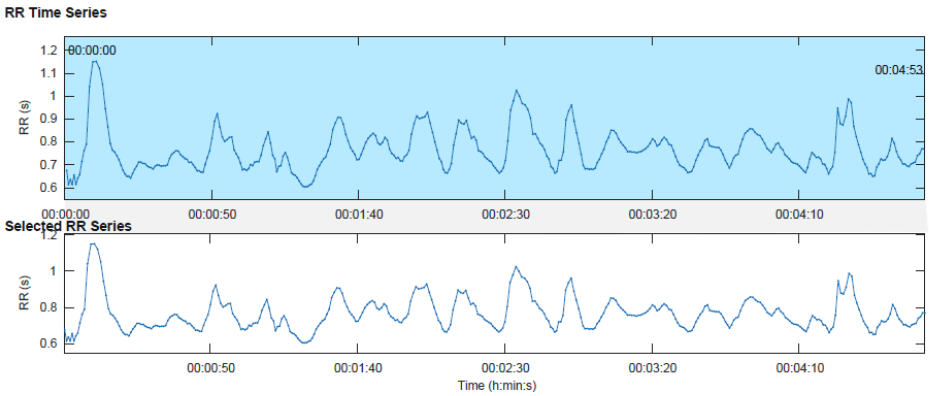

Figure 5.26: Tract of selected RR intervals in the ortho signal for time and frequency domain analysis.

Figure 5.27 shows the distributions of the beat-to-beat RR intervals and the heart rate HR recorded during the ortho phase.

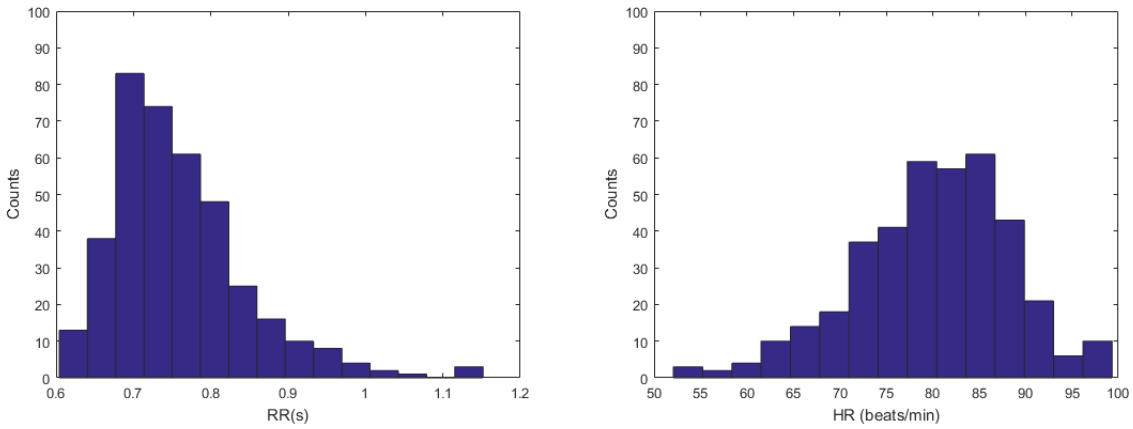

(a) (b)

Figure 5.27: Distributions of the RR intervals (a) and the heart rate HR (b) of the ortho phase.

Table 5.7 shows the parameters that quantify the variability of heart rate in the time domain.

Time-Domain Results	
Variable	**Value**
Mean RR	758 ms
STD RR	688 ms
Mean HR	79 beats/min
STD HR	2 beats/min
Min HR	54 beats/min
Max HR	99 beats/min

Table 5.7: Variables that quantify HRV during ortho phase in the time domain.

Figure 5.28 shows Poincarè plot and the values SD1 and SD2 standard deviations of the distributions along the transverse axis and the bisector.

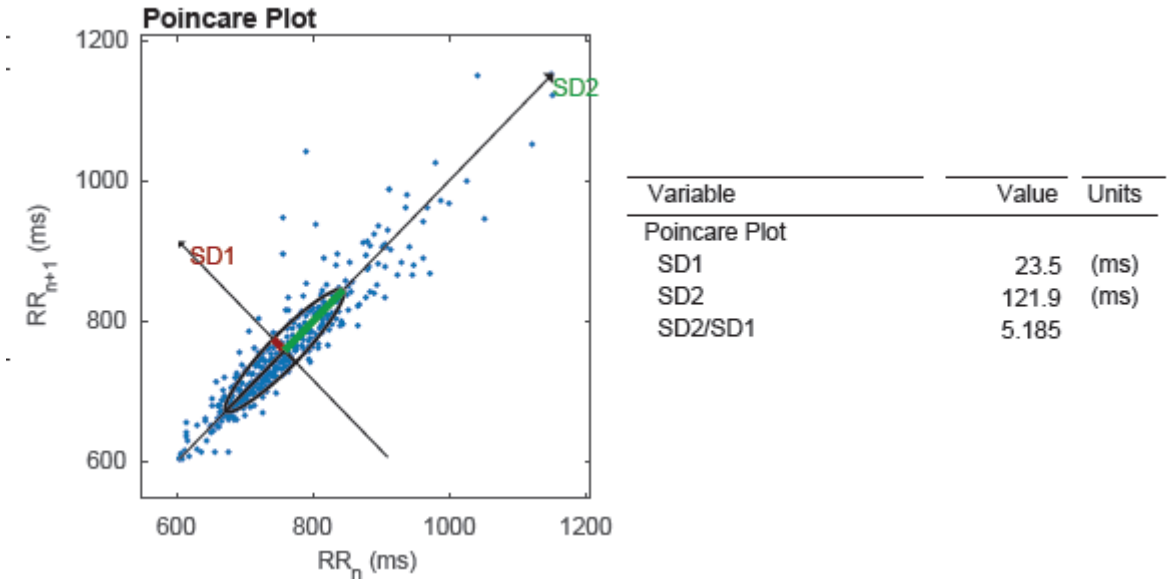

Figure 5.28: Poincarè plot of each RR interval according to the previous one.

Figure 5.29 shows the Fast Fourier Transform (FFT) of the RR intervals of the ortho signal ECG, ie the power spectrum is represented, which indicates how the power carried by a signal of a given frequency has been distributed.

Figure 5.30 shows analysis of the ortho signal obtained with autoregressive methods.

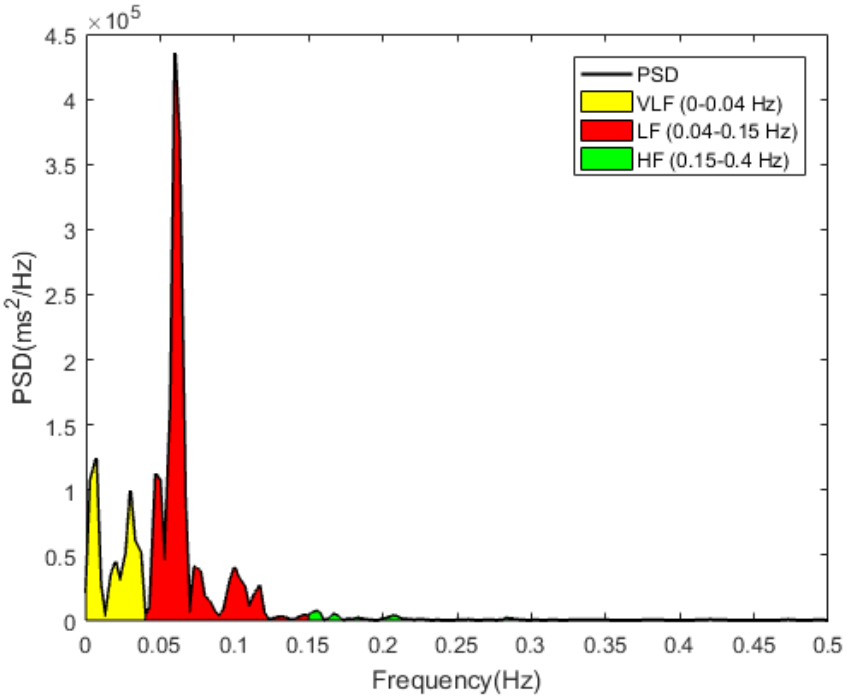

Figure 5.29: Fast Fourier Transform (FFT) of the ortho sygnal.

In the Figure 5.29 and 5.30 it is possible to distinguish three different frequency bands that characterize the sympathetic and vagal activity of the autonomic nervous system.

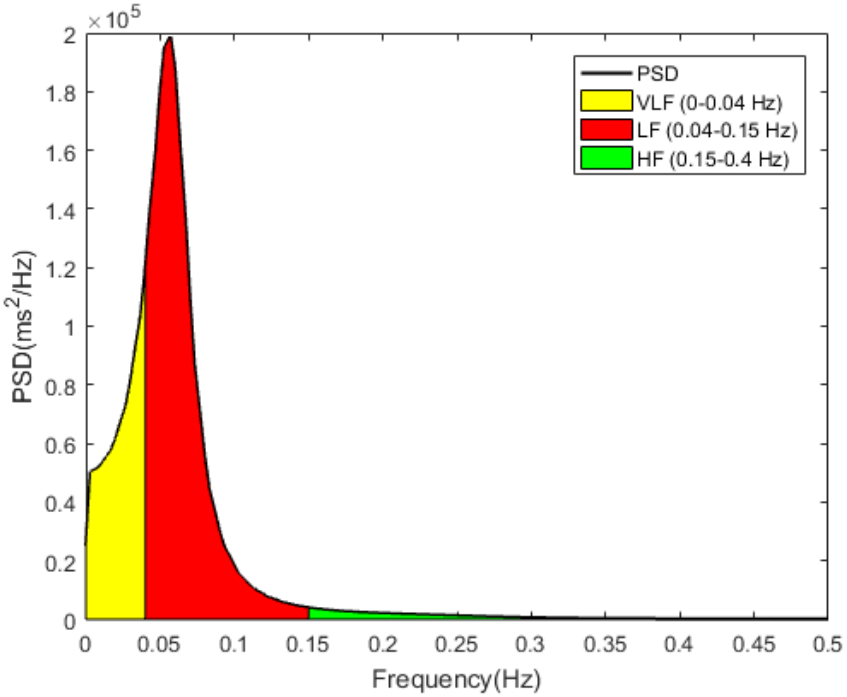

Figure 5.30: Autoregressive analysis of the ortho sygnal.

Table 5.8 shows the parameters that quantify the heart rate variability in the frequency domain.

Frequency-Domain Results				
Variable	**VLF**	**LF**	**HF**	**LF/HF**
FFT Results				
Peak (Hz)	0,007	0,06	0,16	
Power (ms^2)	2165,0	5640,6	186,1	30,3
Power (%)	27,1	70,6	2,3	
Power (n.u.)		96,8	3,2	
AR Results				
Peak (Hz)	0,040	0,057	0,15	
Power (ms^2)	2722,2	6781,5	298,3	22,7
Power (%)	27,8	69,2	3,04	
Power (n.u.)		95,8	4,2	

Table 5.8: Variables that quantify HRV during ortho phase in the frequency domain.

Figure 5.31 shows the ECG signal recorded during the top test execution and the relative tacogram.

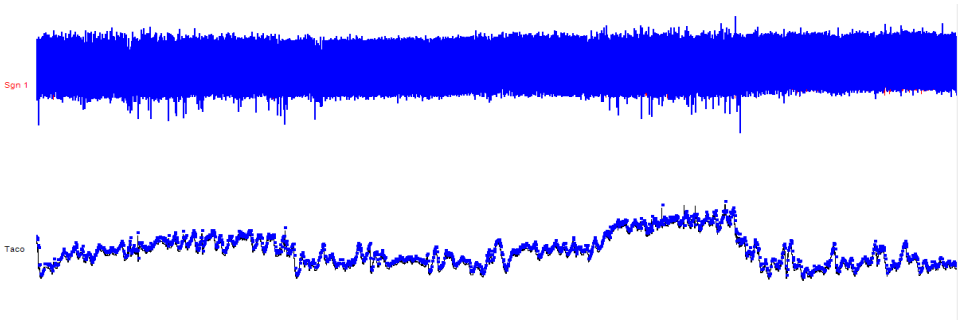

Figure 5.31: Heart rate trend as a function of time during the top test.

Figure 5.32 shows the heart rate trend during the top test execution, highlighting in blue the areas where there is a growth and decrease of the frequency in the transition phases in which the workload is added or removed.

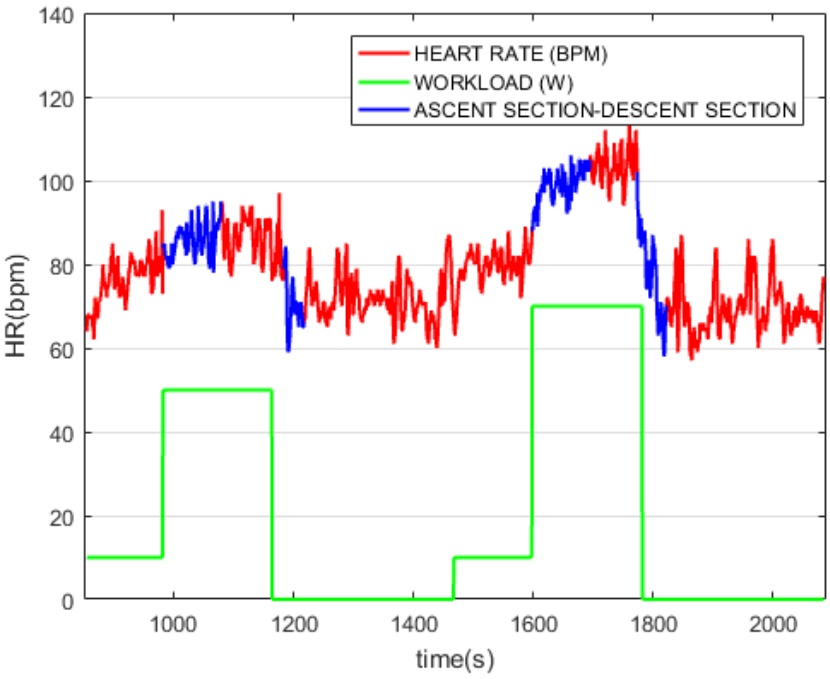

Figure 5.32: Heart rate trend as a function of time during the top test.

Figure 5.33 shows the exponential interpolation in the phase of heart rate increase at the insertion of the first workload (beginning of step 1).

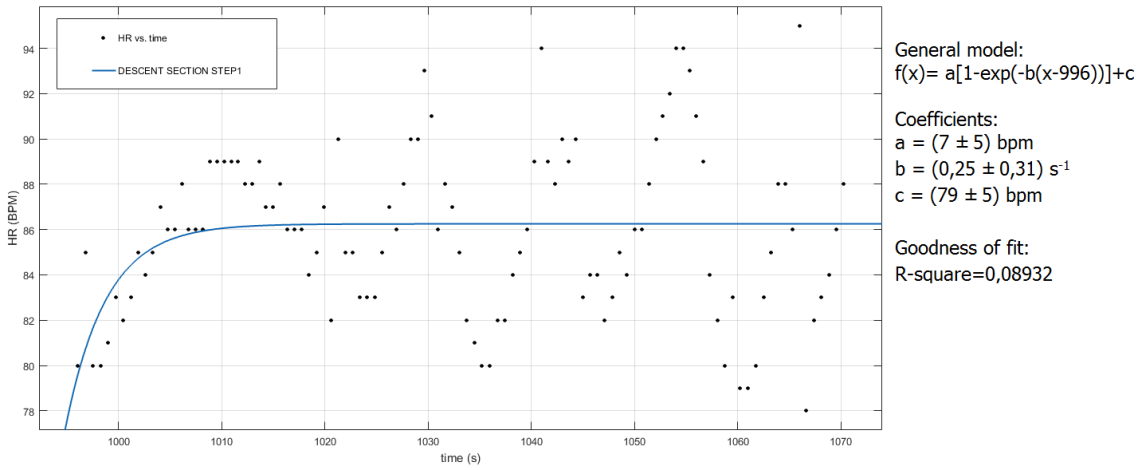

Figure 5.33: Exponential interpolation of the stress adaptation curve in response to the first workload.

Figure 5.34 shows the exponential interpolation in the passive recovery phase in which the heart rate decreases at the removal of the first workload (end of step 1).

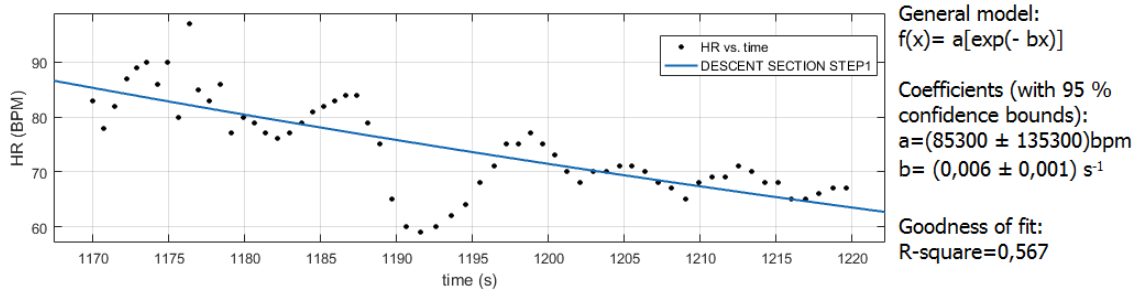

Figure 5.34: Exponential interpolation of the passive recovery curve after removal of the first workload.

Figure 5.35 shows the exponential interpolation in the phase of heart rate increase at the insertion of the first workload (beginning of step 2).

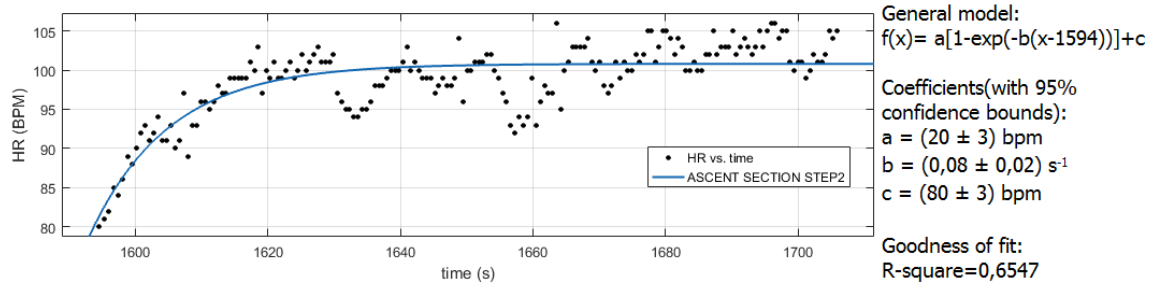

Figure 5.35: Exponential interpolation of the stress adaptation curve in response to the second workload.

Figure 5.34 shows the exponential interpolation in the passive recovery phase in which the heart rate decreases at the removal of the second workload (end of step 2).

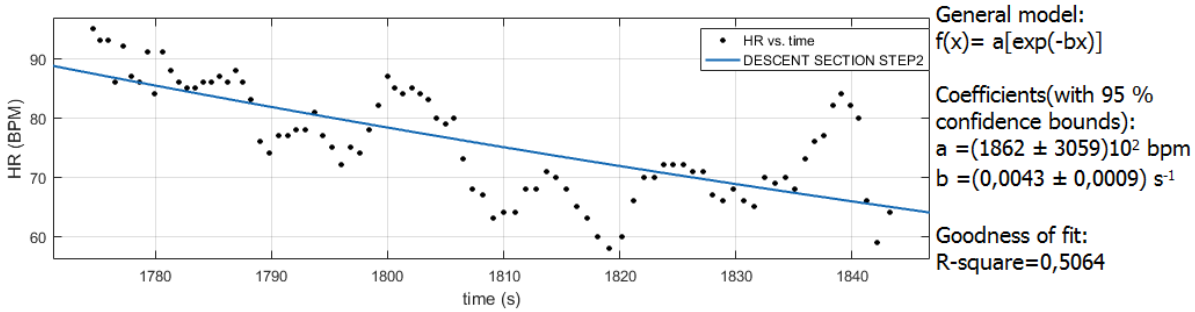

Figure 5.36: Exponential interpolation of the passive recovery curve after removal of the second workload.

5.3 Results of third subject

Figure 5.37 shows the tachogram of the whole recorded signal ECG.

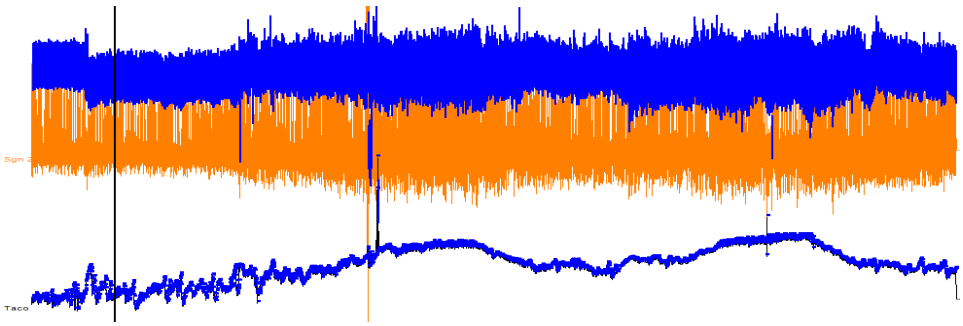

Figure 5.37: Complete tachogram of the signal ECG.

Figure 5.38 shows the trend of the heart rate during the entire test, both for the tilt test phase and for the top test phase in which the patient was subjected to two different workloads, before a light one (50 W) and then a moderate one (70 W).

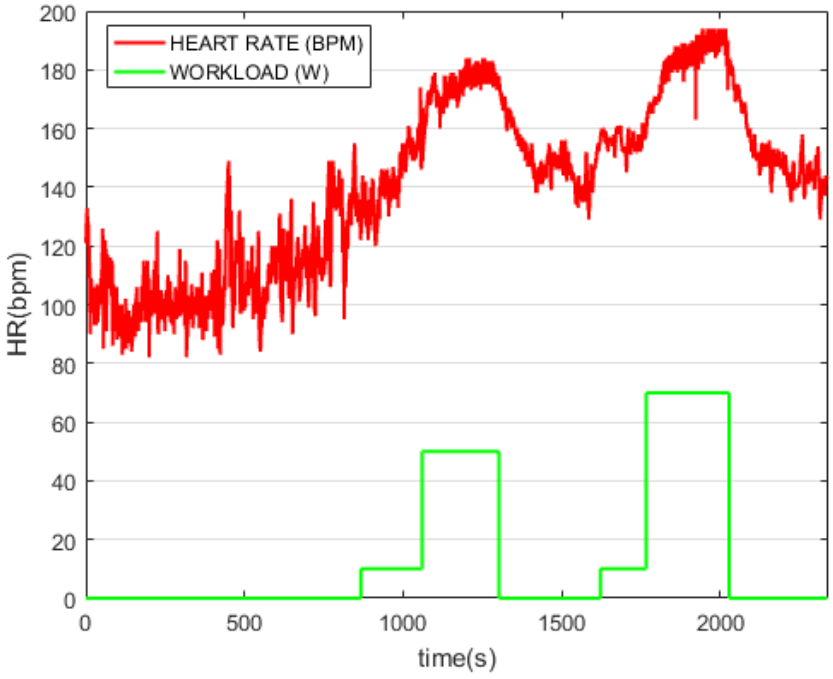

Figure 5.38: Heart rate trend as a function of time.

Figure 5.39 shows the section of the RR intervals, selected through the Kubios software, related to the clinium phase in which the subject is lying on the bed.

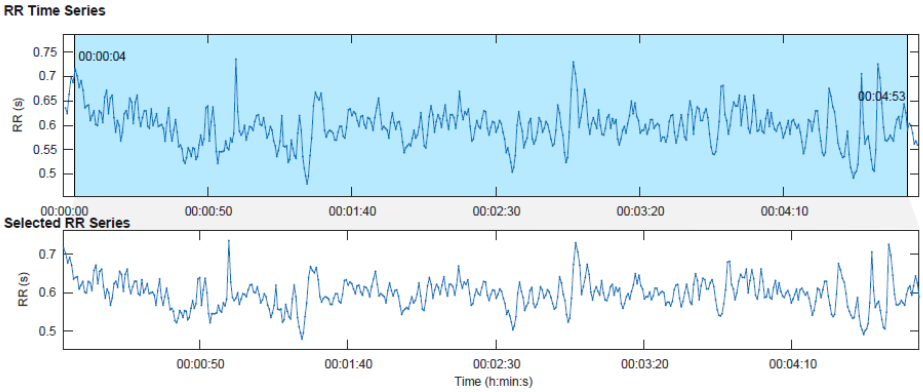

Figure 5.39: Tract of selected RR intervals in the clino signal for time and frequency domain analysis.

Figure 5.40 shows the distributions of the beat-to-beat RR intervals and the heart rate HR recorded during the clinium phase.

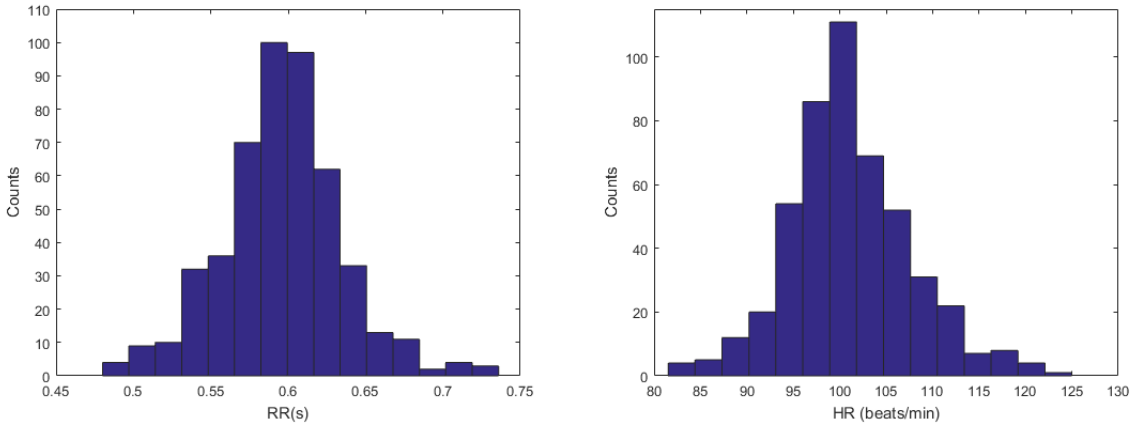

(a) (b)

Figure 5.40: Distributions of the RR intervals (a) and the heart rate HR (b) of the clino phase.

Table 5.9 shows the parameters that quantify the heart rate variability in the time domain.

Time-Domain Results	
Variable	**Value**
Mean RR	596 ms
STD RR	39 ms
Mean HR	101 beats/min
STD HR	2 beats/min
Min HR	87 beats/min
Max HR	119 beats/min

Table 5.9: Variables that quantify HRV during clino phase in the time domain.

Figure 5.41 shows Poincarè plot and the values SD1 and SD2 standard deviations of the distributions along the transverse axis and the bisector.

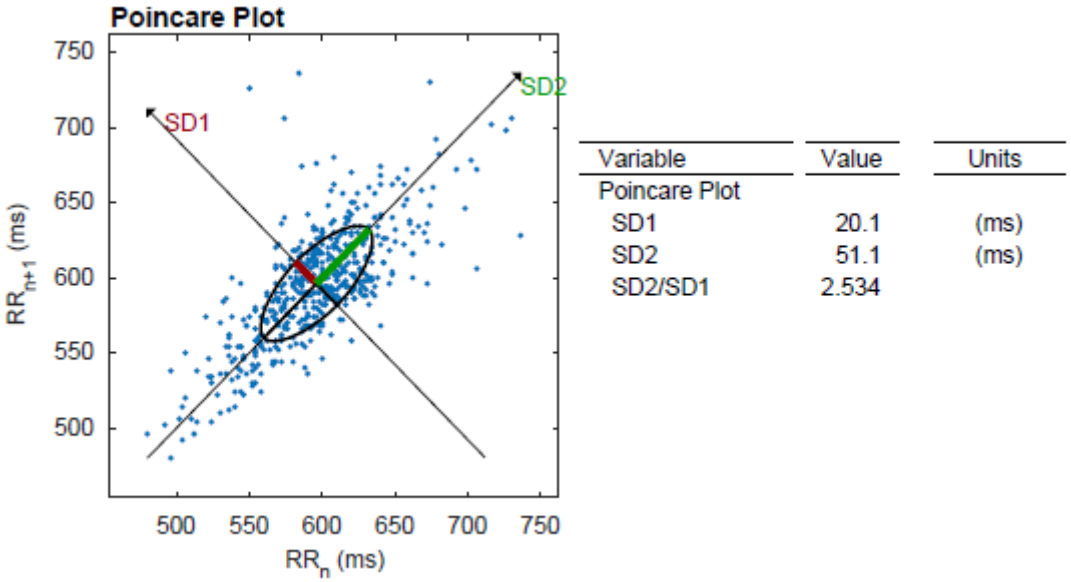

Figure 5.41: Poincarè plot of each RR interval according to the previous one.

Figure 5.42 shows the Fast Fourier Transform (FFT) of the RR intervals of the clino signal ECG, ie the power spectrum is represented, which indicates how the power carried by a signal of a given frequency has been distributed.

Figure 5.43 shows analysis of the clino signal obtained with autoregressive methods.

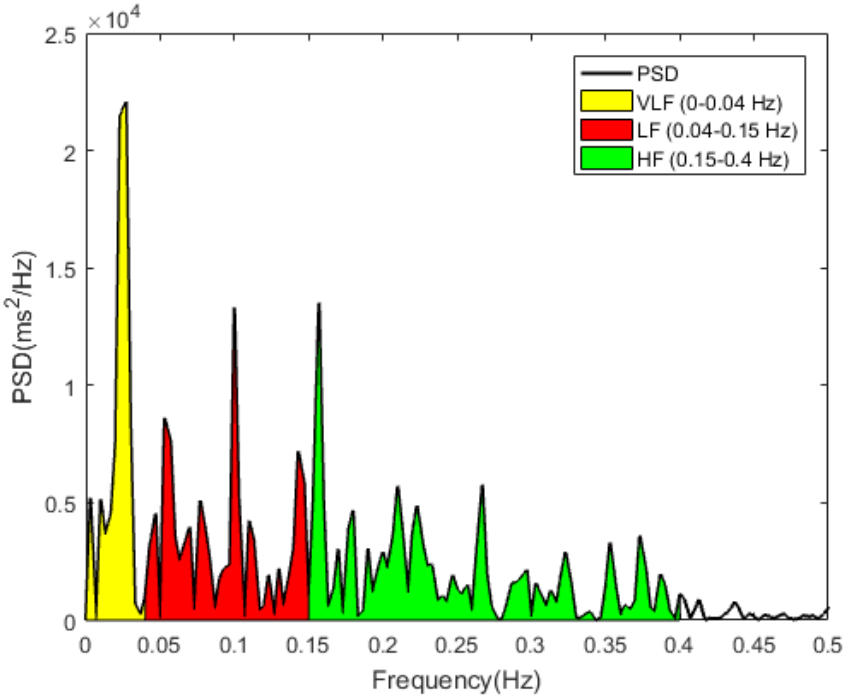

Figure 5.42: Fast Fourier Transform (FFT) of the clinium sygnal.

In the figure 5.42 and 5.43 it is possible to distinguish three different frequency bands that characterize the sympathetic and vagal activity of the autonomic nervous system.

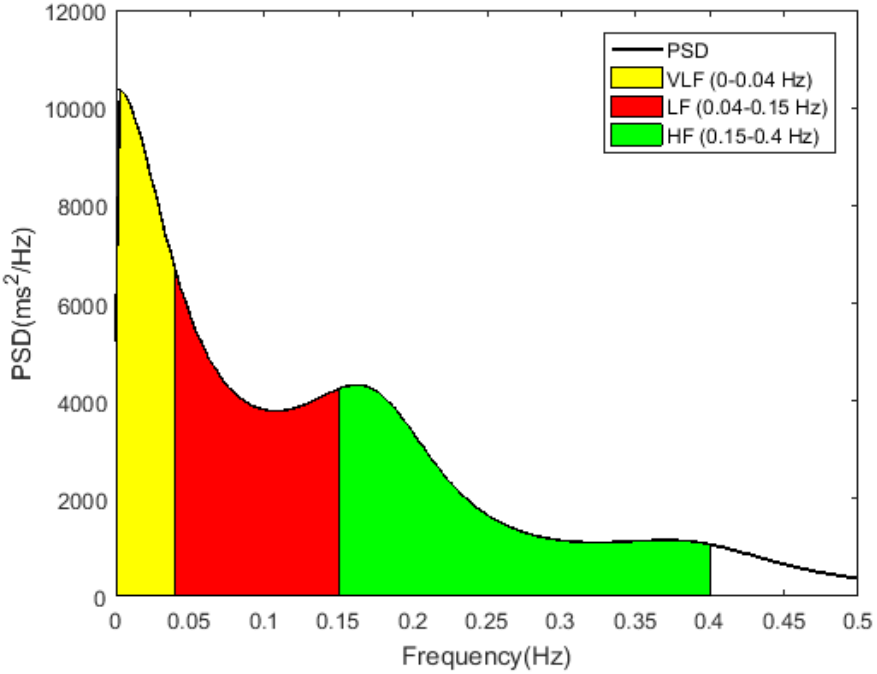

Figure 5.43: Autoregressive analysis of the clinium sygnal.

Table 5.10 shows the parameters that quantify the variability of heart rate in the frequency domain.

Frequency-Domain Results				
Variable	**VLF**	**LF**	**HF**	**LF/HF**
FFT Results				
Peak (Hz)	0,027	0,100	0,16	
Power (ms^2)	264,3	359,6	468,6	0,77
Power (%)	24,1	32,9	42,8	
Power (n.u.)		43,3	56,4	
AR Results				
Peak (Hz)	0,0033	0,040	0,163	
Power (ms^2)	345,5	481,8	499,4	0,97
Power (%)	26,0	36,3	37,6	
Power (n.u.)		49,0	50,8	

Table 5.10: Variables that quantify HRV during clino phase in the frequency domain.

Figure 5.44 shows the section of the RR intervals, selected through the Kubios software, related to the ortho phase in which the subject is standing.

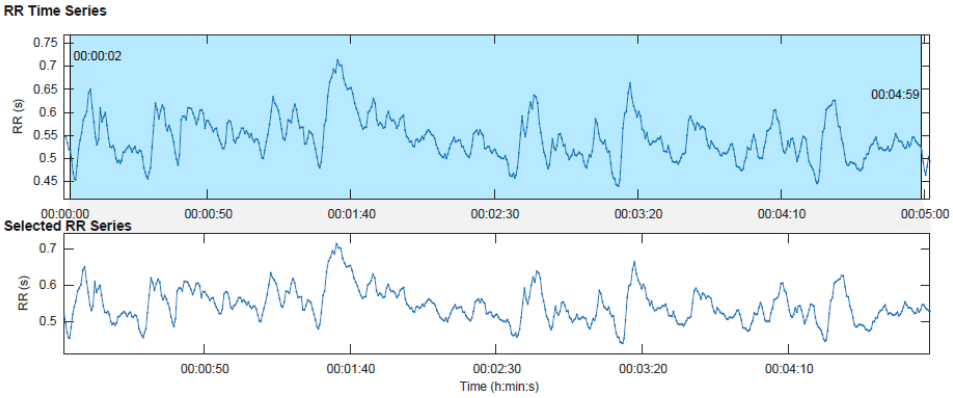

Figure 5.44: Tract of selected RR intervals in the ortho signal for time and frequency domain analysis.

Figure 5.45 shows the distributions of the beat-to-beat RR intervals and the heart rate HR recorded during the ortho phase.

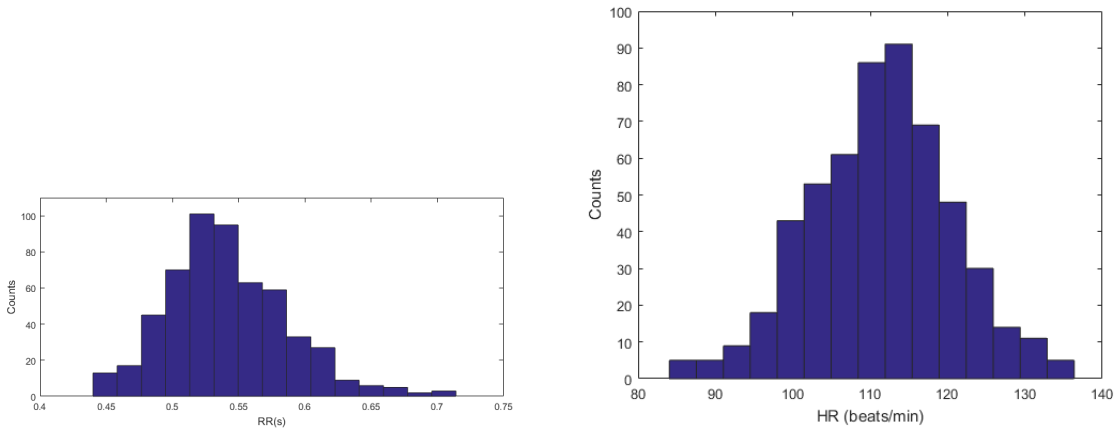

(a) (b)

Figure 5.45: Distributions of the RR intervals (a) and the heart rate HR (b) of the ortho phase.

Table 5.11 shows the parameters that quantify the heart rate variability in the time domain.

Time-Domain Results	
Variable	**Value**
Mean RR	542 ms
STD RR	46 ms
Mean HR	111 beats/min
STD HR	2 beats/min
Min HR	86 beats/min
Max HR	134 beats/min

Table 5.11: Variables that quantify HRV during ortho phase in the time domain.

Figure 5.46 shows Poincarè plot and the values SD1 and SD2 standard deviations of the distributions along the transverse axis and the bisector.

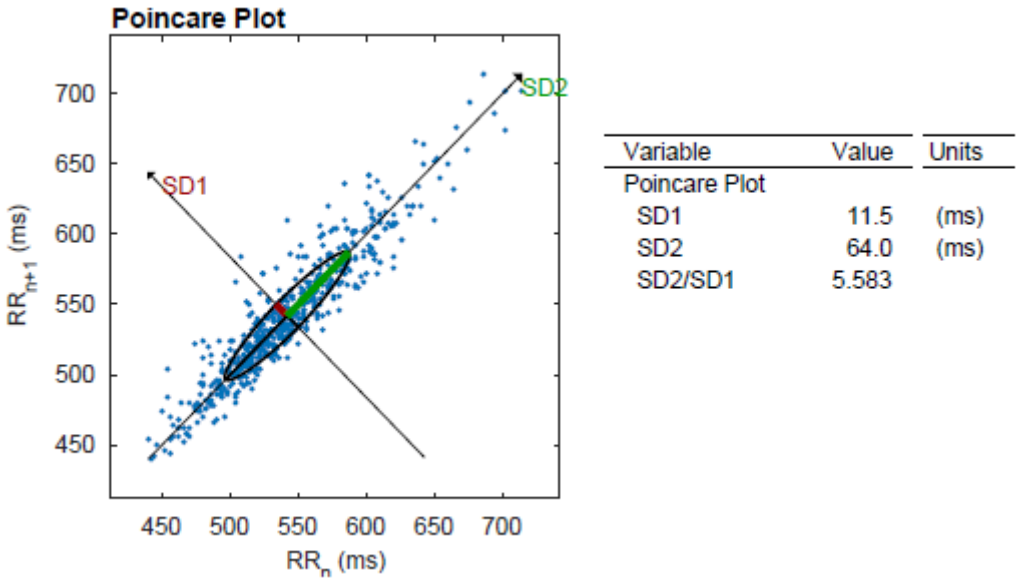

Figure 5.46: Poincarè plot of each RR interval according to the previous one.

Figure 5.47 shows the Fast Fourier Transform (FFT) of the RR intervals of the ortho signal ECG, ie the power spectrum is represented, which indicates how the power carried by a signal of a given frequency has been distributed.

Figure 5.48 shows analysis of the ortho signal obtained with autoregressive methods.

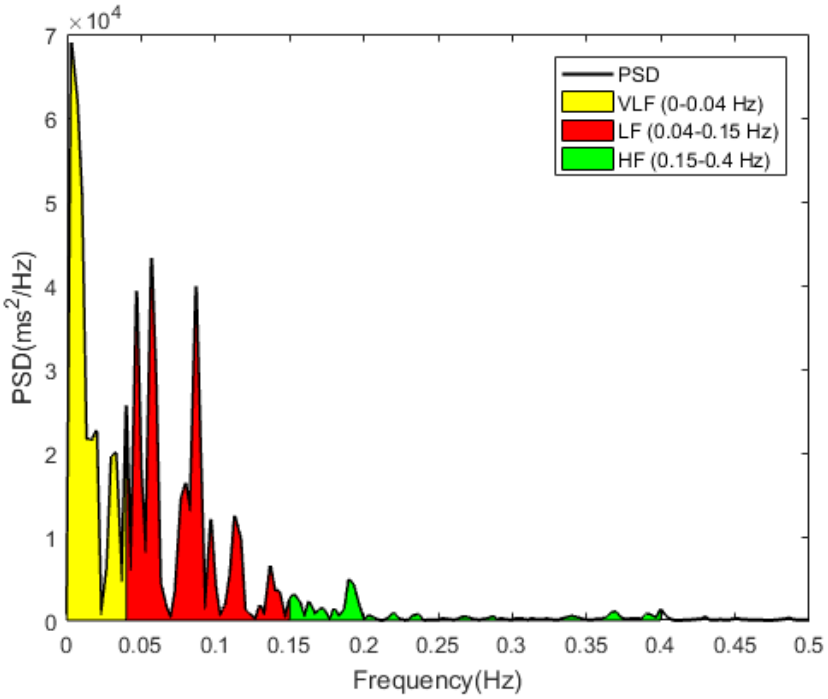

Figure 5.47: Fast Fourier Transform (FFT) of the ortho sygnal.

In the Figure 5.47 and 5.48 it is possible to distinguish three different frequency bands that characterize the sympathetic and vagal activity of the autonomic nervous system.

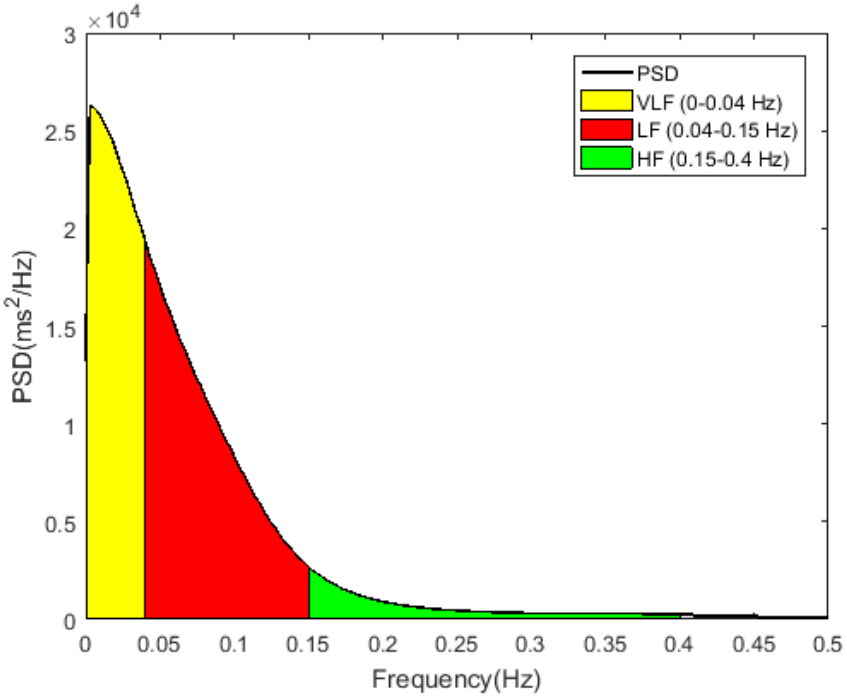

Figure 5.48: Autoregressive analysis of the ortho sygnal.

Table 5.12 shows the parameters that quantify the variability of heart rate in the frequency domain.

Frequency-Domain Results				
Variable	**VLF**	**LF**	**HF**	**LF/HF**
FFT Results				
Peak (Hz)	0,0033	0,057	0,19	
Power (ms^2)	1038,8	1124,7	140,9	7,98
Power (%)	45,03	46,8	6,1	
Power (n.u.)		88,7	11,1	
AR Results				
Peak (Hz)	0,0033	0,040	0,15	
Power (ms^2)	921,2	1055,1	154,0	6,85
Power (%)	43,2	49,5	7,2	
Power (n.u.)		87,2	12,7	

Table 5.12: Variables that quantify HRV during ortho phase in the frequency domain.

Figure 5.49 shows the ECG signal recorded during the execution of the top test and the relative tacogram.

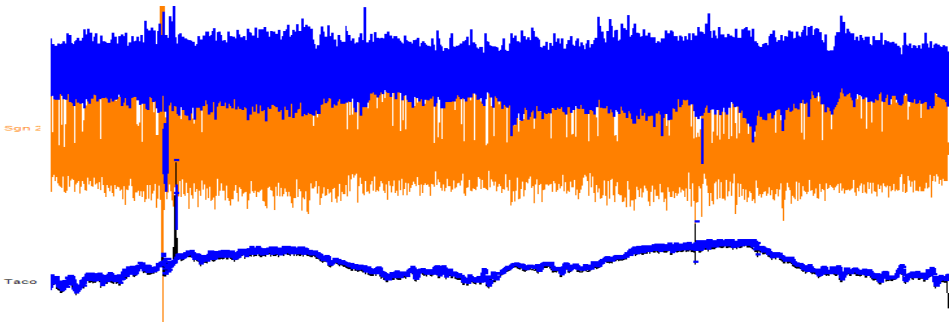

Figure 5.49: Tachogram of the signal ECG recorded during top test.

Figure 5.50 shows the trend of the heart rate during the execution of the top test, highlighting in blue the areas where there is a growth and decrease of the frequency in the transition phases in which the workload is added or removed.

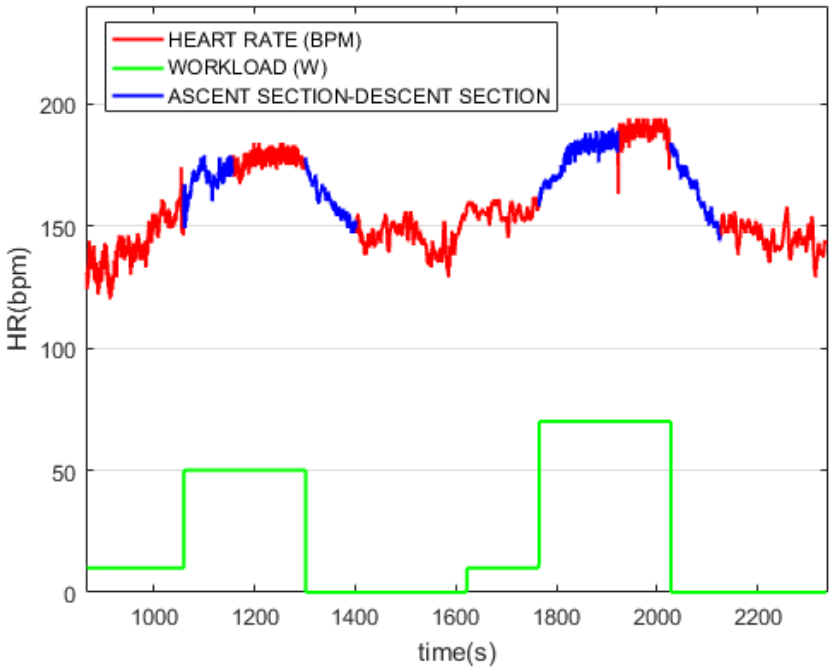

Figure 5.50: Heart rate trend as a function of time during the top test.

Figure 5.51 shows the exponential interpolation in the phase of heart rate increase at the insertion of the first workload (beginning of step 1).

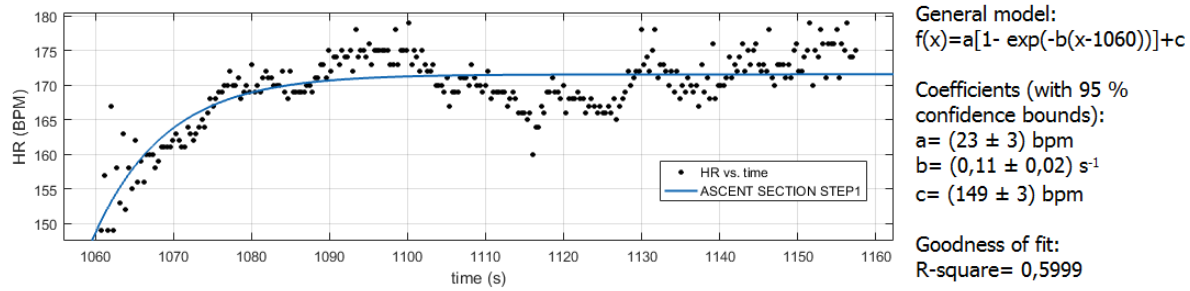

Figure 5.51: Exponential interpolation of the stress adaptation curve in response to the first workload.

Figure 5.52 shows the exponential interpolation in the passive recovery phase in which the heart rate decreases at the removal of the first workload (end of step 1).

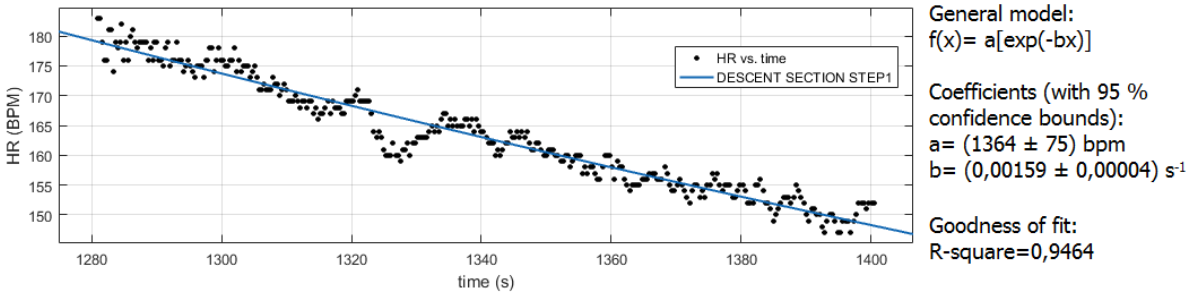

Figure 5.52: Exponential interpolation of the passive recovery curve after removal of the first workload.

Figure 5.53 shows the exponential interpolation in the phase of heart rate increase at the insertion of the first workload (end of step 2).

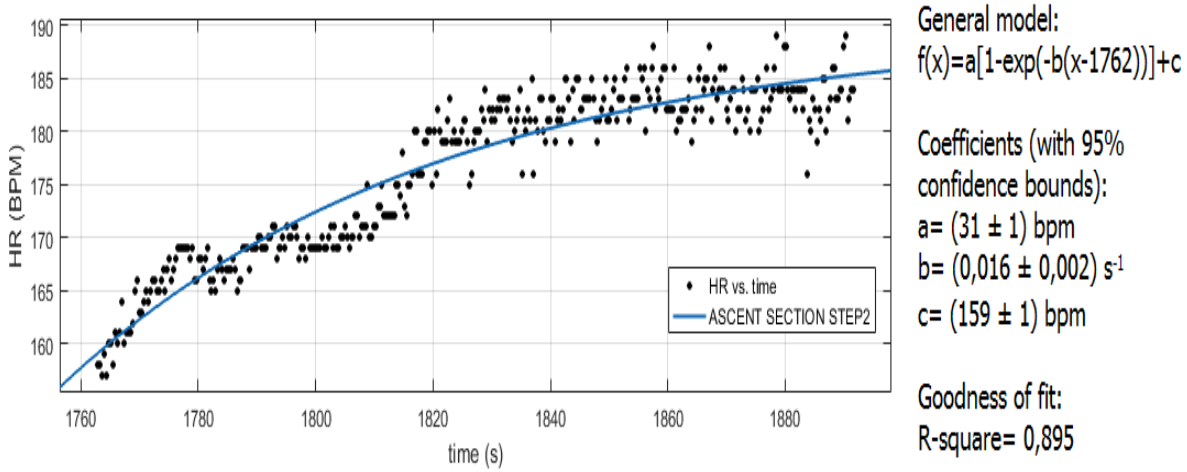

Figure 5.53: Exponential interpolation of the stress adaptation curve in response to the second workload.

Figure 5.54 shows the exponential interpolation in the passive recovery phase in which the heart rate decreases at the removal of the first workload (end of step 2).

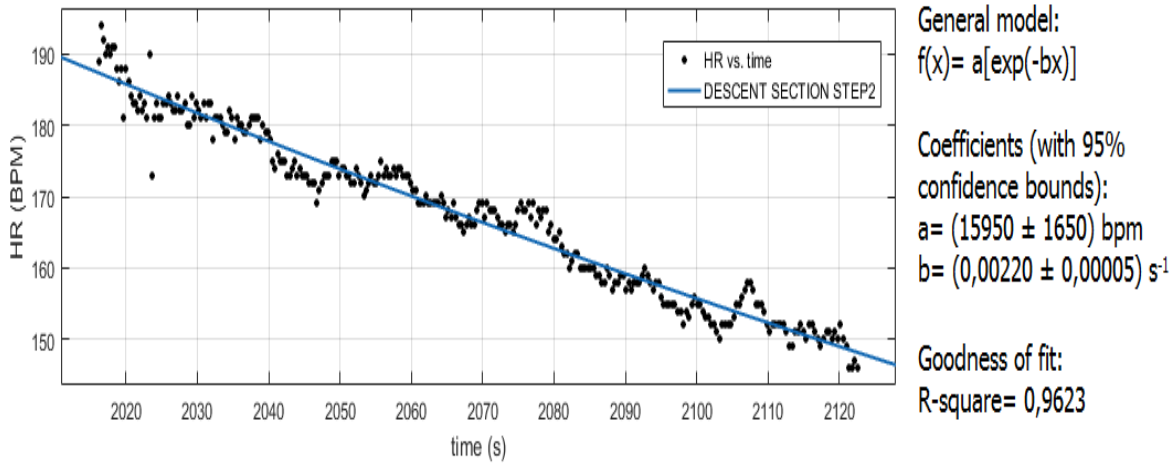

Figure 5.54: Exponential interpolation of the passive recovery curve after removal of the second workload.

5.4 Results of fourth subject

Figure 5.55 shows the tachogram of the whole recorded signal ECG.

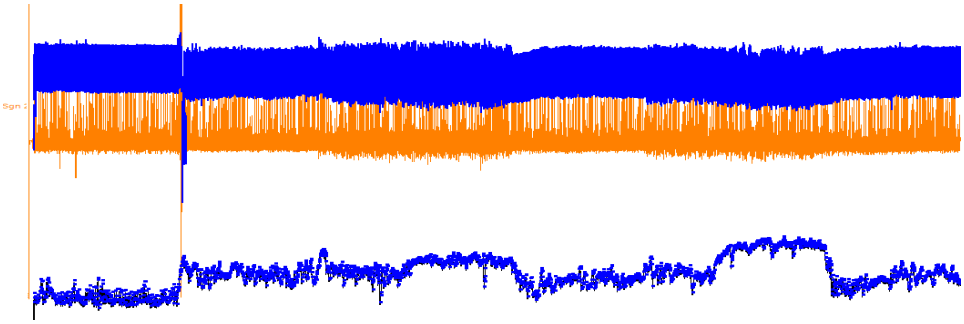

Figure 5.55: Complete tachogram of the signal ECG.

Figure 5.56 shows the heart rate trend during the entire test, both for the tilt test phase and for the top test phase in which the patient was submitted to two different workloads, before a light one (50 W) and then a moderate one (70 W).

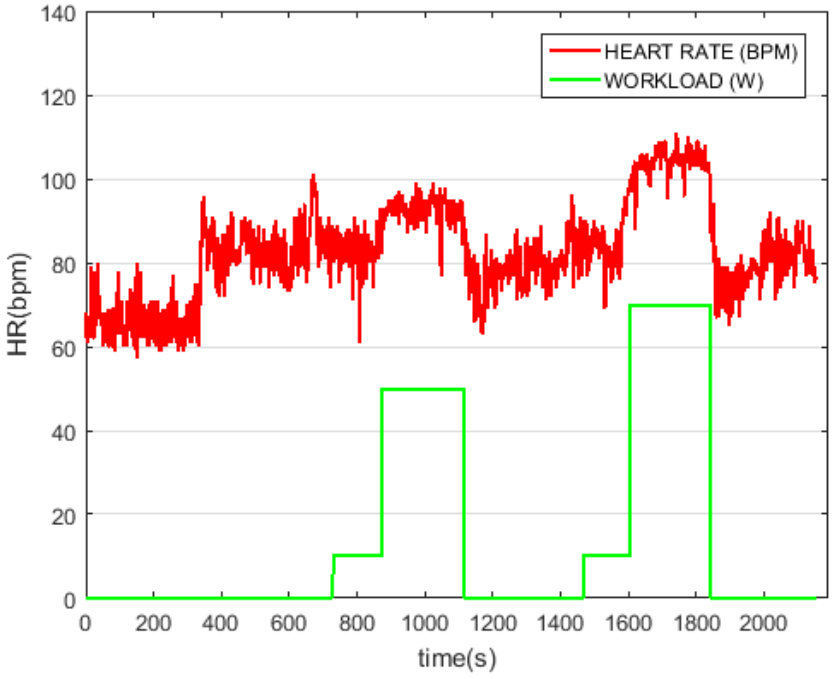

Figure 5.56: Heart rate trend as a function of time and workload inserted or removed.

Figure 5.57 shows the section of the RR intervals, selected through the Kubios software, related to the clinium phase in which the subject is lying on the bed.

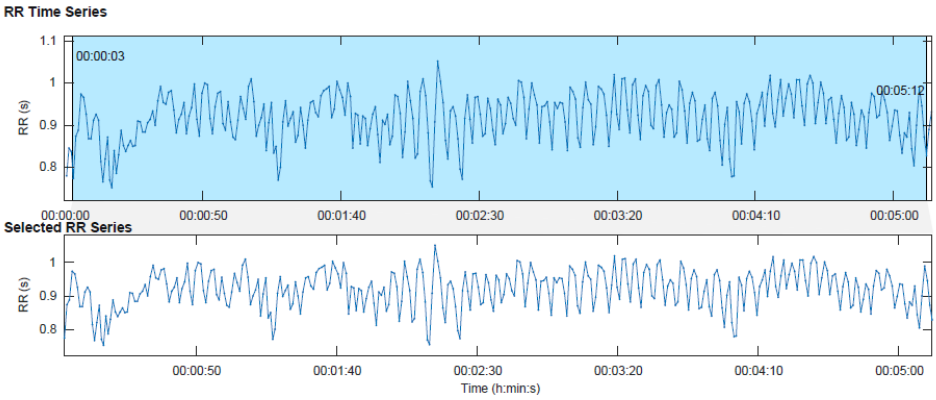

Figure 5.57: Tract of selected RR intervals in the clino signal for time and frequency domain analysis.

Figure 5.58 shows the distributions of the beat-to-beat RR intervals and the heart rate HR recorded during the clinium phase.

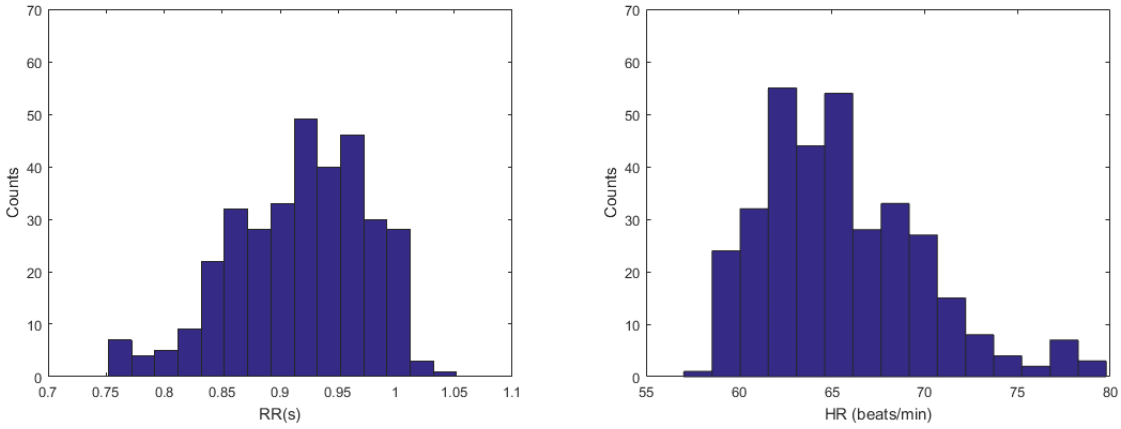

(a) (b)

Figure 5.58: Distributions of the RR intervals (a) and the heart rate HR (b) of the clino phase.

Table 5.13 shows the parameters that quantify the variability of heart rate in the time domain.

Time-Domain Results	
Variable	**Value**
Mean RR	920 ms
STD RR	57 ms
Mean HR	65 beats/min
STD HR	1 beats/min
Min HR	61 beats/min
Max HR	75 beats/min

Table 5.13: Variables that quantify HRV during ortho phase in the time domain.

Figure **??** shows Poincarè plot and the values SD1 and SD2 standard deviations of the distributions along the transverse axis and the bisector.

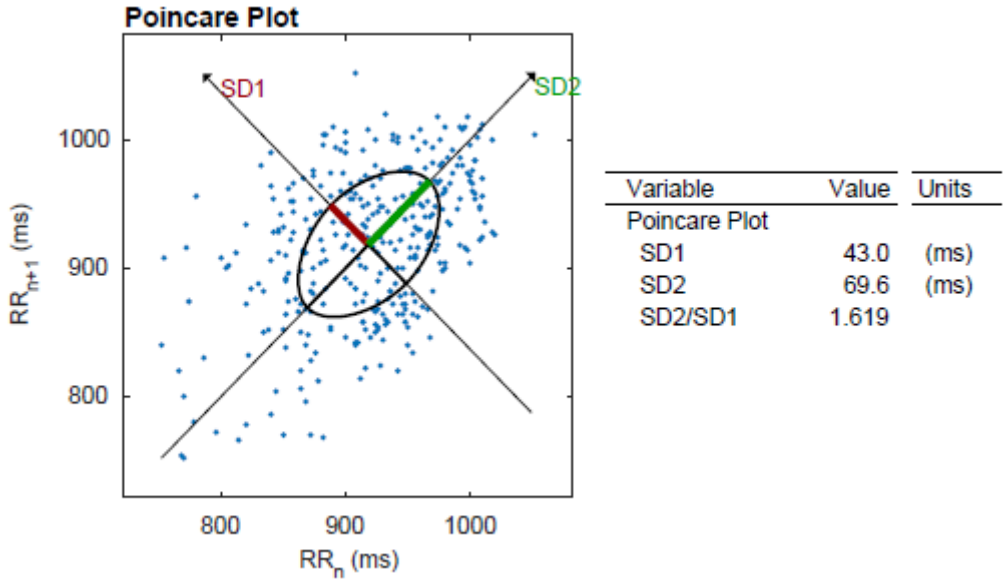

Figure 5.59: Poincarè plot of each RR interval according to the previous one.

Figure 5.60 shows the Fast Fourier Transform (FFT) of the RR intervals of the clino signal ECG, ie the power spectrum is represented, which indicates how the power carried by a signal of a given frequency has been distributed.

Figure 5.61 shows analysis of the clinium signal obtained with autoregressive methods.

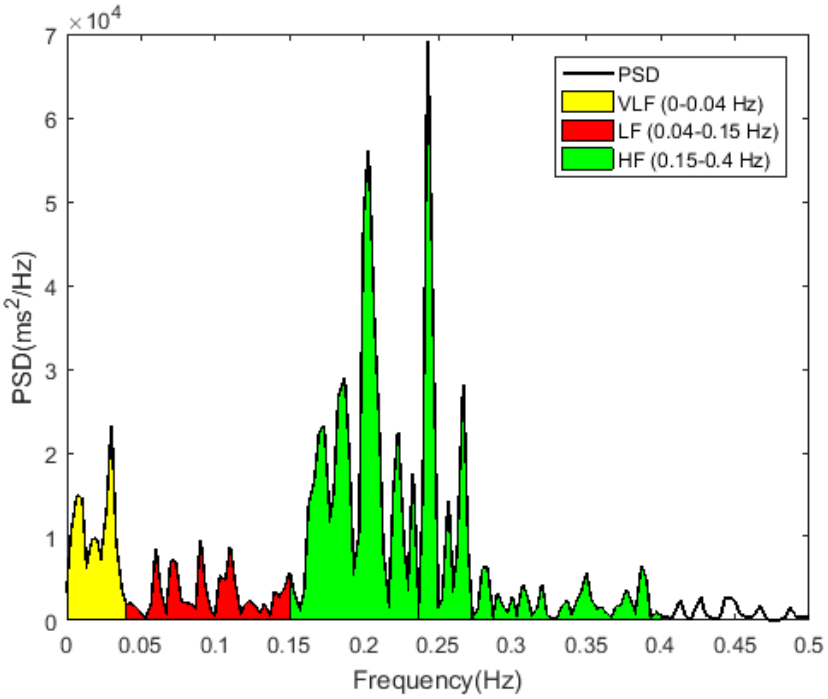

Figure 5.60: Fast Fourier Transform (FFT) of the clinium sygnal.

In the Figure 5.60 and 5.61 it is possible to distinguish three different frequency bands that characterize the sympathetic and vagal activity of the autonomic nervous system.

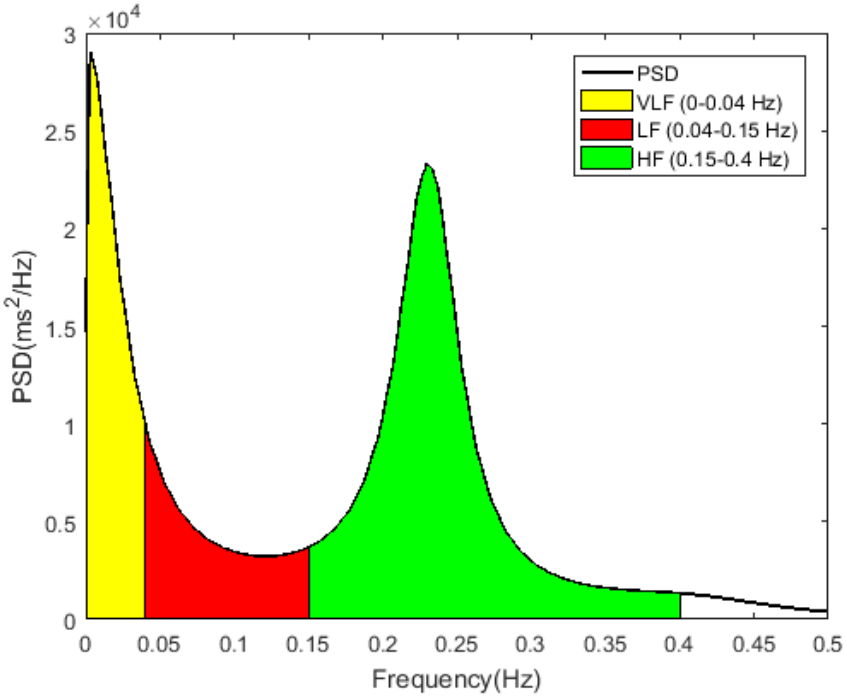

Figure 5.61: Autoregressive analysis of the clinium sygnal.

Table 5.14 shows the parameters that quantify the variability of heart rate in the frequency domain.

Frequency-Domain Results				
Variable	**VLF**	**LF**	**HF**	**LF/HF**
FFT Results				
Peak (Hz)	0,030	0,090	0,243	
Power (ms^2)	401,5	320,7	2358,4	0,14
Power (%)	13,03	10,4	76,5	
Power (n.u.)		12,0	88,0	
AR Results				
Peak (Hz)	0,0033	0,040	0,230	
Power (ms^2)	851,4	477,5	1842,5	0,26
Power (%)	26,8	15,0	58,0	
Power (n.u.)		20,6	79,3	

Table 5.14: Variables that quantify HRV during clino phase in the frequency domain.

Figure 5.62 shows the section of the RR intervals, selected through the Kubios software, related to the ortho phase in which the subject is standing.

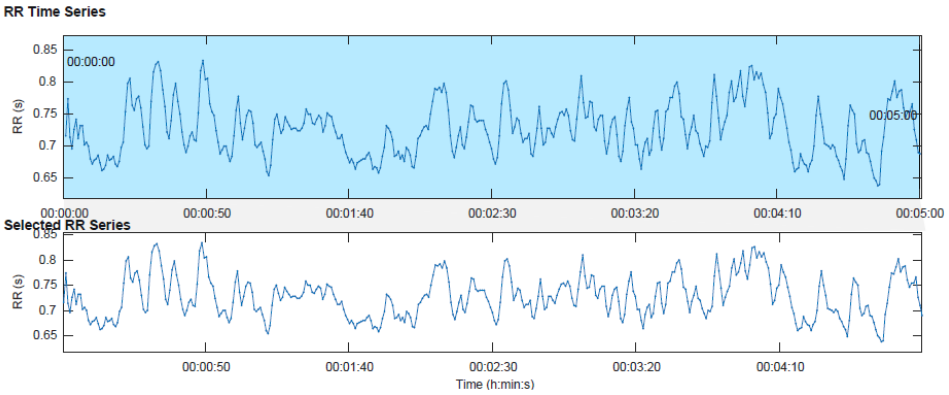

Figure 5.62: Tract of selected RR intervals in the ortho signal for time and frequency domain analysis.

Figure 5.63 shows the distributions of the beat-to-beat RR intervals and the heart rate HR recorded during the ortho phase.

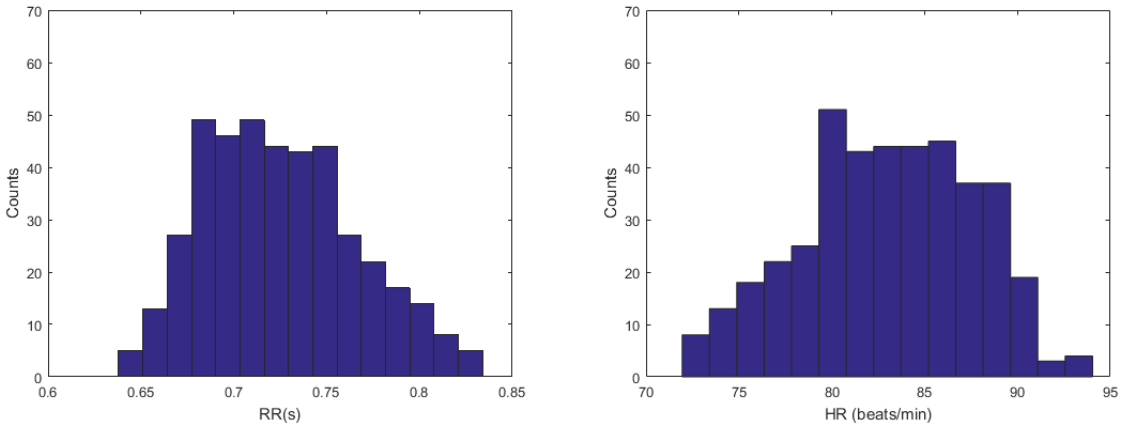

(a) (b)

Figure 5.63: Distributions of the RR intervals (a) and the heart rate HR (b) of the ortho phase.

Table 5.15 shows the parameters that quantify the variability of heart rate in the time domain.

Time-Domain Results	
Variable	**Value**
Mean RR	726 ms
STD RR	41 ms
Mean HR	83 beats/min
STD HR	1 beats/min
Min HR	74 beats/min
Max HR	93 beats/min

Table 5.15: Variables that quantify HRV during ortho phase in the time domain.

Figure 5.64 shows Poincarè plot and the values SD1 and SD2 standard deviations of the distributions along the transverse axis and the bisector.

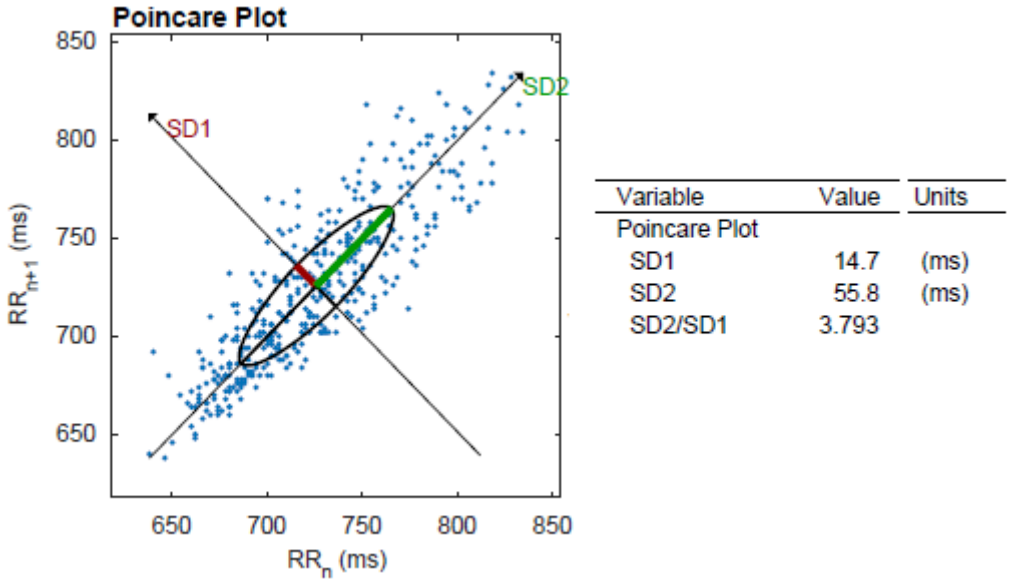

Figure 5.64: Poincarè plot of each RR interval according to the previous one.

Figure 5.65 shows the Fast Fourier Transform (FFT) of the RR intervals of the ortho signal ECG, ie the power spectrum is represented, which indicates how the power carried by a signal of a given frequency has been distributed.

Figure 5.66 shows analysis of the ortho signal obtained with autoregressive methods.

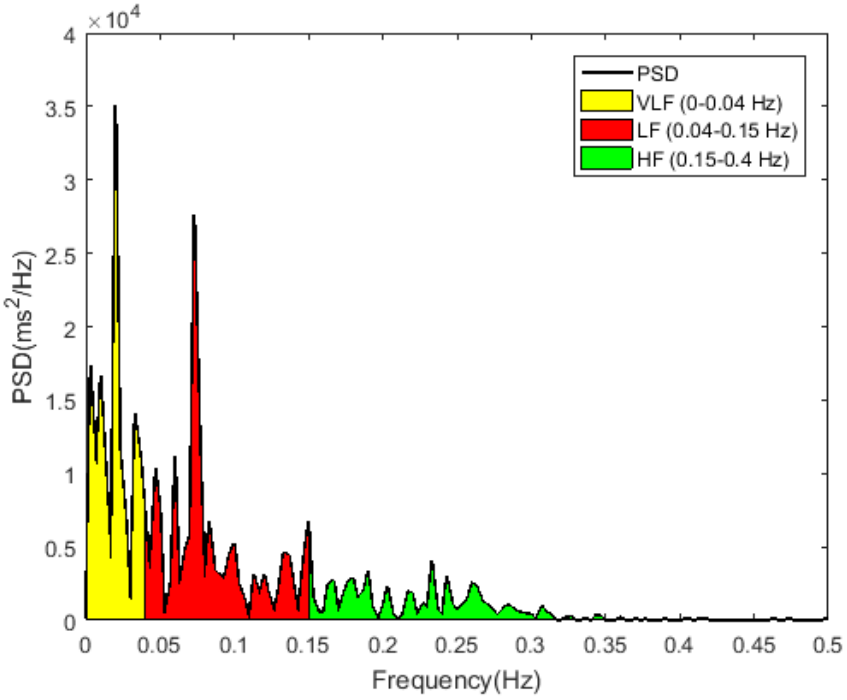

Figure 5.65: Fast Fourier Transform (FFT) of the ortho sygnal.

In the Figure 5.65 and 5.66 it is possible to distinguish three different frequency bands that characterize the sympathetic and vagal activity of the autonomic nervous system.

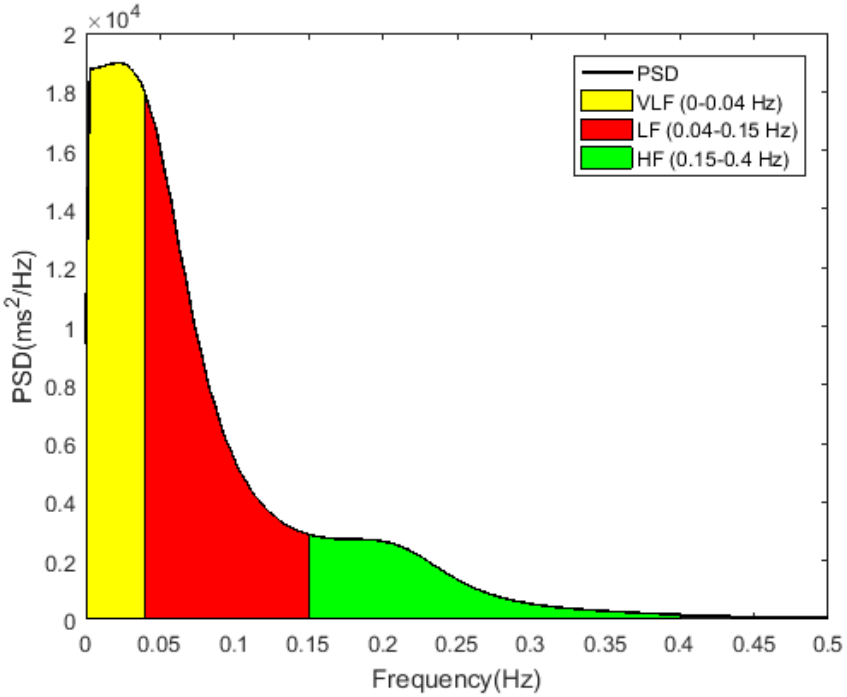

Figure 5.66: Autoregressive analysis of the ortho sygnal

Table 5.16 shows the parameters that quantify the heart rate variability in the time domain.

Frequency-Domain Results				
Variable	**VLF**	**LF**	**HF**	**LF/HF**
FFT Results				
Peak (Hz)	0,020	0,073	0,15	
Power (ms^2)	480,8	525,2	224,7	2,34
Power (%)	39,1	42,7	18,3	
Power (n.u.)		70,0	29,96	
AR Results				
Peak (Hz)	0,023	0,040	0,15	
Power (ms^2)	734,1	860,0	312,2	2,75
Power (%)	38,5	45,1	16,4	
Power (n.u.)		73,4	26,6	

Table 5.16: Variables that quantify HRV during ortho phase in the frequency domain.

Figure 5.67 shows the ECG signal recorded during the execution of the top test and the relative tacogram.

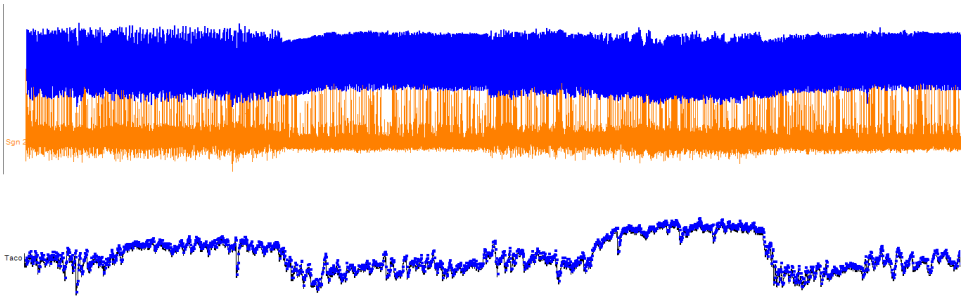

Figure 5.67: Tachogram of the signal ECG recorded during top test. Heart rate trend as a function of time during the top test.

Figure 5.68 shows the heart rate trend during the execution of the top test, highlighting in blue the areas where there is a growth and decrease of the frequency in the transition phases in which the workload is added or removed.

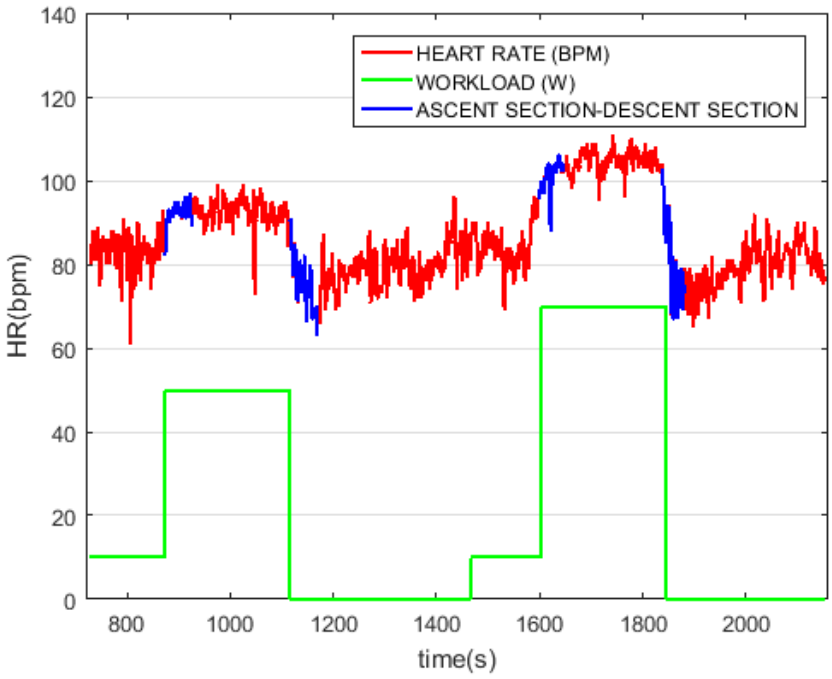

Figure 5.68: Heart rate trend as a function of time during the top test.

Figure 5.69 shows the exponential interpolation in the phase of heart rate increase at the insertion of the first workload (beginning of step 1).

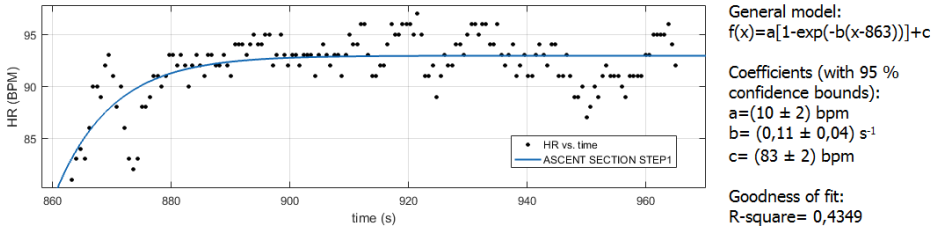

Figure 5.69: Exponential interpolation of the stress adaptation curve in response to the first workload.

Figure 5.70 shows the exponential interpolation in the passive recovery phase in which the heart rate decreases at the removal of the first workload (end of step 1).

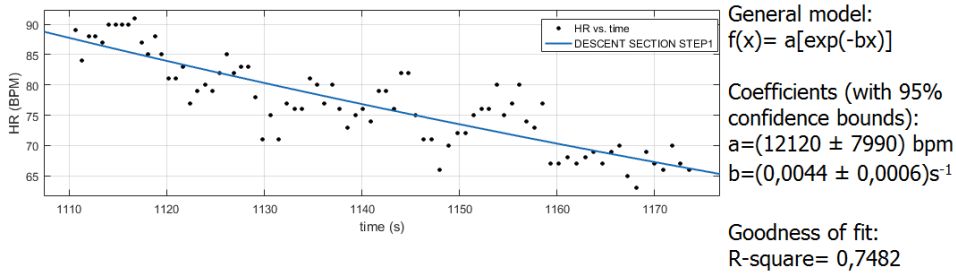

Figure 5.70: Exponential interpolation of the passive recovery curve after removal of the first workload.

Figure 5.71 shows the exponential interpolation in the phase of heart rate increase at the removal of the second workload (end of step 2).

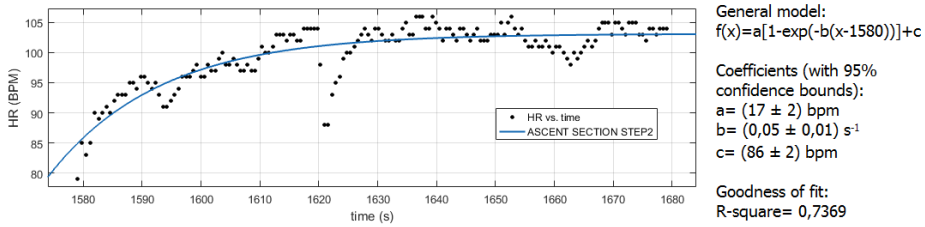

Figure 5.71: Exponential interpolation of the stress adaptation curve in response to the first workload.

Figure 5.72 shows the exponential interpolation in the passive recovery phase in which the heart rate decreases at the removal of the first workload (end of step 1).

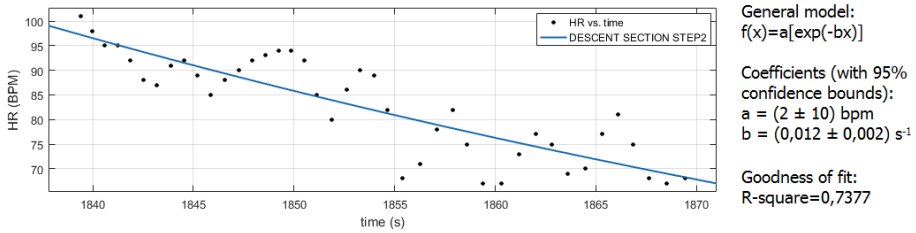

Figure 5.72: Exponential interpolation of the passive recovery curve after removal of the second workload.

5.5 Results of fifth subject

Figure 5.73 shows the tachogram of the whole recorded signal ECG.

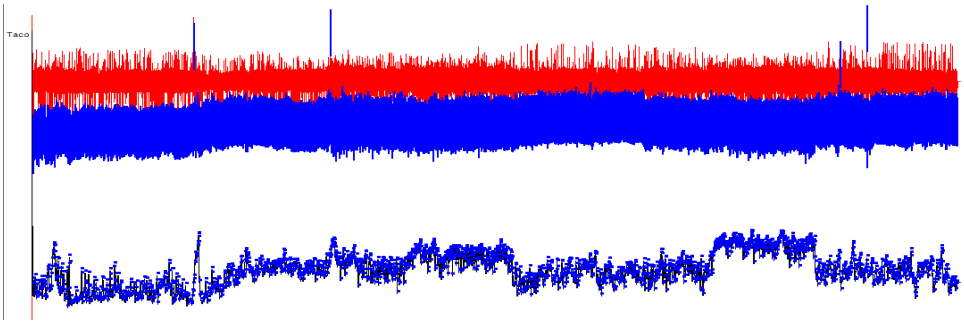

Figure 5.73: Complete tachogram of the signal ECG.

Figure 5.74 shows the trend of the heart rate during the entire test, both for the tilt test phase and for the top test phase in which the patient was subjected to two different workloads, before a light one (50 W) and then a moderate one (70 W).

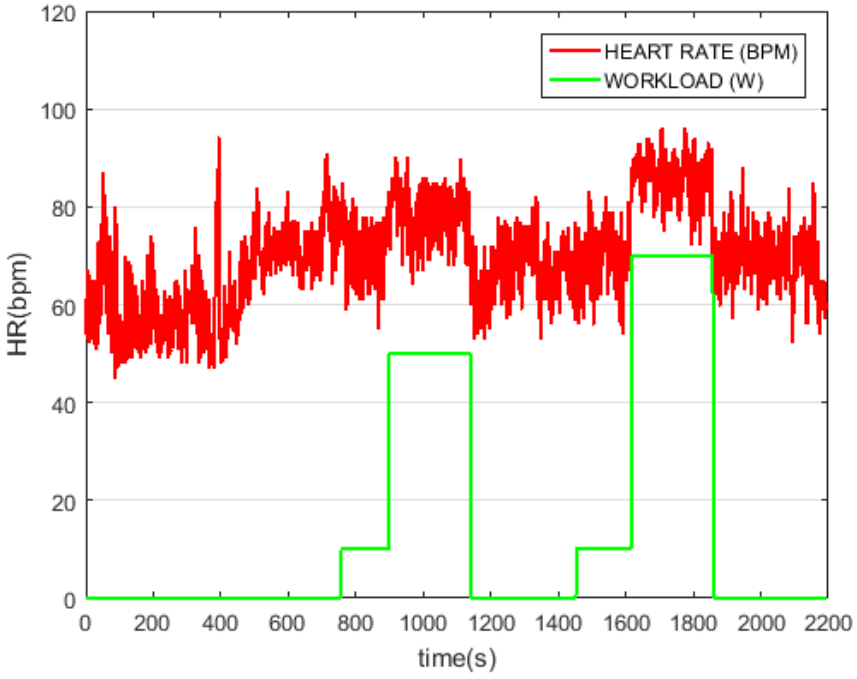

Figure 5.74: Heart rate trend as a function of time.

Figure 5.75 shows the section of the RR intervals, selected through the Kubios software, related to the clinium phase in which the subject is lying on the bed.

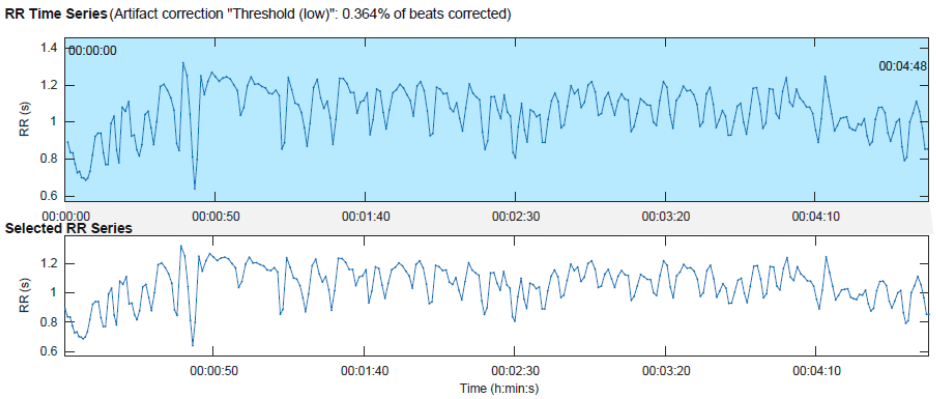

Figure 5.75: Tract of selected RR intervals in the clino signal for time and frequency domain analysis.

Figure 5.76 shows the distributions of the beat-to-beat RR intervals and the heart rate HR recorded during the clinium phase.

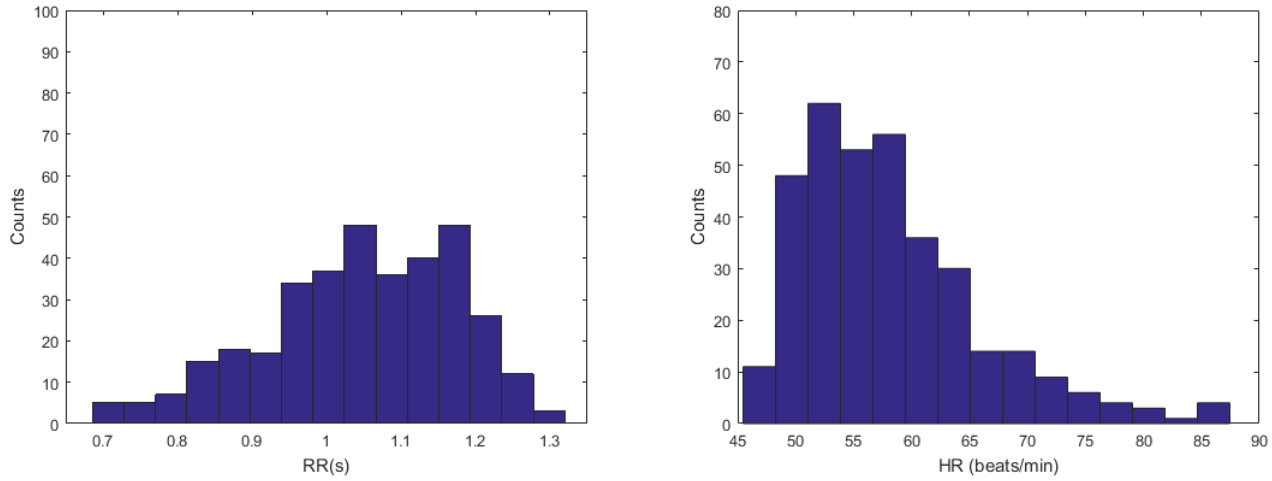

(a) (b)

Figure 5.76: Distributions of the RR intervals (a) and the heart rate HR (b) of the clino phase.

Table 5.17 shows the parameters that quantify the variability of heart rate in the time domain.

Time-Domain Results	
Variable	**Value**
Mean RR	1045 ms
STD RR	133 ms
Mean HR	57 beats/min
STD HR	2 beats/min
Min HR	48 beats/min
Max HR	85 beats/min

Table 5.17: Variables that quantify HRV during clino phase in the time domain.

Figure 5.77 shows Poincarè plot and the values SD1 and SD2 standard deviations of the distributions along the transverse axis and the bisector.

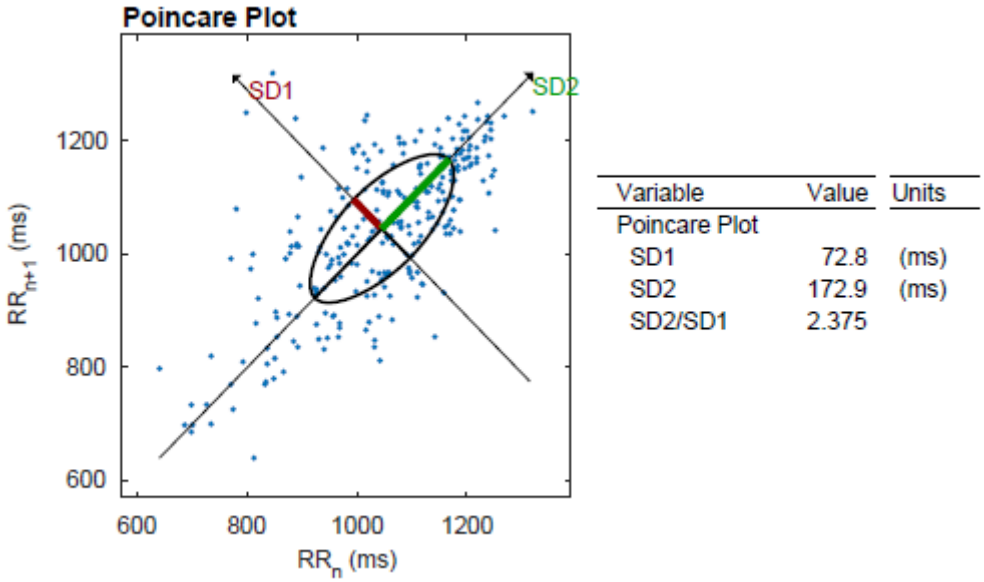

Figure 5.77: Poincarè plot of each RR interval according to the previous one.

Figure 5.78 shows the Fast Fourier Transform (FFT) of the RR intervals of the clino signal ECG, ie the power spectrum is represented, which indicates how the power carried by a signal of a given frequency has been distributed.

Figure 5.79 shows analysis of the clinium signal obtained with autoregressive methods.

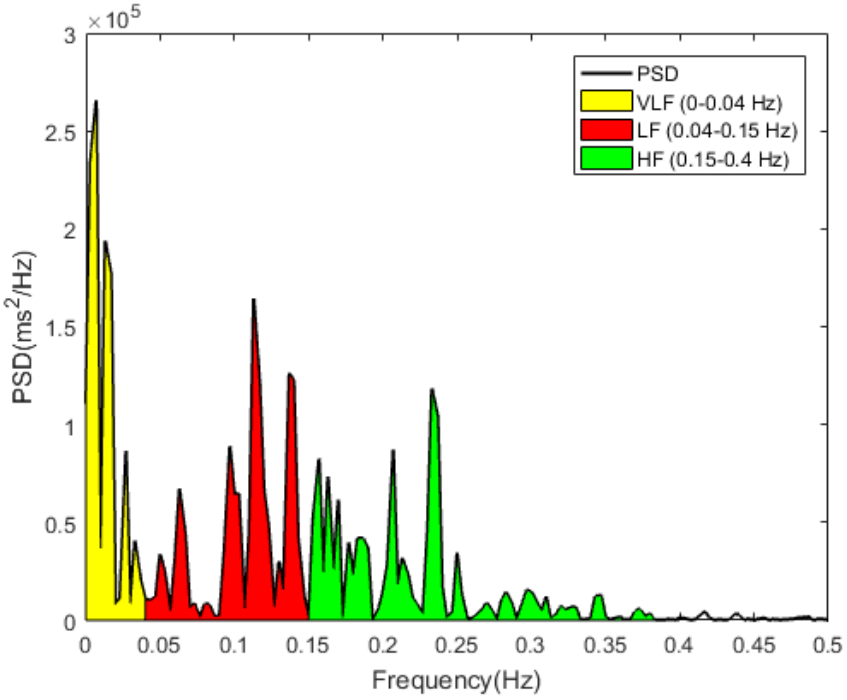

Figure 5.78: Fast Fourier Transform (FFT) of the clinium sygnal.

In the Figure 5.78 and 5.79 it is possible to distinguish three different frequency bands that characterize the sympathetic and vagal activity of the autonomic nervous system.

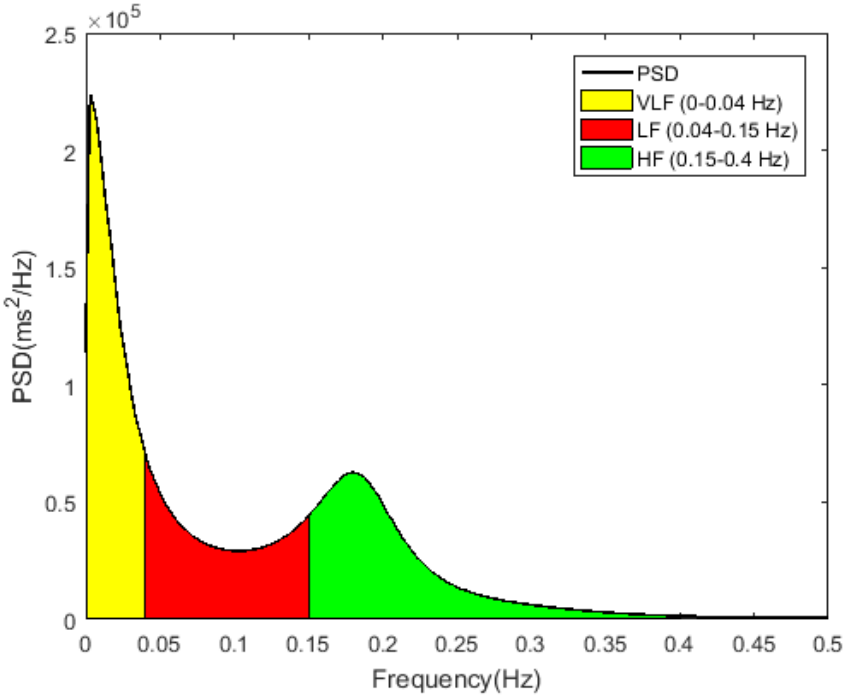

Figure 5.79: Autoregressive analysis of the clinium sygnal.

Table 5.18 shows the parameters that quantify the heart rate variability in the frequency domain.

Frequency-Domain Results				
Variable	**VLF**	**LF**	**HF**	**LF/HF**
FFT Results				
Peak (Hz)	0,0167	0,113	0,207	
Power (ms^2)	2548,7	3129,9	3933,7	0,80
Power (%)	26,5	32,6	40,9	
Power (n.u.)		44,3	55,7	
AR Results				
Peak (Hz)	0,0033	0,040	0,17	
Power (ms^2)	5450,1	3861,3	4937,4	0,78
Power (%)	38,2	27,1	34,6	
Power (n.u.)		43,9	56,1	

Table 5.18: Variables that quantify HRV during clino phase in the frequency domain.

Figure 5.80 shows the section of the RR intervals, selected through the Kubios software, related to the ortho phase in which the subject is standing.

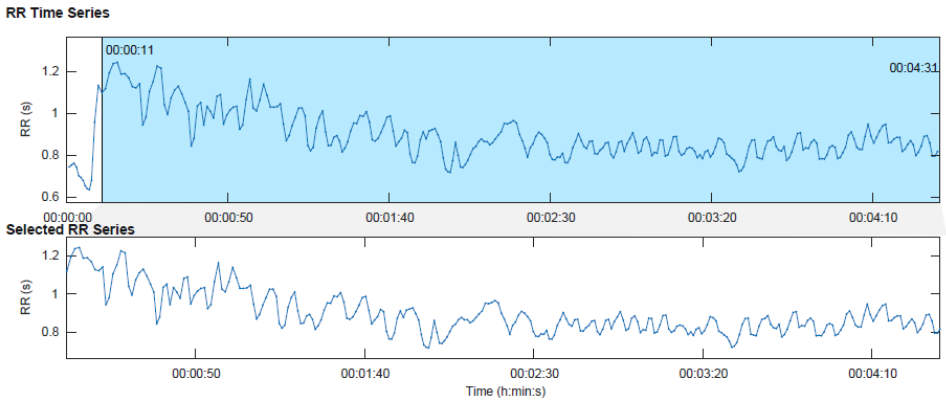

Figure 5.80: Tract of selected RR intervals in the ortho signal for time and frequency domain analysis.

Figure 5.81 shows the distributions of the beat-to-beat RR intervals and the heart rate HR recorded during the ortho phase.

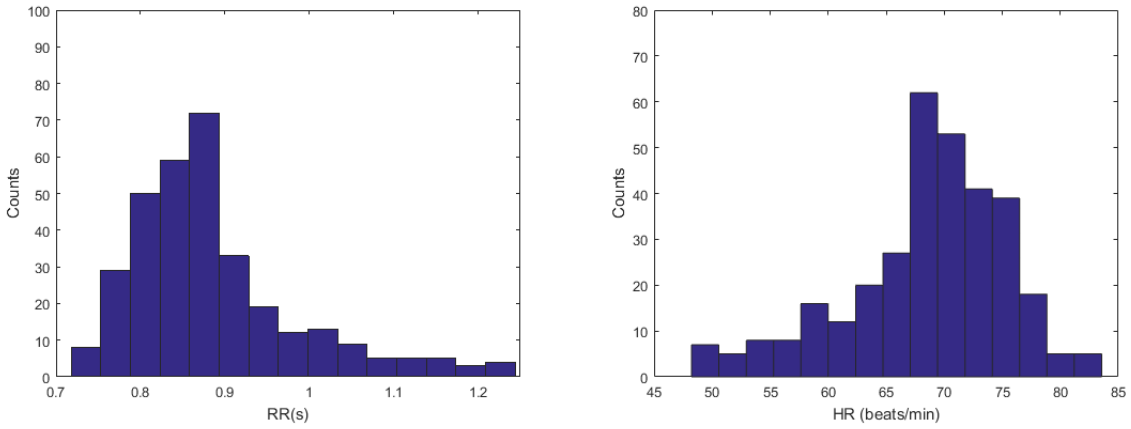

(a) (b)

Figure 5.81: Distributions of the RR intervals (a) and the heart rate HR (b) of the ortho phase.

Table 5.19 shows the parameters that quantify the variability of heart rate in the time domain.

Time-Domain Results	
Variable	**Value**
Mean RR	891 ms
STD RR	105 ms
Mean HR	67 beats/min
STD HR	2 beats/min
Min HR	50 beats/min
Max HR	81 beats/min

Table 5.19: Variables that quantify HRV during ortho phase in the time domain.

Figure 5.82 shows Poincarè plot and the values SD1 and SD2 standard deviations of the distributions along the transverse axis and the bisector.

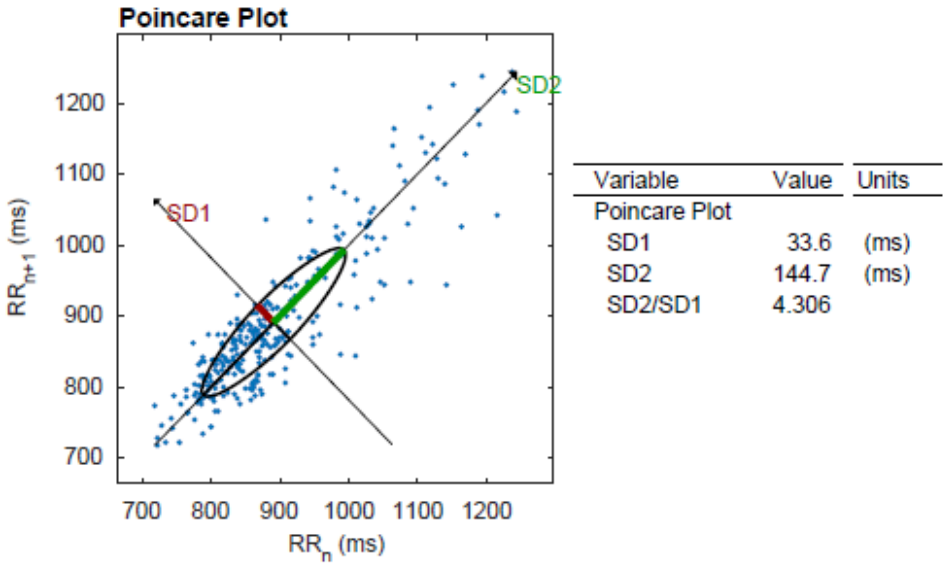

Figure 5.82: Poincarè plot of each RR interval according to the previous one.

Figure 5.83 shows the Fast Fourier Transform (FFT) of the RR intervals of the ortho signal ECG, ie the power spectrum is represented, which indicates how the pow Figure 5.84 shows analysis of the ortho signal obtained with autoregressive methods.

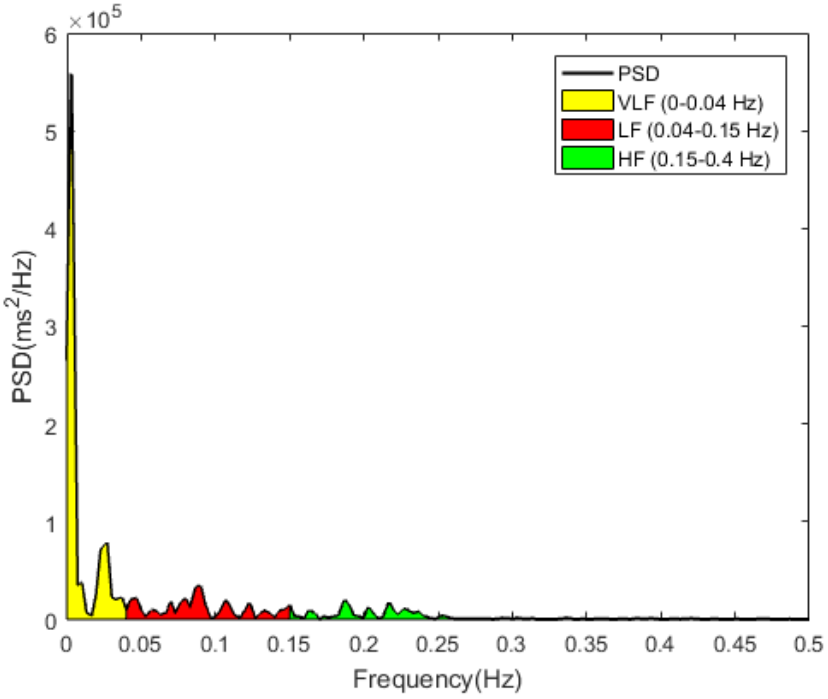

Figure 5.83: Fast Fourier Transform (FFT) of the ortho sygnal.

In the Figure 5.83 and 5.84 it is possible to distinguish three different frequency bands that characterize the sympathetic and vagal activity of the autonomic nervous system.

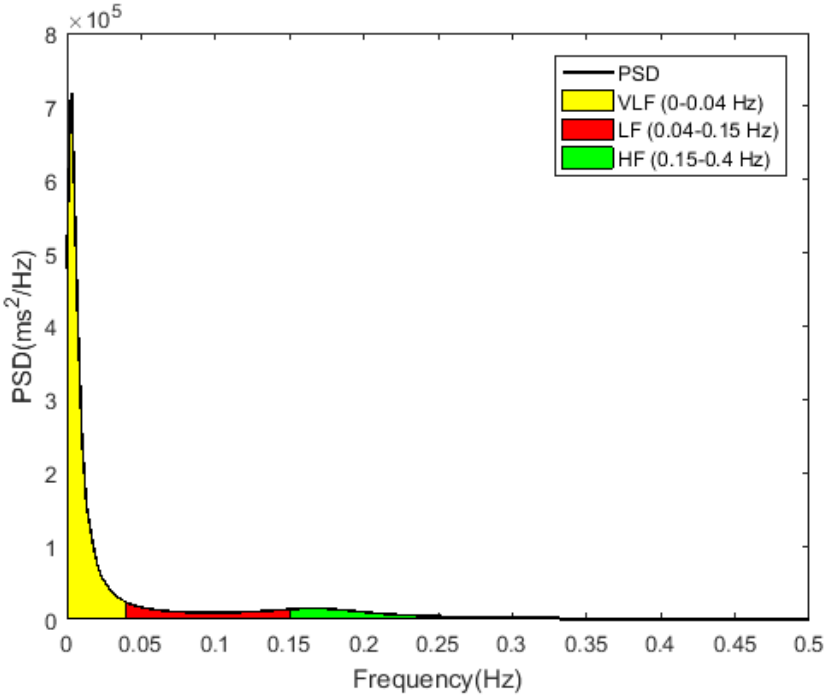

Figure 5.84: Autoregressive analysis of the ortho sygnal.

Table 5.20 shows the parameters that quantify the variability of heart rate in the frequency domain.

Frequency-Domain Results				
Variable	**VLF**	**LF**	**HF**	**LF/HF**
FFT Results				
Peak (Hz)	0,0033	0,090	0,187	
Power (ms^2)	3812,9	1454,7	693,92	2,10
Power (%)	64,0	24,4	11,6	
Power (n.u.)		67,7	32,3	
AR Results				
Peak (Hz)	0,0033	0,040	0,16	
Power (ms^2)	7684,8	1326,4	1169,3	1,13
Power (%)	75,5	13,0	11,5	
Power (n.u.)		53,1	46,8	

Table 5.20: Variables that quantify HRV during ortho phase in the frequency domain.

Figure 5.85 shows the ECG signal recorded during the top test execution and the relative tachogram.

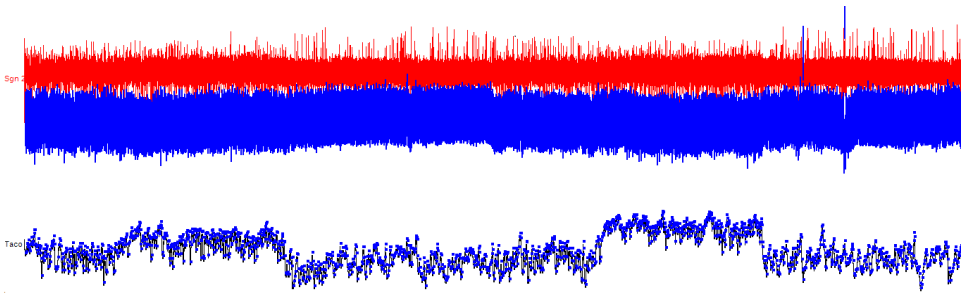

Figure 5.85: Tachogram of the signal ECG recorded during top test.

Figure 5.86 shows the heart rate trend during the top test execution, highlighting in blue the areas where there is a growth and decrease of the frequency in the transition phases in which the workload is added or removed.

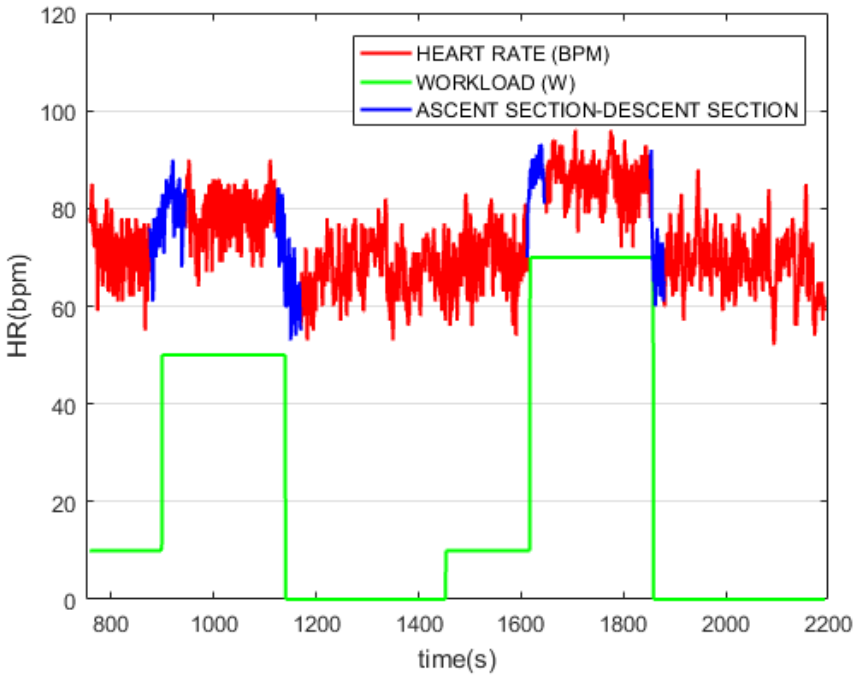

Figure 5.86: Heart rate trend as a function of time during the top test.

Figure 5.87 shows the exponential interpolation in the phase of heart rate increase at the insertion of the first workload (beginning of step 1).

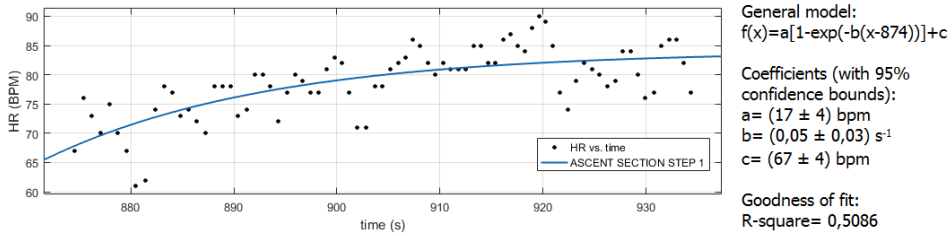

Figure 5.87: Exponential interpolation of the stress adaptation curve in response to the first workload.

Figure 5.88 shows the exponential interpolation in the passive recovery phase in which the heart rate decreases at the removal of the first workload (end of step 1).

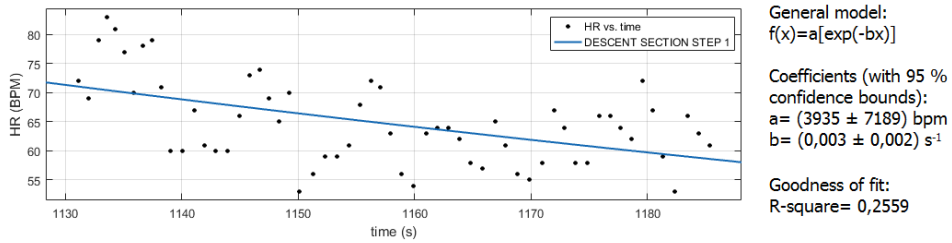

Figure 5.88: Exponential interpolation of the passive recovery curve after removal of the first workload.

Figure 5.89 shows the exponential interpolation in the phase of heart rate increase at the insertion of the second workload (beginning of step 2).

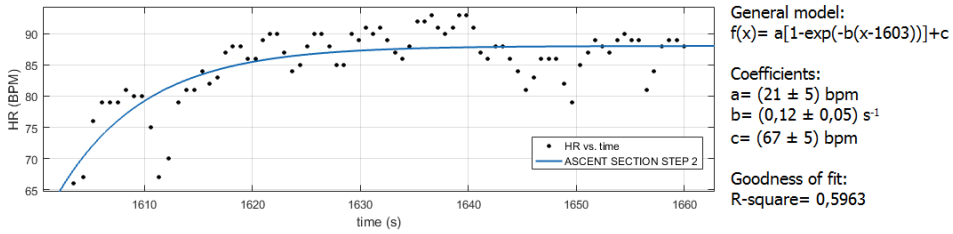

Figure 5.89: Exponential interpolation of the stress adaptation curve in response to the second workload.

Figure 5.90 shows the exponential interpolation in the passive recovery phase in which the heart rate decreases at the removal of the second workload (end of step 2).

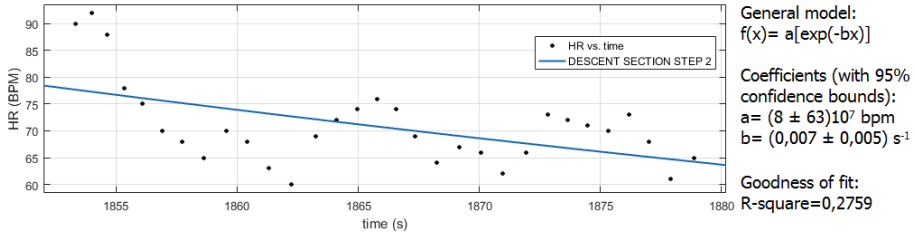

Figure 5.90: Exponential interpolation of the passive recovery curve after removal of the second workload.

5.6 Results of sixth subject

Figure 5.91 shows the tachogram of the whole recorded signal ECG.

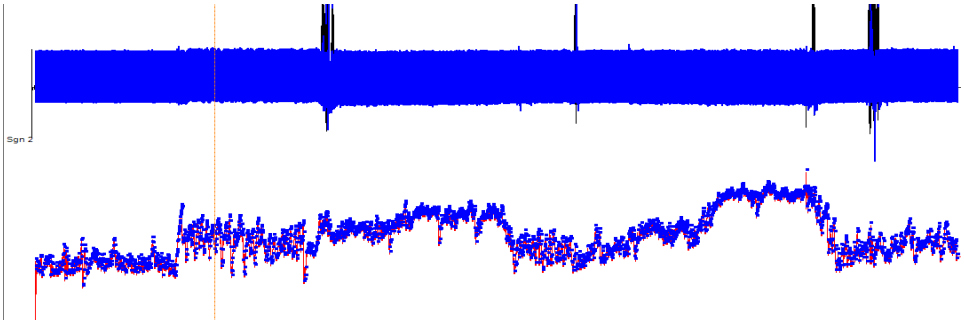

Figure 5.91: Complete tachogram of the signal ECG.

Figure 5.92 shows the trend of the heart rate during the entire test, both for the tilt test phase and for the top test phase in which the patient was submitted to two different workloads, before a light one (50 W) and then a moderate one (70 W).

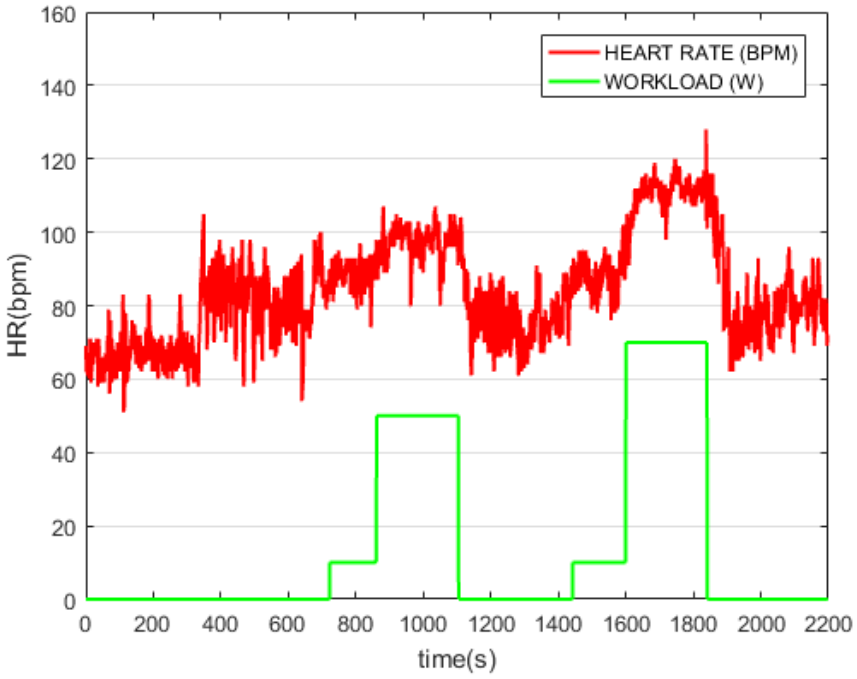

Figure 5.92: Heart rate trend as a function of time.

Figure 5.93 shows the section of the RR intervals, selected through the Kubios software, related to the clinium phase in which the subject is lying on the bed.

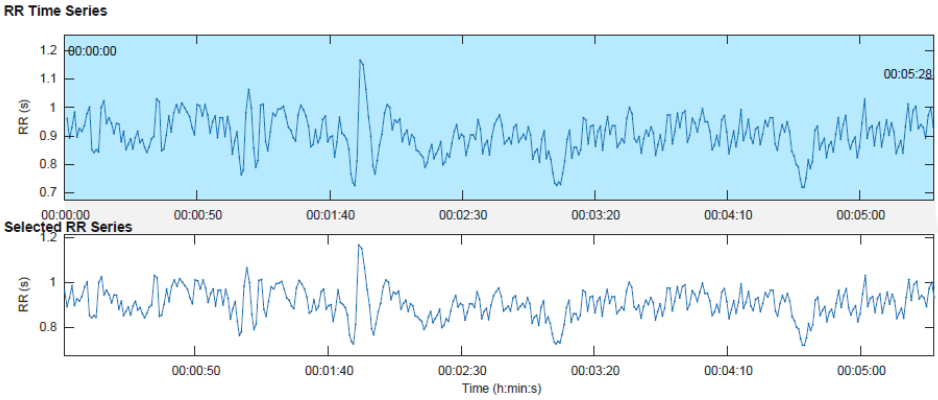

Figure 5.93: Tract of selected RR intervals in the clino signal for time and frequency domain analysis.

Figure 5.94 shows the distributions of the beat-to-beat RR intervals and the heart rate HR recorded during the clinium phase.

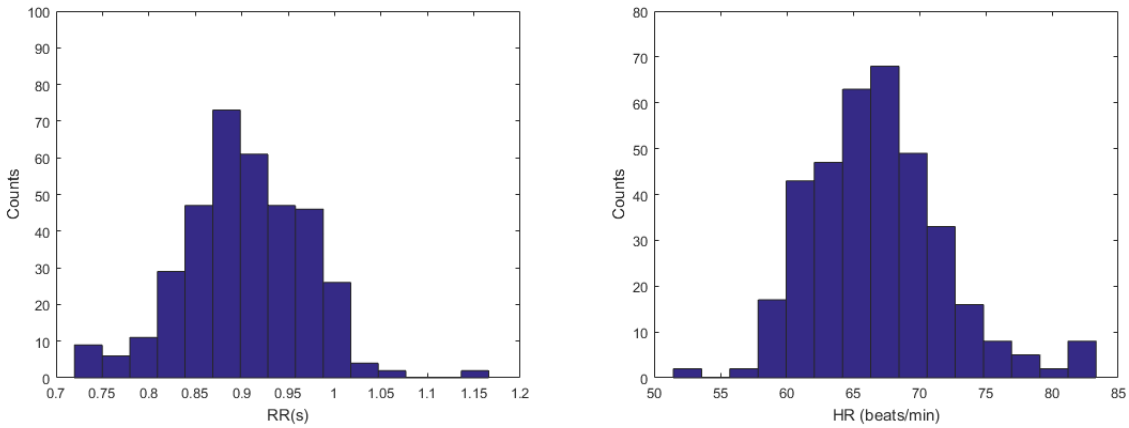

(a) (b)

Figure 5.94: Distributions of the RR intervals (a) and the heart rate HR (b) of the clino phase.

Table 5.21 shows the parameters that quantify the variability of heart rate in the time domain.

Time-Domain Results	
Variable	**Value**
Mean RR	903 ms
STD RR	67 ms
Mean HR	67 beats/min
STD HR	1 beats/min
Min HR	57 beats/min
Max HR	81 beats/min

Table 5.21: Variables that quantify HRV during clino phase in the time domain.

Figure 5.95 shows Poincarè plot and the values SD1 and SD2 standard deviations of the distributions along the transverse axis and the bisector.

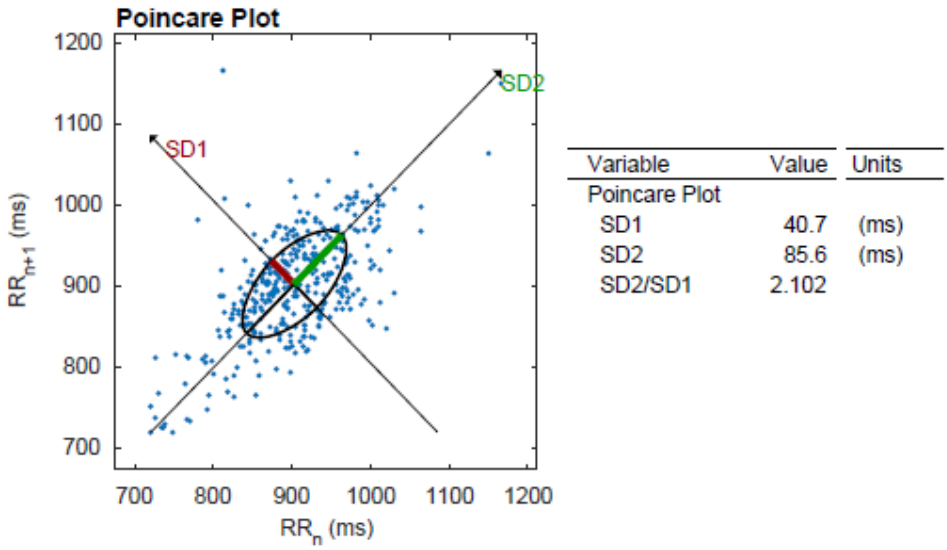

Figure 5.95: Poincarè plot of each RR interval according to the previous one.

Figure 5.96 shows the Fast Fourier Transform (FFT) of the RR intervals of the ortho signal ECG, ie the power spectrum is represented, which indicates how the power carried by a signal of a given frequency has been distributed.

Figure 5.97 shows analysis of the clinium signal obtained with autoregressive methods.

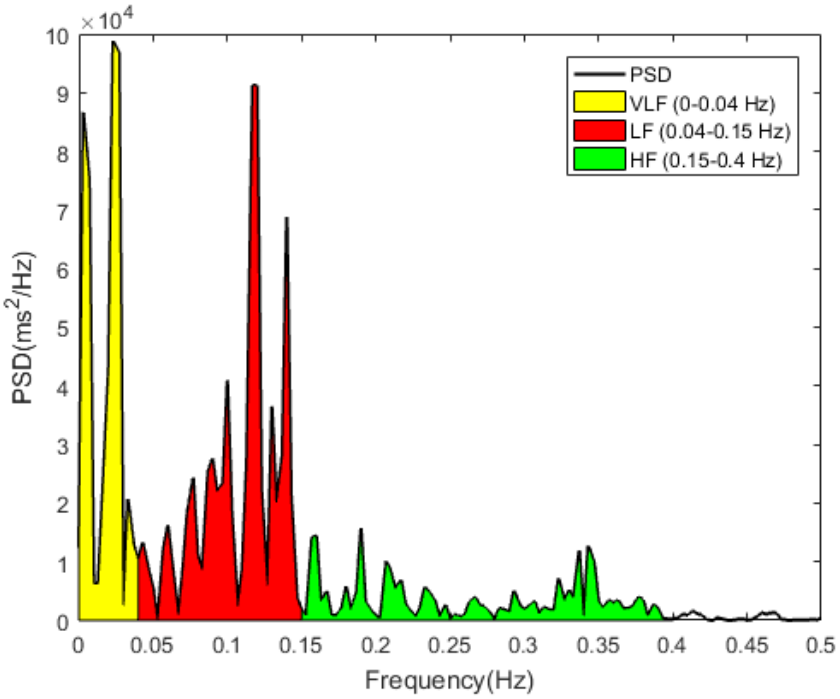

Figure 5.96: Fast Fourier Transform (FFT) of the clinium sygnal.

in the figure 5.96 and 5.97 it is possible to distinguish three different frequency bands that characterize the sympathetic and vagal activity of the autonomic nervous system.

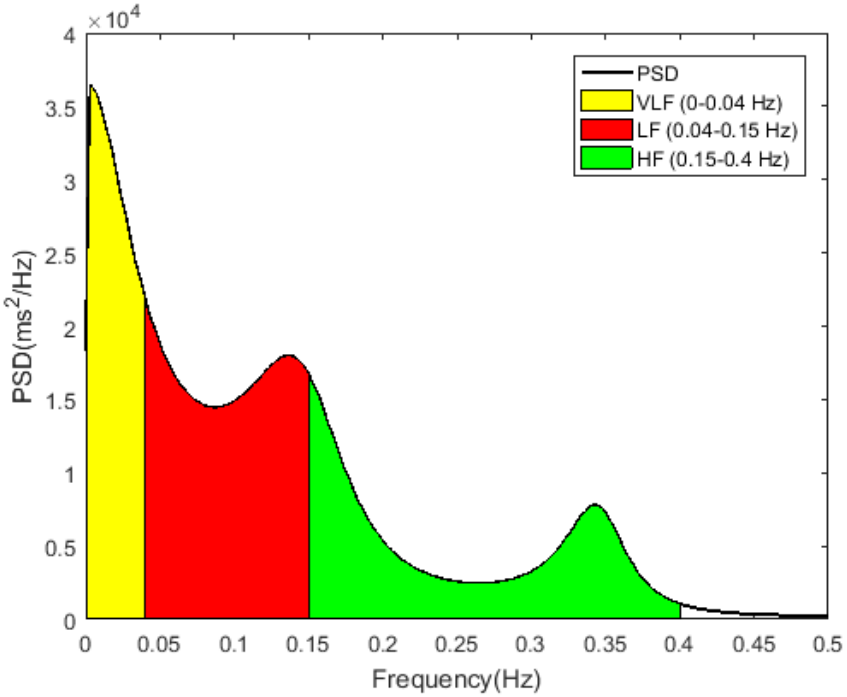

Figure 5.97: Autoregressive analysis of the clinium sygnal.

Table 5.22 shows the parameters that quantify the heart rate variability in the frequency domain.

Frequency-Domain Results				
Variable	**VLF**	**LF**	**HF**	**LF/HF**
FFT Results				
Peak (Hz)	0,023	0,117	0,19	
Power (ms^2)	1613,9	2437,1	892,31	2,73
Power (%)	32,6	49,3	18,0	
Power (n.u.)		73,2	26,8	
AR Results				
Peak (Hz)	0,0033	0,040	0,15	
Power (ms^2)	1178,3	1817,6	1282,3	1,42
Power (%)	27,5	42,5	30,0	
Power (n.u.)		58,6	41,3	

Table 5.22: Variables that quantify HRV during clinium phase in the frequency domain.

Figure 5.98 shows the section of the RR intervals, selected through the Kubios software, related to the ortho phase in which the subject is standing.

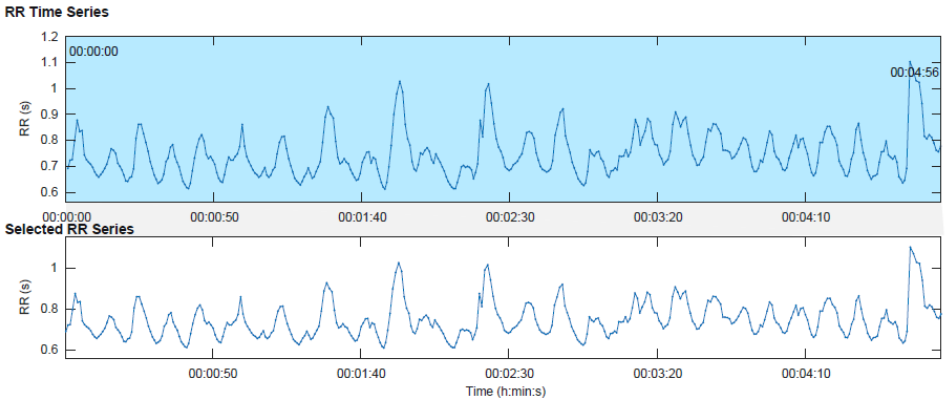

Figure 5.98: Tract of selected RR intervals in the ortho signal for time and frequency domain analysis.

Figure 5.99 shows the distributions of the beat-to-beat RR intervals and the heart rate HR recorded during the ortho phase.

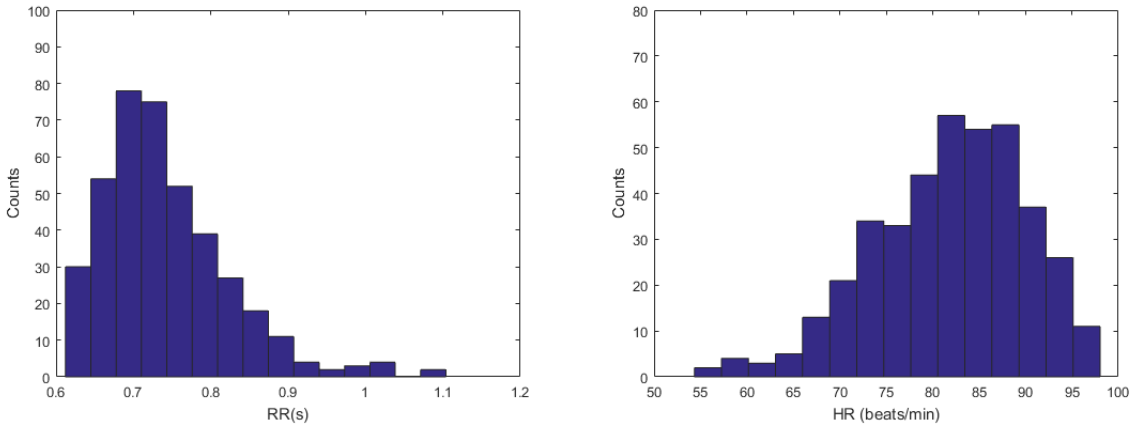

(a) (b)

Figure 5.99: Distributions of the RR intervals (a) and the heart rate HR (b) of the ortho phase.

Table 5.23 shows the parameters that quantify the variability of heart rate in the time domain.

Time-Domain Results	
Variable	**Value**
Mean RR	742 ms
STD RR	82 ms
Mean HR	81 beats/min
STD HR	2 beats/min
Min HR	58 beats/min
Max HR	96 beats/min

Table 5.23: Variables that quantify HRV during ortho phase in the time domain.

Figure 5.100 shows Poincarè plot and the values SD1 and SD2 standard deviations of the distributions along the transverse axis and the bisector.

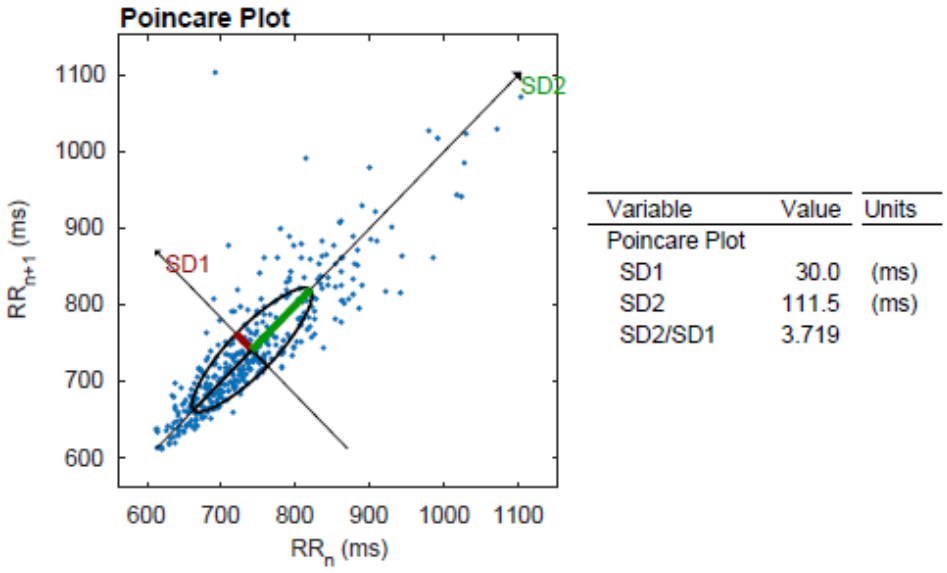

Figure 5.100: Poincarè plot of each RR interval according to the previous one.

Figure 5.101 shows the Fast Fourier Transform (FFT) of the RR intervals of the ortho signal ECG, ie the power spectrum is represented, which indicates how the power carried by a signal of a given frequency has been distributed.

Figure 5.102 shows analysis of the ortho signal obtained with autoregressive methods.

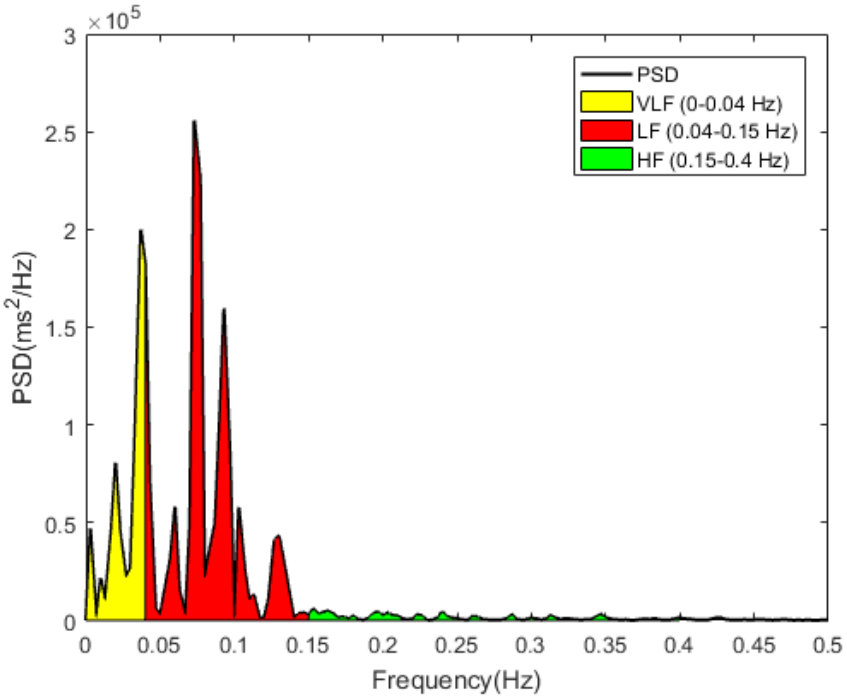

Figure 5.101: Fast Fourier Transform (FFT) of the ortho sygnal.

In the Figure 5.101 and 5.102 it is possible to distinguish three different frequency bands that characterize the sympathetic and vagal activity of the autonomic nervous system.

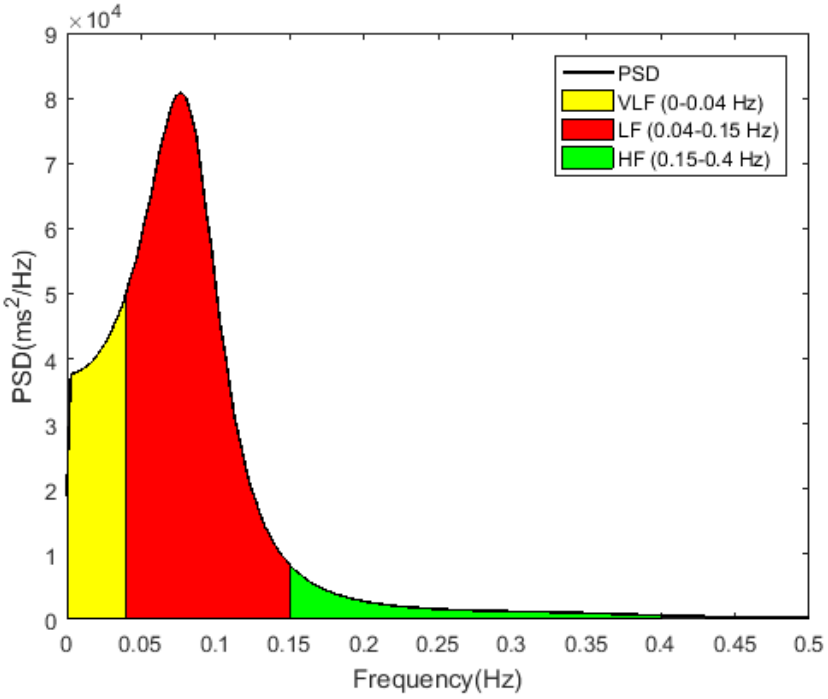

Figure 5.102: Autoregressive analysis of the ortho sygnal.

Table 5.24 shows the parameters that quantify the heart rate variability in the frequency domain.

Frequency-Domain Results				
Variable	**VLF**	**LF**	**HF**	**LF/HF**
FFT Results				
Peak (Hz)	0,037	0,073	0,15	
Power (ms^2)	2281,3	5126,8	343,1	14,95
Power (%)	29,4	66,1	4,4	
Power (n.u.)		93,7	6,3	
AR Results				
Peak (Hz)	0,0033	0,040	0,15	
Power (ms^2)	1627,4	5212,1	490,2	10,63
Power (%)	22,2	71,1	6,7	
Power (n.u.)		91,4	8,6	

Table 5.24: Variables that quantify HRV during ortho phase in the frequency domain.

Figure 5.103 shows the ECG signal recorded during the execution of the top test and the relative tacogram.

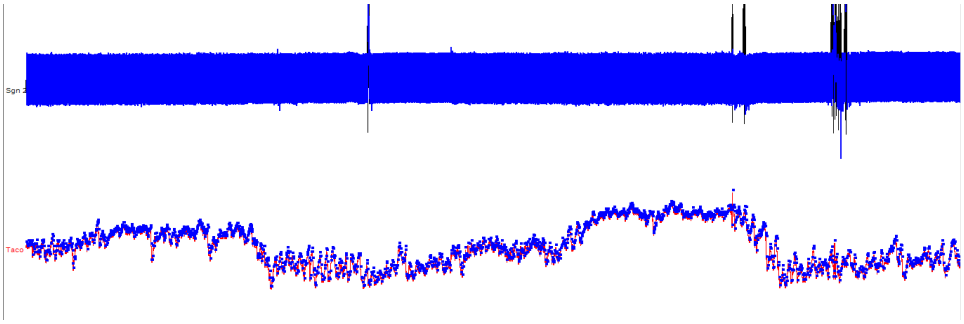

Figure 5.103: Tachogram of the signal ECG recorded during top test.

Figure 5.104 shows the heart rate trend during the top test execution, highlighting in blue the areas where there is a growth and decrease of the frequency in the transition phases in which the workload is added or removed.

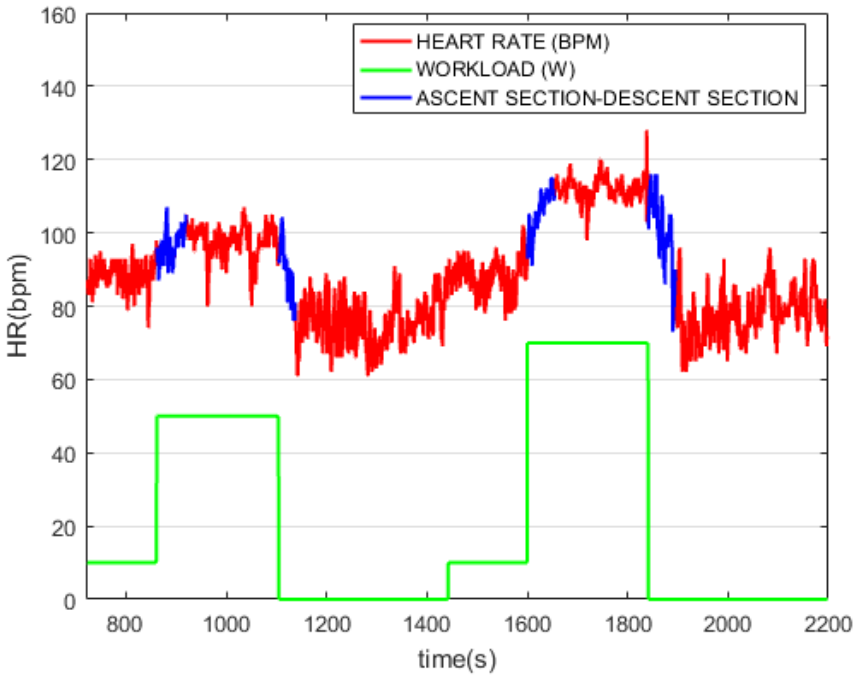

Figure 5.104: Heart rate trend as a function of time during the top test.

Figure 5.105 shows the exponential interpolation in the phase of heart rate increase at the insertion of the first workload (beginning of step 1). Figure 5.106 shows the

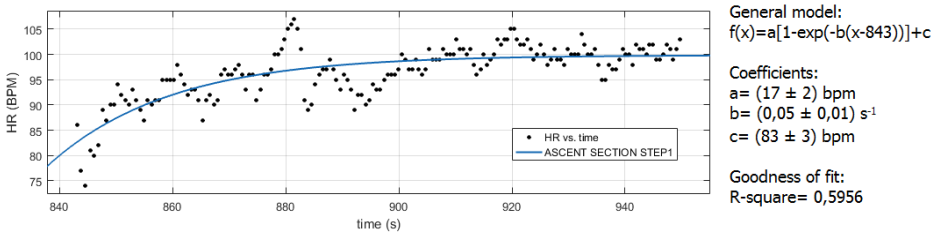

Figure 5.105: Exponential interpolation of the stress adaptation curve in response to the first workload.

exponential interpolation in the passive recovery phase in which the heart rate decreases at the removal of the first workload (end of step 1).

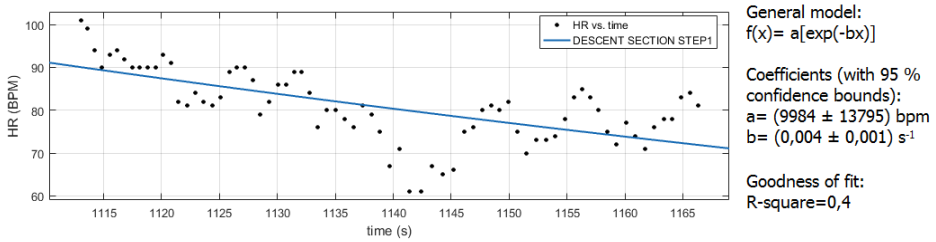

Figure 5.106: Exponential interpolation of the passive recovery curve after removal of the first workload.

Figure 5.107 shows the exponential interpolation in the phase of heart rate increase at the removal of the second workload (beginning of step 2).

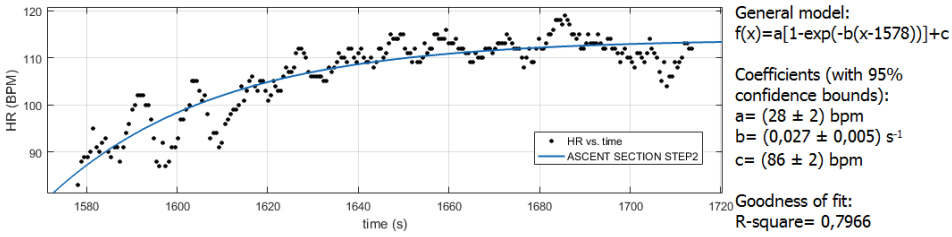

Figure 5.107: Exponential interpolation of the stress adaptation curve in response to the second workload.

Figure 5.108 shows the exponential interpolation in the passive recovery phase in which the heart rate decreases at the removal of the first workload (end of step 2).

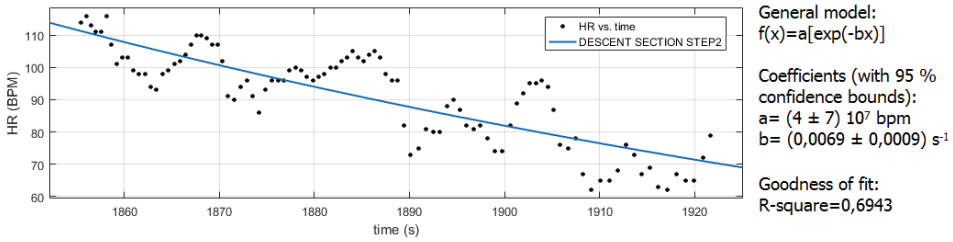

Figure 5.108: Exponential interpolation of the passive recovery curve after removal of the second workload.

5.7 Summary of the results for each subject

Table 5.25 shows the results obtained in the frequency domain through Fourier analysis and autoregressive methods.

Table 5.26 shows the results obtained from the exponential interpolation of the adaptation curve to the first workload and to the passive recovery curve after step1.

Table 5.27 shows the results obtained from the exponential interpolation of the adaptation curve to the second workload and to the passive recovery curve after step2.

N.S.	RR_c **(ms)**	HR_c **(bpm)**	$(LF/HF)_{FFTc}$	$(LF/HF)_{ARc}$	RR_o **(ms)**	HR_o **(bpm)**	$(LF/HF)_{FFTo}$	$(LF/HF)_{ARo}$
R.Z.	894 ± 48	67 ± 1	1,83	3,41	797 ± 29	75 ± 1	6,83	4,1
M.F.M.	949 ± 66	63 ± 1	3,44	3,11	758 ± 688	79 ± 2	30,3	22,7
M.Z.	596 ± 39	101 ± 2	0,77	0,97	542 ± 46	111 ± 2	7,98	6,85
S.C.	920 ± 57	65 ± 1	0,14	0,26	726 ± 41	83 ± 1	2,34	2,75
A.L.	1045 ± 133	57 ± 2	0,80	0,78	891 ± 105	67 ± 2	2,10	1,13
A.M.	903 ± 67	67 pm 1	2,73	1,42	742 ± 82	81 ± 2	14,95	10,63

Table 5.25: RR_c RR interval during clino phase, HR_c Heart Rate during clino phase, $(LF/HF)_{FFTc}$ ratio between LF and HF calculated through FFT during clino phase, $(LF/HF)_{ARc}$ ratio between LF and HF calculated through autoregressive method during clino phase, RR_o RR interval during ortho phase, HR_o Heart Rate during ortho phase, $(LF/HF)_{FFTo}$ ratio between LF and HF calculated through FFT during ortho phase, $(LF/HF)_{ARc}$ ratio between LF and HF calculated through autoregressive method during ortho phase.

N.S.	HR_{w1} **(BPM)**	HR_{s1} **(BPM)**	HR_{d1} **(BPM)**	τ_{1inc} (s^{-1})	τ_{1decr} (s^{-1})
R.Z.	85 ± 3	102 ± 3	73 ± 4	0,017 ± 0,003	0,0025 ± 0,0003
M.F.M.	76 ± 5	87 ± 4	71 ± 5	0,25 ± 0,31	0,006 ± 0,001
M.Z.	137 ± 7	176 ± 5	149 ± 8	0,11 ± 0,02	0,00159 ± 0,00004
S.C.	83 ± 4	93 ± 4	78 ± 5	0,11 ± 0,04	0,0044 ± 0,0006
A.L.	72 ± 6	80 ± 5	68 ± 6	0,05 ± 0,03	0,003 ± 0,002
A.M.	89± 3	98 ± 4	76 ± 7	0,05 ± 0,01	0,004 ± 0,001

Table 5.26: HR_{w1} heart rate during warm-up phase before step1, HR_{s1} heart rate during the first step, HR_{d1} heart rate during defacting after step1, τ_{1inc} exponential interpolation coefficient during the heart rate increase phase, τ_{1decr} exponential interpolation coefficient during the heart rate decrease phase.

N.S.	HR_{w2} **(BPM)**	HR_{s2} **(BPM)**	HR_{d2} **(BPM)**	τ_{2inc} (s^{-1})	τ_{2decr} (s^{-1})
R.Z.	85 ± 1	122 ± 1	85 ± 4	0,026 ± 0,002	0,0046 ± 0,0004
M.F.M.	80 ± 3	103 ± 5	70 ± 7	0,08 ± 0,02	0,0043 ± 0,0009
M.Z.	155 ± 3	188 ± 4	148 ± 7	0,016 ± 0,002	0,00220 ± 0,00005
S.C.	83 ± 4	105 ± 2	80 ± 5	0,05 ± 0,01	0,012 ± 0,002
A.L.	71 ± 6	86 ± 4	69 ± 6	0,12 ± 0,05	0,007 ± 0,005
A.M.	87± 4	113 ± 3	78 ± 7	0,027 ± 0,005	0,0069 ± 0,0009

Table 5.27: HR_{w2} heart rate during warm-up phase before step2, HR_{s2} heart rate during the second step, HR_{d2} heart rate during defacting after step2, τ_{2inc} exponential interpolation coefficient during the heart rate increase phase, τ_{2decr} exponential interpolation coefficient during the heart rate decrease phase.

Chapter 6

Discussion and conclusions

In this chapter the results reported in the previous chapter are discussed.

For each subject there has been an increase in the LF/HF ratio (Low Frequency/High Frequency) when we pass from the analysis of the clino signal to the analysis of the ortho signal in the frequency domain, this increase is due to the activation of the sympathetic nervous system (SNS) that accelerates the heart rate working at low frequencies. Instead, when the patient is lying on the bed (clinium phase) the HF component that determines the PNS activity is predominant, and the LF/HF ratio is lower.

The increase in the LF/HF ratio is noted by comparing the values $(LF/HF)_{FFTc}$, $(LF/HF)_{ARc}$ with the values $(LF/HF)_{FFTo}$, $(LF/HF)_{ARo}$ in Table 5.25.

The mild and moderate workloads inserted during the top test determine a physical exercise increase associated with an increase of sympathetic activity and a decrease of the parasympathetic one with a consequent heart rate increase. The rate at which the heart rate drops after exercise is an index of the vagal system reactivation.

The heart rate increase during a low intensity exercise (step 1) is due only to the vagal system inhibition, while for an exercise of medium-high intensity (step 2) the sympathetic system activation also occurs.

Passive recovery after exercise (defacting) is associated with the interruption of motor stimulation by the brain that is responsible for the initial rapid drop in heart rate.

However, the vagal system activation is considered the main mechanism of exponential decrease after exercise. The speed at which the heart rate drops and the length of recovery time after a moderate to intense exercise are usually used as a cardiovascular

fitness index.

An exponential interpolation of the curve sections corresponding to the insertion or removal of the workload is carried out to evaluate the capacity to adapt to the effort (step1, step2) and the passive recovery (defacting phase). Table5.26 e Table 5.27 show the values of the interpolation coefficients τ_{1inc} and τ_{1decr}, τ_{2inc} and τ_{2decr} to evaluate the increase and decrease of the heart rate respectively.

In addition, it is possible to notice that the second and fifth subject who perform physical activity several times a week have lower heart rate values (see Figure 5.20 and 5.74) compared to sedentary subjects like the first and third subject (see Figure 5.2 and 5.38).

Considering the fifth person who performs physical activity more than five times a week, the τ_{1inc} , τ_{2inc} values in the phases of load adjustment and τ_{1decr}, τ_{2decr} in the passive recovery phases are higher than those of sedentary subjects or those who perform little physical activity (see Table 5.26 and Table 5.27). The highest τ_{1inc} , τ_{2inc} values in the sporting subject indicates a better adjustment to the effort and the higher τ_{1decr}, τ_{2decr} values indicates a faster passive recovery, thus a faster return to the stability condition of the heart rate.

This thesis was focused on the instrumental procedures of a new test for physical evaluation on subjects with limited performance, where the standard submaximal methods are very difficult to apply. By choice, to simplify the process, only the electrocardiogram was sampled and all the interventions were addressed to extract all the possible information from that. First the quantification of the autonomous nervous system driving, by Tilt Test and HRV analysis, then by observing the way of adaptation of cardiac frequency to different, quite low, stress load steps, and recovery. In this work the methods have been described and tested on subjects with different performance, due to age and daily activity, and quantitative differences have been shown. We demonstrated that TOP test is easily executable and that a adequate amount of information is possible to be collected. Now the validation process moves to the clinicians, who have to select different subjects populations, apply the test and highlight the differences. We are sure that this will be possible, with an important contribute of medical Physics.

Bibliography

[1] G.Testoni, R.Zannoli *Fisica: i fenomeni naturali e la loro descrizione*, Bologna, Italy, 2003.

[2] R.Zannoli,C. Orsi *Elementi di strumentazione medica*, Bologna, Italy, 1999.

[3] Mezzani *Cardiopulmonary Exercise Testing: Basics of Methodology and Measurements*, Veruno, Novara , Italy, 2017.

[4] k.Albouaini, M.Egred, A.Alahmar *Cardiopulmonary Exercise Testing and its applicatio*, , 2007, volume 93, pages 1285-92.

[5] I.Corazza, R.Zannoli, D.Bianchini, S.Urbinati *Rehal:a telemedicine platform for home cardiac rehabilitation*, Bologna, Italy, 2014.

[6] N. Nelson, DO,A. Asplund , MD,MPH, FACSM *Exercise Testing: who, when and why?*, Georgia Southern University, Statesboro, 2015.

[7] W.Stringer *Cardiopulmonary exercise Testing: current applications*, Harbor-UCLA Medical Center, Torrance, USA, 2016.

[8] J.Myers *Applications of Cardiopulmonary Exercise Testing in the manegement of cardiovascular and pulmonary disease*, 2004.

[9] Roger Hainsworth *Heart Rate Variability*, chapther 1, New York, United States of America, 1995.

[10] Ivan Corazza, Laura Fabbiani, Romano Zannoli *Measurement of oxygen uptake: validation of a "mask-free" method*,Bologna, Italy, 2006.

[11] Marco Guazzi, Kenneth Dickstein *Six Minute walk test and cardiopulmonary exercise testing in patients with chronic heart failure*, 2009.

[12] Enrico Clini, Ernesto Crisafulli *Exercise Capacity as a pulmonary rehabilitation outcome*, Modena,Pavullo , Italy, 2009.

[13] Ivan Corazza, Romano Zannoli, Sebastiano Zannoli, Angelo Branzi *E-Remedy, Home Cardiac Rehabilitation: A Bologna-European Community Special Project*, 2009.

[14] Mika P. Tarvainen, Jukka Lipponen, Juha-Pekka Niskanen, PhLic Perttu O. Rantaaho, *Kubios HRV (ver. 3.1) User's Guide*, 2018.

[15] SparkBio *Anscovery manuale utente*, Bologna, 2015.

[16] Ivan Corazza *Metodiche "classiche" di acquisizione e quantificazione della variabilità della frequenza cardiaca*, 2012.

[17] Douglas F. Elliot *Handbook of Digital Sygnal Processing*, 1987.